



Universidade de Aveiro
Ano 2012

Departamento de Ambiente e Ordenamento
Departamento de Geociências

**IRENE
VIOLA**

**Mineralogia e geoquímica de carbonatos
autigénicos do Golfo de Cádiz**

***Mineralogy and geochemistry of authigenic
carbonates from the Gulf of Cadiz***



Universidade de Aveiro
Ano 2012

Departamento de Ambiente e Ordenamento
Departamento de Geociências

**IRENE
VIOLA**

**Mineralogia e geoquímica de carbonatos
autigénicos do Golfo de Cádiz**

***Mineralogy and geochemistry of authigenic
carbonates from the Gulf of Cadiz***

Dissertação apresentada à Universidade de Aveiro para cumprimento dos requisitos necessários à obtenção do grau de Mestre em Ciências do Mar e das Zonas Costeiras, realizada sob a orientação científica do Doutor Vitor Hugo da Silva Magalhães, investigador auxiliar do Departamento de Geociências da Universidade de Aveiro e da Doutora Rossella Capozzi, professora de Geologia estratiográfica e sedimentológica, do Dipartimento di Scienze della Terra da Universidade de Bologna.

o júri

presidente

Prof.^a Doutora Filomena Maria Cardoso Pedrosa Ferreira Martins
Professora Associada do Departamento de Ambiente e Ordenamento da Universidade de Aveiro

Doutor Davide Oppo
Investigador da Faculdade de Geociências da Universidade de Bolonha

Doutor Vítor Hugo Da Silva Magalhães
Investigador Auxiliar do Centro de Estudos do Ambiente e do Mar (CESAM) e do Departamento de Geociências da Universidade de Aveiro

Prof.^a Doutora Rossella Capozzi
Professora Associada da Faculdade de Geociências da Universidade de Bolonha

agradecimentos

Esta tese de mestrado beneficiou da ajuda e do apoio de muitas pessoas, laboratórios e instituições.

Agradeço ao Dr. Vitor Hugo Magalhães por todos conselhos e ensinamentos na geoquímica dos carbonatos, que foram muito importantes para este trabalho.

Agradeço à prof. Rossella Capozzi por todos conselhos, ensinamentos, e a disponibilidade prestada a este projecto.

As actividades de investigação desenvolvidas no decorrer desta tese foram realizadas no Departamento de Geociências da Universidade de Aveiro, onde fui muito bem-acolhida e onde encontrei sempre grande disponibilidade e apoio de todos.

Os meus agradecimentos ao director do Departamento de Geociências da Universidade de Aveiro, o Prof. Doutor Fernando Rocha e a todos os membros deste departamento. O meu obrigada especial à Denise Terroso e ao Prof. Doutor Fernando Rocha pelo apoio e sempre disponível e imediato acesso às análises mineralógicas por difracção raios-X.

Quero agradecer todos os colegas do Laboratório de Geologia e Geofísica Marinha pelo suporte, entusiasmo e força que deram durante este período.

A minha gratidão ao Prof. Doutor Luis Menezes Pinheiro, líder deste laboratório, pelo seu apoio, amizade, e sempre estimulantes e úteis comentários e discussões.

As amostras utilizadas neste trabalho foram recolhidas no âmbito de vários projectos, na pessoa dos seus investigadores quem eu também agradeço. Assim, agradeço ao projecto ESF EUROCORES/ Euromargins - MVSEIS (01-LEC-EMA24F DCTM/2003/DIV/40018/99), e aos projectos, SWIMGLO (PTDC/MAR/100522/2008) e GRACE (PTDC/MAR-PRO/3844/2012), financiados para a Fundação Portuguesa da Ciência e da Tecnologia (FTC). Também agradeço o projecto "Stratigraphic and structural control on fluid migration and related carbonate precipitation along conduits" (prot. 2009WCYS5P_001), financiado pelo Ministério da Instrução, Universidade e Pesquisa Italiano.

Por fim, agradeço à minha família e aos meus amigos pelo apoio, ajuda e encorajamento, especialmente à Gea.

Obrigado a todos, a quem está, a quem foi e a quem será.

palavras-chave

MDAC, Mineralogia, geoquímica, Golfo de Cádiz, oxidação anaeróbica de metano.

resumo

Este trabalho apresenta a caracterização mineralógica e geoquímica de carbonatos autigênicos do Golfo de Cádiz. Divide-se numa primeira parte introdutória onde se apresenta um resumo dos conceitos teóricos e o enquadramento geológico e estrutural da área em estudo, seguido da investigação realizada, incluindo a caracterização das amostras estudadas, a descrição dos métodos analíticos e apresentação e discussão dos resultados obtidos, que permitiram a sua caracterização mineralógica e geoquímica. As amostras estudadas provêm de vários vulcões de lama do Golfo de Cádiz, localizados em diferentes enquadramentos tectónico - sedimentares. A caracterização mineralógica e geoquímica dos carbonatos autigênicos indicam uma formação em resultado da oxidação anaeróbica de metano na coluna sedimentar, a pouca profundidade, e reflectem características típicas de três processos de formação que deram origem aos três tipos litológicos presentes: chaminés, crostas e concreções carbonatadas.

Acknowledgments

This master degree thesis benefited from the help and support of many people, laboratories and institutions.

I'd like to thank Dr. Vitor Hugo Magalhães for all the advices and the teaching about carbonates geochemistry that were very important for this thesis.

I'd like to thank also to prof. Rossella Capozzi for her availability and for make this cooperation work.

These research activities were carried out at the Geosciences Department of the University of Aveiro where I was very welcomed and all the facilities and research laboratories were always available for this project.

Therefore, my thanks to the Geosciences Department director Prof. Doctor Fernando Rocha, and to all the Geosciences Department members. A special acknowledge to Denise Terroso and Prof. Doctor Fernando Rocha by their support and the always available access to the x-ray diffraction analysis.

I am grateful to my colleagues of the Marine Geology and Geophysics Laboratory for all the support, enthusiasm and strength that gave me during this period of time.

My appreciation and my acknowledgements to Prof. Doctor Luis Menezes Pinheiro, head of this laboratory, for his support, the friendship, helpful comments and discussions.

The samples used in this work were collected in the framework of several research projects, to whom I also acknowledge, to the ESF EUROCORES/Euromargins project MVSEIS (01-LEC-EMA24F PDCTM/2003/DIV/40018/99), to the SWIMGLO (PTDC/MAR/100522/2008) and GRACE (PTDC/MAR-PRO/3844/2012) projects, financed by the Portuguese Foundation for Science and Technology (FCT). I also acknowledge the project "Stratigraphic and structural control on fluid migration and related carbonate precipitation along conduits "(prot. 2009WCYS5P_001), financed by the Italian Ministry of Education, University and Research.

In the end, a great thank you to all my family and friends for the encouragement, support and help, especially to Gea.

Thanks to everyone, the ones that are, the ones that were and the ones that will be there.

keywords

MDAC, mineralogy, geochemistry, Gulf of Cadiz, anaerobic oxidation of methane.

abstract

This work is focused on the mineralogy and geochemistry of authigenic carbonates from the Gulf of Cadiz. It is divided in an introductory part where the background concepts and the geological setting of the study area are presented, followed by the research work carried out in this master thesis project. The studied samples, the methods and the techniques applied are described, followed by the presentation of the main results and their discussion, concluding on their mineralogical and geochemical characterization and significance. The samples came from several mud volcanoes, on three different geological and tectonic settings of the Gulf of Cadiz. This mineralogical and geochemical characterization of the authigenic carbonates show the methane derived origin, especially the C and O isotopes, as resulting from anaerobic oxidation of methane in shallow sediments and permit to divide the samples in three main group based on mineralogy and morphology: chimneys, crusts and concretions. The data obtained compared with the literature model proposed, permit to prove the hypothesis about the formation processes of the three type. On the different type of carbonates is possible to recognize the influence of the MOW on the oxidation and bio-erosion of the chimneys and gas hydrates influence on two samples from the Michael Ivanov Mud Volcano. It is possible, due the isotopic data, move hypothesis on age of the three different type of carbonate, in particular has been possible to distinguish between the recent formation of the concretions and older formation of the chimneys.

Index

Figures Index	iii
Tables Index	viii
Chapter 1: Introduction	1
Chapter 2: Theoretical Background	8
2.1 Carbonate Rocks	8
2.1.1 Mineralogy	8
2.1.2 Classification of carbonate rocks	9
2.2 Authigenic Carbonates	16
2.3 Fluid escape structures	24
2.3.1 Cold Seepages	24
2.3.2 Mud Volcanoes	29
2.3.3 Pockmarks	30
2.4 Chemiosynthetic Fauna	32
2.4.1 Gas hydrates and chemosynthetic biota at cold seeps	34
Chapter 3: The Gulf of Cadiz	37
3.1 Study Area	37
3.2 Geological Setting	37
3.3 Oceanographic setting	41
3.4 Carbonate Chimneys	42
3.5 Carbonate Crusts	44
3.6 Mud Volcanoes	45
Chapter 4: Materials	48
4.1 Cruises	50
Cruise TTR 14	50
Cruise TTR 15	51
Cruise TTR 16	53
Cruise METEOR 86/5	53
Chapter 5: Methods	58
5.1 Thin Sections	58
5.1.1 What is a petrographic thin section?	58

5.1.2 <i>Thin Section Preparation Systems</i>	58
5.2 X-ray diffraction	59
5.2.1 <i>X-ray Generation and Properties</i>	60
5.2.2 <i>Lattice Planes and Bragg's Law</i>	60
5.2.3 <i>Powder Diffraction</i>	61
5.2.4 <i>X-ray Crystallography</i>	62
5.2.5 <i>MacDiff 4.2.6</i>	62
5.3 Geochemistry	64
5.3.1 <i>LECO C, O, N and S elemental analysis</i>	64
5.3.2 <i>Carbon and Oxygen Isotopes</i>	65
5.4 Scanning Electron Microscopy (SEM)	66
5.4.1 <i>Fundamental Principles of Scanning Electron Microscopy (SEM)</i>	67
5.4.2 <i>Applications</i>	68
Chapter 6: Results	69
6.1 Samples description	69
6.2 Petrography	73
6.3 XRD	78
6.3.1 <i>Total Mineral Composition</i>	78
6.3.2 <i>Carbonate Content</i>	84
6.4 Isotopes	87
Chapter 7: Discussion	96
7.1 Types of authigenic carbonates	96
7.2 Methane-derived origin of these carbonates	97
7.3 Relative formation ages	101
7.4 Formation model	102
Chapter 8: Conclusions	104
References	106
Annex I R Statistic Script	116
Annex II GCD kit extension	118

Figures Index

Figure 1: The Gulf of Cadiz. (Source: google heart).....	4
Figure 2: Folk classification of carbonates rocks. (Folk, 1965).....	10
Figure 3: Dunham classification of carbonates rocks. (Dunham, 1961)	11
Figure 4: Carbonate depositional environments. (Schlager W., 1992).....	13
Figure 5: Schematic representation of the carbon species and carbon isotope compositions of different reservoirs involved in hydrothermal systems at mid-ocean ridge environments. (a) Lost City-type hydrothermal system (b) Black smoker type system. Abbreviations: DOC, dissolved organic carbon; DIC, dissolved inorganic carbon; TOC, total organic carbon; TIC, total inorganic carbon; TC, total carbon (Delacour et al., 2008).....	17
Figure 6: Location of the studied regions with authigenic carbonates in the ocean. (1) Subduction zones; (2) spreading zones; (1) Gulf of California; (2) Sea of Okhotsk, Paramushir Isl. area; (3) Black Sea, Dnepr canyon; (4) Norwegian Sea, Haakon Mosby mud volcano (HMMV); (5) mud volcanoes of the Gulf of Cadiz; (6, 7) active hydrothermal fields of the Mid-Atlantic Ridge (MAR): (6) Lost City (30° N); (7) Logachev (14° N). (Lein, 2004).....	19
Figure 7: Map showing the global distribution of onshore and offshore oil seeps many of which also emit natural gas. Numbers indicate the count of seeps in a given region. Modified from Wilson et al. (1973, 1974) (Kvenvolden et al, 2005).....	29
Figure 8: Illustration of a pockmark and underlying gas chimney during a phase of active expulsion of free gas. The passage of free gas through the hydrate stability zone is aided by the formation of hydrate around the pathways through which the gas is passing, inhibiting access of the gas to pore water and preventing conversion of all the gas to hydrate. Progressive formation of hydrate and carbonate near the seabed seals pathways, causing an outward migration of the active gas vents. (Foucher et al, 2007).....	31
Figure 9: Illustration of a pockmark and underlying gas chimney when only pore water is migrating through the system. Methane from hydrate created during the free-gas expulsion phase keeps the methane in solution in the migrating pore water at saturation concentration, supporting chemosynthetic biota in the pockmark, until all the hydrate is removed in solution. This process may continue for thousands of years, with only moderate amounts of hydrate and concentration of methane in solution in the pore water entering the chimney from below. (Foucher et. al, 2007).....	32
Figure 10: Schematic representation of the control of methane concentration beneath the seabed	

by the initial concentration of methane in solution in upwardly migrating pore water, the presence of hydrate, and sulfate in the seawater. The concentration of dissolved methane in the rising pore water controls the depth at which hydrate begins to form. If it is less than the lowest value of methane solubility, then all previously formed hydrate will be removed, but the rate of removal depends upon the degree to which the pore water is undersaturated and the rate of pore-water flow (Foucher et. al 2007).....35

Figure 11: Tectonic map of the Gulf of Cádiz (Medialdea et al, 2009) showing the main outcropping and very shallow diapirs, faults, mud volcanoes and mud-carbonate mounds. FSb: Subbetic Front; FF: Flysch Front. Mud volcanoes recently discovered after Somoza et al. (2008). B) Line-drawing derived from the Multi-Channel Seismic profile TASYO 1 that crosses the Gulf of Cádiz.....38

Figure 12: Regional map of the contourite depositional system on the middle slope of the Gulf of Cádiz and West Iberian margin with proposed site locations. Morphosedimentary sectors (1–5). (Hernandez-Molina et al., 2006).....40

Figure 13 : Location sketch with main water-mass circulation along the margin (modified from Hernández-Molina et al., 2006) (Stow et al, 2011)42

Figure 14: Map of the Mud Volcanoes discovered and confirmed in the Gulf of Cadiz until 2008. (Golnzález et al., 2009).....46

Figure 15: Map showing the location of the samples used in this Master thesis project (green stars). Red triangles indicate the location of the present-day confirmed mud volcanoes.....48

Figure 16: Location of the samples collected during the TTR 14 Cruise that were used in this project. On the background, low resolution NRL Seemap backscatter overlaid by the deep-towed high resolution MAK side-scan sonar acquired during the TTR 14 cruise. The location of the 3 sampling stations: 550D and 551D dredge samples are marked by the red squares and the TV- controlled grab sample 552Gr marked by the red hexagon.....50

Figure 17. Onboard pictures of the samples collected on the stations 550D, 551D and 552Gr.....51

Figure 18: Location of the samples collected during the TTR 15 and TTR16 Cruises that were used in this project. A hillshade of the bathymetry is shown on the background.....52

Figure 19: Location of the samples collected during the TTR 15 and TTR16 Cruises on the Meknes mud volcano, used in this project. on the background is shown a deep towed side-scan sonar backscatter imagery of the mud volcano with the crater and mud flows characterized by a strong backscatter intensity (corresponding to dark colors).....52

Figure 20: Onboard pictures of the samples collected on the stations 569Gr, 574D, and 581Gr,

from which the representative samples IV23, IV24 and IV25, studied in this work, were collected from.....53

Figure 21: Core log and onboard picture of the gravity core TTR15 – 583G, from where the concretions sample IV26, that was studied in this work, was collected from.....54

Figure 22: Onboard picture of the sample TTR 16 – 600Gr collected on Pen Duick escarpment, from which a representative samples IV27 was collected from and studied in this work.....55

Figure 23: Location of the samples collected during the Meteor 86/5 Cruises on the Michael Ivanov mud volcano and used in this project. On the background is shown a autonomous underwater vehicle side-scan sonar backscatter imagery of the mud volcano, with multiple craters, mud flows and pockmarks.....56

Figure 24: Gravity cores M86/5-24GC04 and M86/5-42GC10 and respective core logs from where the samples IV20 and IV22 were collected from. Gravity core M86/5-100GC25, where a gas hydrate chunk was observed, is also shown.....57

Figure 25: MacDiff 4.0.4 screenshot. Example of visualization.....63

Figure 26: Examples of chimneys samples from TTR-14.....69

Figure 27: Examples of two crusts (a and c) and a concretion (b).....70

Figure 28: Scans of the catted surface of the chimneys samples. On that have been identify the sub sampling point.....72

Figure 29: Microscope photos show examples of different textures of the thin sections. From the top: IV03.01, IV03.02, IV04.01, IV08.01, IV11.01 and IV16.01.....73

Figure 30: Scans of the thin section IV03.01, IV03.02 and IV04.01.....74

Figure 31: Scans of the thin sections IV04.02, IV08.01, IV09.01 and IV10.01.....76

Figure 32: Scans of the thin sections for the samples IV11.01, IV14.01, IV16.01 and IV19.01.....77

Figure 33: Example of diffractogram in Macdiff showing the peaks for calcite, dolomite and quartz.....78

Figure 34: Box-plot of mineral composition for TTR 14 chimney samples. Box-plots indicate the minimum, maximum median and lower and upper quartiles for a variable. The box represents the interquartile range that contains 50% of values. The whiskers are lines or points that extend from the box to the highest and lowest values. A line across the box indicate the median. The number of sub samples used in the statistic elaboration in reposted

as n and calcite and dolomite are indicated by light and dark gray respectively.....81

Figure 35: Box-plot of mineral composition for M86/5 concretion samples. Box-plots indicate the minimum, maximum median and lower and upper quartiles for a variable. The box represents the interquartile range that contains 50% of values. The whiskers are lines or points that extend from the box to the highest and lowest values. A line across the box indicate the median. The number of sub samples used in the statistic elaboration in reposted as n and calcite and dolomite are indicated by light and dark gray respectively.....83

Figure 36: Box-plot of mineral composition for TTR 15 and 16 crust samples. Box-plots indicate the minimum, maximum median and lower and upper quartiles for a variable. The box represents the interquartile range that contains 50% of values. The whiskers are lines or points that extend from the box to the highest and lowest values. A line across the box indicate the median. The number of sub samples used in the statistic elaboration in reposted as n and calcite and dolomite are indicated by light and dark gray respectively.....84

Figure 37: Ternary mineral and compositional plots.....85

Figure 38: Column graph between quantification of carbonate fractions by XRD and LECO for TTR 14 chimneys samples.....85

Figure 39: Column graph between quantification of carbonate fractions by XRD and LECO for TTR 15, TTR 16 crust and M86/5 concretion samples.....86

Figure 40: Correlation between Total Organic Carbon and total carbonate fraction in LECO and correlation between XRD and LECO carbonate fractions.....86

Figure 41: $\delta^{18}\text{O}$ vs $\delta^{13}\text{C}$ for the three types of samples. The values of the isotopes (VPDB) are expressed in ‰.....88

Figure 42: Correlation between total carbonate fraction from LECO and the $\delta^{18}\text{O}$ isotope for the three type of samples.....90

Figure 43: Correlation between the two main carbonate fractions, Calcite and Dolomite, from XRD and the $\delta^{18}\text{O}$ isotope for the three type of samples.....91

Figure 44: Correlation between total carbonate fraction from LECO and the $\delta^{13}\text{C}$ isotope for the three type of samples.....92

Figure 45: Correlation between the two main carbonate fractions, Calcite and Dolomite, from XRD and the $\delta^{13}\text{C}$ isotope for the three type of samples.....93

Figure 46: isotopes profiles for chimneys samples of TTR-14. In blue the $\delta^{13}\text{C}$, in red the $\delta^{18}\text{O}$. The values of both the isotopes are expressed in ‰ (VPDB).....93

Figure 47: isotopes profiles for concretions samples of M86/5. In blue the $\delta^{13}\text{C}$, in red the $\delta^{18}\text{O}$. The values of both the isotopes are expressed in ‰(VPDB).....94

Figure 48: isotopes profiles for crusts samples of TTR-15 and 16. In blue the $\delta^{13}\text{C}$, in red the $\delta^{18}\text{O}$. The values of both the isotopes are expressed in ‰ (VPDB).....94

Figure 49: $\delta^{18}\text{O}$ and $\delta^{13}\text{C}$ values for the samples used in this thesis (colored ones) and the samples values taken from Magalhães, V. 2007 (black-gray). The values of the isotopes are expressed in ‰ (VPDB).....99

Figure 50: screenshot of R-statistics showing an example of data input from .txt file.....116

Tables Index

Table 1: Main regions of authigenic carbonate investigation. (Source: Lein, 2004).....	16
Table 2: List of samples used in this Master thesis project. Allong this thesis, samples will be identified by her lab code.....	49
Table 3: results from XRD, LECO and isotopes for all the samples.....	79

Chapter 1: Introduction

This master thesis project has been developed in the Geosciences department of the Aveiro University. It is related to three different projects:

- the *"Stratigraphic and structural control on fluid migration and related carbonate precipitation along conduits"* project. This project addresses the study of modern and ancient carbonate conduits and chimneys recovered in different, offshore and onshore geologic contexts, as the Northern Apennines, the Adriatic Sea, the emerged northern part of the Crotone basin (Calabria) and the Gulf of Cadiz. The study aims to constrain the nature of the authigenic carbonate samples and to investigate their proposed origin as methane-derived carbonates, based on their similarity with other occurrences but not yet totally confirmed. This type of samples are frequently interpreted as surface indicators of shallow or deep hydrocarbons reservoirs and can therefore be useful for exploration purposes. As the leakage of fluids up to the surface, previously needs the achievement of favorable conditions leading to expulsion from source rocks, migration and accumulation within stratigraphic and structural traps. This project, and this thesis, are developed in collaboration with the University of Bologna (Italy).
- The Euromargins/Eurocores programme project MVSEIS *"Tectonic control, deep crustal structure and fluid escape pathways in the Gulf of Cadiz mud volcano field"* started on June 2003 and integrates Portuguese, Spanish, Belgium and French teams under the coordination of the Portuguese team (L. M. Pinheiro). The Portuguese work package has been funded by the Portuguese Science Foundation - FCT. The objective of the MVSEIS project is to investigate the deep crustal structure, the sedimentary section and sediment dynamics, the tectonic control and the detailed geometry of the fluid escape pathways in this area with active mud volcanism and cold seeps, using a multidisciplinary

approach. The multidisciplinary approach gives the opportunity to link the tectonic, sedimentological, geochemical and biological processes associated with the mud volcanism and gas seepage.

- The SWIMGLO project: “*The Gloria-SWIM plate boundary Faults connection and its importance on the propagation of tectonic deformation and deep*” (PTDC/MAR/100522/2008). The SWIM Fault system constitutes a 600 km long active plate boundary between the Rif-Tell continental plate boundary and the Gloria Fault plate boundary. Mud volcanoes, the loci of chemosynthetic biological communities, are found in association with the SWIM Faults. The interconnectivity between chemosynthetic ecosystems in the Gulf of Cadiz can be mediated by local oceanographic processes. This project will investigate the geological connection between the SWIM Faults and the Gloria Fault, the channeling of fluids along the SWIM Faults in the deep oceanic domain and the chemosynthetic communities along the SWIM Faults and SWIM-Gloria connection. The geological, chemical and biological data will contribute to clarify i) the role of trans-continental-oceanic faults in the dispersal of deep-sea chemosynthetic organisms across the Atlantic, ii) the fluids exhaled along this plate boundary and, iii) the geometry and seismicity of the connection of two plate boundaries that are merging into each other at Present.

The samples analyzed in this thesis have been collected during four different cruises. Three of them are Training-Through-Research (or TTR) cruises, in particular the TTR-14, TTR-15 and TTR-16, that operated largely in the area. The fourth cruise is the METEOR cruise M86/5.

The subject of this thesis are Authigenic Carbonate formation, in the Gulf of Cadiz. In particular three type of authigenic carbonates have been considered in this work: chimneys, crusts and concretion (usually associated with mud volcanoes structures). Those samples came from 4 different cruises list before, that operate in different parts of the Gulf. So have been analyzed in this work four different data sets of samples collected from three different settings:

- On the Mediterranean Outflow Water channel in front of Gibraltar
- On the deep portuguese mud volcano Michael Ivanov MV

- On the Marocco margin: Vernadesky ridge
 - Pen Duick Escarpment
 - Mercator Mud Volcano
 - Merkator Mud Volcano

The main objective of this thesis is the identification and characterization of authigenic carbonate associated with cold seeps from these three different settings in the area of the Gulf of Cadiz. In particular prove, using mineralogy and geochemistry, that the three types of carbonates that have been considered in this thesis are actually different between them and that are clearly recognizable on the basis of the analysis done. Prove also that is possible to define trends of evolution and characterization for the three types of carbonate and for the samples in each group. Another important objective in this master degree thesis, is to investigate and try to relate the geochemical and mineralogical characteristics to the formational processes of the three types of authigenic carbonate considered in this thesis. After reaching all the previous objectives, this master degree thesis address itself to prove that the authigenic carbonate considered are, in all the cases methane derived.

The characterization of the samples has been done using geochemical properties and mineralogy of the samples to identify and distinguish the different types of samples.

Based on the characterization of the carbonate samples from these different settings, the composition and formation processes of authigenic carbonates will be constrained. Three types of authigenic carbonates have been considered in this work: chimneys, crusts and concretions (usually associated with mud volcanoes and similar structures).

In this study, the samples were characterized by petrographic and geochemical analysis through:

- Thin section petrographic description
- Scanning electro microscopy analysis
- X-ray diffraction (XRD)
- Carbon and Oxygen stable isotopes

- Chemical analysis of Carbonate content and Total Organic Carbon content

Area

The Gulf of Cadiz, situated in the south-west of Europe, is a very important area of



Figure 1: the Gulf of Cadiz. (Source: google earth)

the Atlantic ocean. This gulf is confined in the North by Spain and Portugal southern coasts and on the south by Moroccan atlantic coasts. The most characteristic limits are the East and West-ones: they are respectively the Gibraltar Strait and the open Atlantic Ocean. This region is the area in which the water of Mediterranean sea mixes with water from the Atlantic Ocean.

The importance of the oceanographic literature and marine

geological studies on the Gulf of Cadiz continental margin (SW Europe) emanates of its proximity to the Strait of Gibraltar, a point of singular geographic interest, being it the place where the Atlantic Ocean and Mediterranean Sea interchange their water masses, starting a thermodynamical system that is one of the most important in the global water circulation, and where the Western Mediterranean Alpidic Orogen (Betic and Rif Mountain range) meet through the Gibraltar Tectonic Arch. Therefore, this zone has been object of numerous studies in a large variety of disciplines.

Geologically speaking, the Gulf of Cadiz is located at the front of the Betic-Rifian Arc. It has had a very complex geological history and undergone several episodes of rifting, compression and strike-slip motion, since the Triassic (Wilson et al., 1996; Maldonado et al., 1999). The westward migration of the Gibraltar arc during the Mesozoic caused the Gulf of Cadiz to form as a forearc basin (Maldonado et al., 1999). In the forearc basin, due to different movement, rotation and gravitational processes resulted in the implantation of the Gibraltar Olistostrome. This is a chaotic consequence of units that involve a huge volume of mud and salt

diapirism of Triassic salt units and undercompacted Early-Middle Miocene plastic marls (Maldonado et al. 1999).

Throughout this area, pockmarks, extensive mud volcanism, carbonate mounds and chimney structures related to hydrocarbon rich fluid venting and mud diapirism are observed (Ivanov et al., 2000; Somoza et al., 2003; Pinheiro et al., 2003).

At the East part of the Gulf of Cadiz it is possible to observe a large NE-SW diapiric ridge, the Guadalquivir Diapiric Ridge (GDR), that runs from the shelf break up to 1200 m water depth. This ridge controls the orientation of the main channel of the Mediterranean Outflow Water (MOW) undercurrent. The GDR is comprised of a series of wide sub-circular conical mounds surrounded by ring-shaped seafloor depressions. Most of these depressions are filled by contourite deposits as results of the MOW undercurrent interaction with the seafloor. Some of them, mainly on the right side of the main MOW channel, are developed into sediment "shadows", formed on the down-current side of the mounds and with asymmetrical moats (Kenson et al., 2006).

Thesis Outline

This thesis has been divided in 8 chapters.

Chapter 1: Introduction. This is the chapter that you are reading now, it describes the work, the subject and objectives of this thesis. It also contains a breve general and simple description of the area of interest and of the work that has been done to arrive at the objectives of this master thesis.

Chapter 2: Theoretical Background. In this section I have reviewed all the necessary background knowledge on the carbonates petrography, fluid escapes processes and structures to arrive to the conclusions. Here will be described all the main the formation process, environments and the mineralogy of this kind of rocks.

Then I'll review the Authigenic Carbonates: those are exactly the type of carbonate rocks studied in this thesis. Is possible to identify different types of Authigenic carbonates and especially Methane Derived Authigenic Carbonate. Those are deeply related with cold seeps and hydrothermal vents phenomenon that are

treated in the following part of the chapter. In the end let's do a little survey on the significance and importance of the chemiosynthetic fauna.

Chapter 3: Gulf of Cadiz. This chapter describes the settings of the area both geological and oceanographic, description of processes and of the main type of authigenic carbonates present in the area and that are analyzed in this thesis. Will be described the formation and main geology of the gulf because it is important to discriminate the composition of the samples and of the rock in the area. Also there is the description of the actual setting of the ocean currents and this is very important to understand the influence of the MOW that enter in the gulf and processes and interaction water-sediment.

Chapter 4 Materials. In this chapter is presented the characterization of the different samples set used in this master project and the description of the cruises in which the samples were recovered . Not all samples have been recovered with the same sampling instruments and also the data sets are very different between them, one is composed by chimneys formation, one by carbonate concretions and the other by carbonate crusts.

Chapter 5: Methods. Here are described all the methods used the analysis done on the samples such as thin section technique, X-ray diffraction, and all the analysis and the meaning of the variables that has been measured or calculated on the samples.

Chapter 6: Results. In this chapter are showed all the results of the analysis, commented and linked together. All the data results have been analyzed and plotted with Microsoft Excel, R-Statistic and GCDkit extension for R.

Chapter 7: Discussion. In this chapter are discussed all the results showed in the previous one. Trends and anomalies between the different groups and within individuals will be investigated.. Then sample relationships and trends linking the different groups and samples in the different groups with the variables will be

discussed and analyzed.

Chapter 8: Conclusions. In this Chapter results and main conclusions are presented. the formation processes and their signature on the different types of samples is presented. It will discussed about if the carbonate in this thesis really are MDAC and why, and the importance and significance of this in general and especially in the area of the Gulf of Cadiz.

Chapter 2: Theoretical Background

2.1 Carbonate Rocks

Sedimentary carbonates are very important, they cover about 7% of the earth surface and correspond to 10-15% of the total sedimentary rocks (Morse et al., 1990).

The economic importance of this type of sedimentary rocks is close related with the hydrocarbons industry. In fact more than 50% of the oil and gas reservoirs are related with carbonate reservoirs. Because carbonate minerals generally are soluble in slightly acidic waters, they often have high porosity and permeability, making them ideal reservoirs for petroleum.

Also a large part of carbon on earth is stored in carbonate sediments and therefore carbonates play a major role in the global carbon cycle (Lein, 2004).

Carbonates are of interest not only to the oil industry they have also economic importance as industrial "mineral" resource to the agriculture, as natural stone, and to the cement and concrete composites industry. Two main types of carbonate rocks can be considered:

- Limestones, composed mostly of calcite (CaCO_3) or high Mg calcite [(Ca,Mg) CO_3];
- Dolostones, composed mostly of dolomite [$\text{CaMg}(\text{CO}_3)_2$].

2.1.1 Mineralogy

Carbonate rocks contain a variety of minerals. Calcite and dolomite are the most abundant, aragonite is rarer, and other carbonate minerals, such as [ankerite, ...] are largely considered as result of special deposits and called "trace minerals".

Is appropriate to divide carbonate minerals by the environments in which they are deposited, in fact the factors controlling the source, mineralogy and diagenesis are very different in deep, intermediate and shallow water.

The main characteristics of those minerals and will be discussed now and subsequently the environmental differences between the different carbonates.

CaCO_3 minerals: Is possible to distinguish between three polymorphs of this composition. Calcite (rhombohedral mineral) is the most abundant carbonate

mineral and is the most stable thermodynamically. Aragonite (orthorhombic mineral) is 1,5 times more soluble than calcite. Viterite, of hexagonal structure, has been rarely observed in natural systems and always in condition in which it is metastable relative to calcite and aragonite. Viterite is 3,7 times more soluble than calcite and 2,5 than aragonite (Morse et al., 1990).

Dolomite: is one of the most abundant sedimentary carbonate minerals. Its formation remains controversial because of the complex and well-ordered structure and because of the many different types of dolomites that exist. There is a deep relation of stability between dolomite and calcite, in fact in different environment the two minerals exchange in percentage of Ca and Mg to increase their stability. In marine waters mostly, but also in others, dolomite is the stable carbonate phase.

High temperature dolomite, it happen dolomitization process. it is the process by which limestone is altered into dolomite; when limestone comes into contact with magnesium-rich water, the mineral dolomite, calcium and magnesium carbonate, $\text{CaMg}(\text{CO}_3)_2$, replaces the calcite in the rock, volume for volume. Dolomitization involves recrystallization on a large scale.

Low temperature dolomite give problem in formation, in the water, and can be substitute by aragonite (Morse et al., 1990).

Other carbonate phases: The carbonates tends to form a variety of hydrates. Magnesite, for example, cannot form directly from liquid to solid in surface condition, but a variety of magnesium carbonate hydrates form from solution.

The possible substitution in the carbonate mineral general structure between the calcium or magnesium and iron or manganese produce a very large number of mineral compositions and structures (Morse et al., 1990).

2.1.2 Classification of carbonate rocks

There are two main classifications that can be used to classify carbonates rocks.

Folk Classification

The Folk classification divides carbonates into two groups. Allochemical rocks are those that contain grains brought in from elsewhere (i.e. similar to detrital grains in

clastic rocks). Allochemical rocks have grains that may consist of fossiliferous material, ooids, peloids, or intraclasts. These are embedded in a matrix consisting

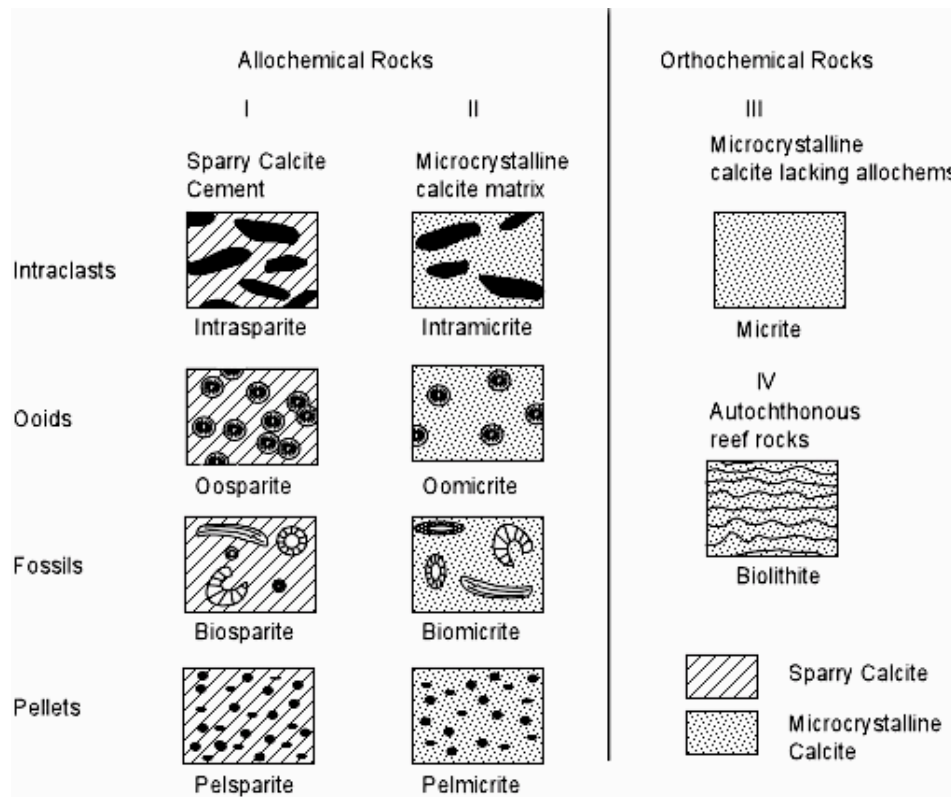


Figure 2: Folk classification of carbonates rocks. (Source: Folk, 1965)

of microcrystalline carbonate (calcite or dolomite), called micrite when cement crystals are less than 5 microns, or larger visible crystals of carbonate, called sparite. Sparite is clear granular carbonate that has formed through recrystallization of micrite, or by crystallization within previously existing void spaces during diagenesis. Orthochemical rocks are those in which the carbonate crystallized in place (Morse et al., 1990).

Dunham Classification.

The Dunham classification is based on the concept of grain support. Also this classification divides carbonate rocks into two groups, those whose original components were not bound together during deposition and those whose original components formed in place and consist of intergrowths of skeletal material. The latter groups are also called boundstones. The former group is further subdivided as to whether or not the grains are mud-supported or grain supported. If the rock

consists of less than 10% grains it is called a mudstone. If it is mud supported with greater than 10% grains it is called a wackstone. If the rock is grain supported, it is

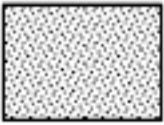
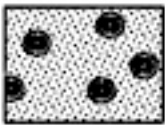

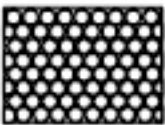
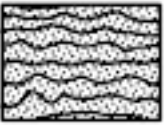
Original components not bound together during deposition				Original components bound together during deposition. Shows intergrown skeletal material, lamination contrary to gravity, or sediment-floored cavities that are roofed over by organic material and are too large to be interstices.
Contains mud (particles of clay and fine silt size)		Lacks mud		
Mud-supported		Grain-supported		
Less than 10% Grains	More than 10% Grains			
Mudstone	Wackstone	Packstone	Grainstone	
				

Figure 3: Dunham classification of carbonates rocks. (source: Dunham, 1961)

called a packstone, if the grains have shapes that allow for small amounts of mud to occur in the interstices, and a grainstone if there is no mud between the grains (Morse et al., 1990).

2.1.3 Carbonate Precipitation

Carbonate precipitation in the marine environment occurs by abiotic and biotic processes and is possible to estimate the degree of biotic influence on the precipitation process using this three stages:

- a) Abiotic precipitation is controlled by the thermodynamic saturation state and the reaction kinetics of the aqueous solution; the influence of organisms is insignificant.
- b) Biologically induced precipitation or mineralization occurs as a byproduct of an organism's metabolic activity or through its interactions with the surrounding environment. The organism is a causative agent only, without control over mineral type or habit, and therefore the minerals resulting from this precipitation differ little from their inorganic counterparts.
- c) Biologically controlled precipitation is a process where composition and form

of the mineral as well as onset and termination of precipitation are determined by organisms. The mineralization is completely regulated, allowing the organism to precipitate minerals that serve some physiological purpose. The organism uses cellular activities to direct the nucleation, growth, morphology and final location of the mineral that is deposited. All the biologically controlled mineralization processes occur in an isolated environment, that can be extracellularly, intercellularly or intracellularly.

Only three modes of carbonate precipitation are significant: the skeletal mode of precipitation (largely of the biotically controlled type), the microbial mode (predominantly biotically induced) and the abiotic mode (Tucker et al., 1990).

2.1.4 Skeletal mode of biologically controlled precipitation

The majority of carbonate material in modern oceans are composed by skeletons of organisms. The formation and the deposition of these skeletons are influenced by various environmental factors, and function of the type of metabolism employed in the formation of skeleton. Is possible to distinguish two main type of metabolism: autotrophy and heterotrophy. Autotrophic organisms use inorganic materials to synthesize organic matter useful to the organism. The heterotrophic organisms use organic material to synthesize the organic matter useful to the organism. Among the carbonate producers , autotrophic organisms are all photo-autotrophic: they perform photosynthesis to live so they strongly depend on light and temperature to survive. Note that the metabolism of extinct groups can only be deduced from circumstantial evidence (Schlager W., 1992).

2.1.5 Microbial mode of biogenic induced precipitation

Shallow water carbonates into skeletal material and abiotic precipitates is inadequate. A significant part of the non-skeletal carbonate material seems to have been precipitated under the influence of organisms and so isn't possible to classify them as abiotic. The precipitation is predominantly induced by micro-organisms, mostly bacteria. Micrite is, usually, the dominant component of these deposits. Often to refer to this rock is used the term "automicrite", it stands for autochthonous micrite as opposed to allochthonous micrite that was transported and deposited as fine-grained sediment. Microbial precipitates may form in the

photic zone or below it, up to water depths of about 400 meters. On modern reefs, the microbial deposits are best developed in the foreereef zones (Schlager W., 1992).

2.1.6 Abiotic mode of precipitation

In this category is included all the carbonate material that was precipitated from sea water during early diagenesis within the depositional setting. Depositional setting implies that the pore waters were very similar to sea water in composition. The products of abiotic precipitation are found in close association with those of the skeletal and the automicrite factory (Schlager W., 1992).

2.1.7 Carbonate Depositional Environments

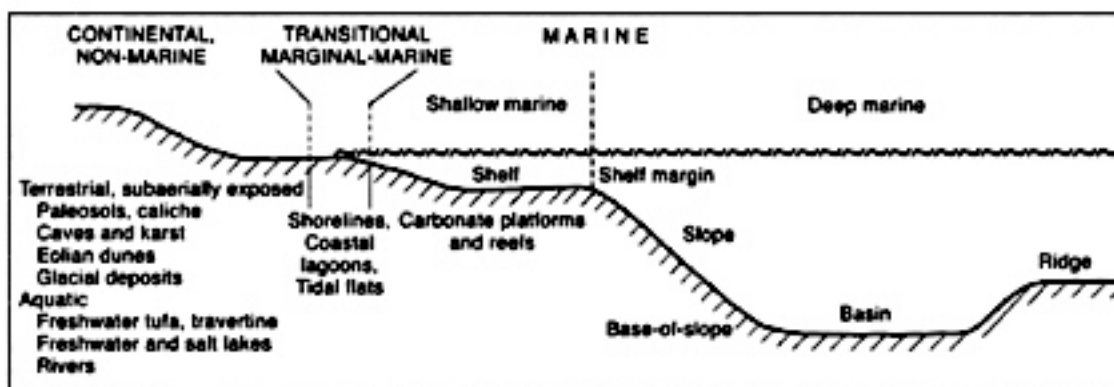


Figure 4: Carbonate depositional environments. (Schlager W., 1992)

The major part of the modern, and probably most ancient, carbonates are predominantly deposited shallow water depths (<10-20 m). This occurs because the organisms involved into the carbonate deposition cycle, as explained before, are mostly photosynthetic. This implies that they need the sun light to survive and to give origin to the reactions involved in carbonate formation. Furthermore, is important to consider also that the carbonate deposition generally occurs in environments where there is a lack of siliciclastic input into the basin. This input increases the turbidity of the water reducing the irradiance and the penetration of the light. In addition, silicate minerals are mechanically harder than the carbonate minerals and so may mechanically abrade the carbonates. High carbonate deposition also requires relatively warm waters conditions that also increase the abundance of carbonate secreting organisms and decrease the solubility of

calcium carbonate in seawater. Nevertheless, carbonate rocks form, with the right conditions, also in deep water and in colder environments (Schlager W., 2002).

2.1.7.1 Main carbonate depositional environments

Carbonate Platforms and Shelves: Are warm shallow seas, generally in continental margins that are ideal places for carbonate deposition. Carbonate shelves can also occur surrounding oceanic islands after volcanism has stopped and the island to eroded. Carbonate platforms are buildups of carbonate rocks in the deeper parts of the oceans on top of continental blocks left behind during extensional processes mostly (Schlager W., 1992).

Tidal Flats. Tidal flats are areas that flood during high tides and are exposed during low tides. Carbonate sands carried in by the tides are cemented together by carbonate secreting organisms, forming algal mats and stromatolites (Schlager W., 1992).

Deep Ocean. Carbonate deposition can also occur in the deep ocean, but only at depths above the Carbonate Compensation Depth, by the accumulation of pelagic carbonate shells of pelagic organisms and of benthic organisms. The location of the Carbonate Compensation Depth is largely dependent on latitude - deeper near the equator and shallower nearer the poles, but is usually located between 3,000 and 5,000 m water depth. The Carbonate Compensation Depth is the depth at which more than 80% of the initial sediment carbonate content, sinking from the surface, is dissolved. Whenever the seawater CO_3^{2-} concentration is higher than the correspondent carbonate mineral saturation value, the carbonate mineral is stable and will not dissolve, but once water CO_3^{2-} concentration becomes lower than the correspondent mineral saturation curve the mineral starts to dissolve. As the carbonate saturation equilibrium increases with depth due to increase in pressure (as dissolved calcium and carbonate ions occupy less volume than as combined in solid form). The main type of carbonate deposition in the deep oceans consists of the accumulation of the remains of planktonic foraminifera to form a carbonate ooze. This ooze are buried and suffer a diagenetic recrystallization to form micritic limestones. Since most oceanic ridges are at a depth shallower than the Carbonate Compensation Depth, carbonate oozes can

accumulate on the flanks of the ridges and can be buried as the oceanic crust moves away from the ridge, but also most oceanic crust and overlying sediment are eventually subducted so the preservation of such deep sea carbonates in the geologic record is rare (Schlager W., 2002).

Non-marine Lakes. Carbonate deposition can occur in non-marine lakes as a result of evaporation, in this case the carbonates are associated to other evaporites deposits. In this kind of environment there is a big consumption of CO₂ by organisms, so the water become oversaturated with respect to calcite (Schlager W., 2002).

Hot Springs. When hot water saturated with calcium carbonate reaches the surface of the Earth at hot springs, the water evaporates and cools resulting in the precipitation of calcite to form a type of limestone called travertine.
(Schlager W., 2002)

2.2 Authigenic Carbonates

The term “authigenic” indicates the in situ formation of a mineral. It comes from greek and literally the meaning is “born in the same place”. The minerals that form those rocks are characterized by the formation in place from the interstitial pores. Authigenic carbonates are, in general, formed by evaporitic deposition or by chemical precipitation of marine and non-marine water in loco.

Oceanic authigenic carbonates are classified according to the origin of carbonate carbon source, evaluated through several methods of sedimentary petrography, mineralogy, isotope geochemistry, and microbiology.

Mg-calcite, proto-dolomite and aragonite predominate among the authigenic carbonates. Their formation is a biogeochemical (microbial) process that involves carbon from ancient sedimentary rocks, abiogenic methane and bicarbonate-ion of hydrothermal fluids into the modern carbon cycle. This process is a very important and powerful in the balance of the carbon cycle, in fact it removes annually about 1 Gt of CaCO₃ from seawater (Lisitsyn, 1978). This process is also very important and focus of intense study due to importance in the equilibrium of the CO₂ balance

Table 1: Main regions of authigenic carbonate investigation. (Lein, 2004)

Region	Coordinates	Depth, m	Specific benthic community, mats	CH ₄ -gas hydrates	CH ₄ seeps, CH ₄ transport	δ ¹³ C-CH ₄ , ‰	Source
Gulf of California: Shelf	24°53.7' N 108°42' W	120			-		Lein <i>et al.</i> , 1978, 1979, 1999
Continental slope	27°09' N 111°08' W	up to 3260			-		
Black Sea: shelf	44°46'-44°52' N 31°50'-31°59' W	60-180	Mats	None	Diagenetic CH ₄	-66	Lein, 1991; Lein <i>et al.</i> , 2001, 2002b
Continental slope	44°46'-44°41' N 31°47'-31°59' W	200-500	Mats		Bubble stream		U'yanova <i>et al.</i> , 1995; Thiel <i>et al.</i> , 2001
Norwegian Sea: Continental slope	72° N	1200	Mats, symbiotrophic polychaets	Air and below bottom surface	Thermogenic + diagenetic diffusion	-60	Lein <i>et al.</i> , 1998, 1999, 2000a, b; Pimenov <i>et al.</i> , 1999
Sea of Okhotsk: Continental slope	49° N	800	Symbiotropha and mats	~1-cm-thick layer	Thermogenic, bubble-stream	-54 average	Lein <i>et al.</i> , 1989
Gulf of Cadiz: continental slope	35°30' N 7°10' W	960	Mats, benthic animals	Within sediments	Thermogenic + diagenetic + hydrothermal, not determined	-32...-63 From -32 to -63, up to -19.2 in homologues	Stadnitskaia <i>et al.</i> , 2001; Lein <i>et al.</i> , 2003
Logachev, MAR	14° N	3400	Mats, symbiotrophic mollusks	None	Hydrothermal, diffusion	-14.6	Lein <i>et al.</i> , 2000a, c, 2001, 2003
Lost City, MAR	30° N	860	Mats and symbiotrophic animals (?)	None	Hydrothermal, diffusion	-16	Lein <i>et al.</i> , 2002b

Note: (-) Not known, no data.

between lithosphere, ocean and atmosphere. It is also important in the Ca balance regulation.

The time necessary for the formation of authigenic carbonates and the mechanisms of their formation were unknown for a long time. The first important study on authigenic carbonates were made by Stakhov (1951) that studied the formation mechanisms of diagenetic carbonates in Black Sea sediments. He believed that “CO₂ generated during diagenetic decay of buried organic matter would play an important role in the migration and redistribution of carbonates fraction in sediments. Stakhov (1951) showed that the content of CO₂ generated during diagenesis, the amount of carbonate dissolved in pore solution, and the redistribution and concentration of carbonates in the form of local segregations have a direct correlation with the organic matter content (Strakhov, 1962, p. 545). However, Strakhov denied the role of bacteria in calcium precipitation. He believed that “bacterial calcite formation” is insignificant, whereas chemical precipitation of CaCO₃ and its transport in suspended form are a dominant process” (Strakhov,

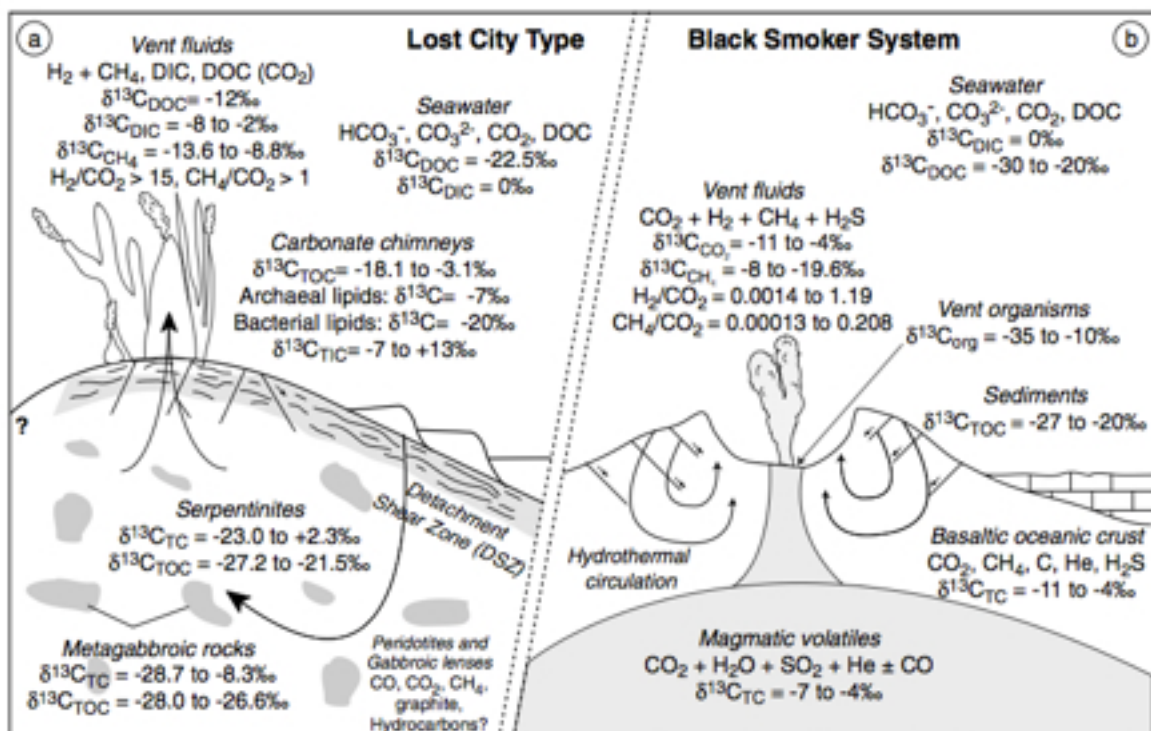


Figure 5: Schematic representation of the carbon species and carbon isotope compositions of different reservoirs involved in hydrothermal systems at mid-ocean ridge environments. (a) Lost City-type hydrothermal system (b) Black smoker type system. Abbreviations: DOC, dissolved organic carbon; DIC, dissolved inorganic carbon; TOC, total organic carbon; TIC, total inorganic carbon; TC, total carbon (Delacour et al., 2008)

1962, p. 102).

After the 1960s the interest about authigenic carbonate formation processes increase with the discover of the methane-derived authigenic carbonates (MDAC) that are related to methane oxidation in the oceanic sediments (Niemann et.al, 1984). In 1984 methane seeps were discovered. These seepage sites correspond to the discharge of methane-bearing solutions and gas jets from bottom sediments. These structures produced a new attention on the authigenic carbonates (Suess et al., 1985). This type of authigenic carbonates is marked by the presence and development of unique biological communities (Sibuet and Olu, 1998) and by the large variability of their morphologies, including carbonate buildups (“chimneys” or “reefs”), plates, crusts, and so on (Lein, 2004).

Since the 1970's and 80's, a large number of active hydrothermal fields have been discovered, especially in the mid-ocean ridges. Those are characterized by the discharge of endogenic gases, like CH₄ and CO₂, and by the formation of authigenic carbonates minerals, that depending from the cases can be formed stockworks or as chimneys and buildups at hydrothermal vents associated with off-axis and serpentinization vents (Lein, 2004). An example of this last possibility is the Lost City field, discovered in 2001. This is a hydrothermal field characterized by low-temperature fluids venting at the seafloor, that is also characterized by about 30 columnar carbonate buildups, up to 10 m across and 60 m high. It was located at the intersection of the Mid-Atlantic Ridge with a transform fault in the North Atlantic 30° N area (Kelley et al., 2001; Lein et al., 2002a). This vent system is located in an off-axis setting where serpentinization of lower oceanic crust and upper mantle peridotite produces large amount of methane and hydrogen released into the surrounding water; they do not produce significant amounts of carbon dioxide, hydrogen sulfide or metals, which are the major outputs of volcanic black smoker vents, in figure 5 is possible to see at the differences between a typical black smoker vent and the Lost City vent. All the methane and hydrogen rich fluid escape as volatiles sustain dense microbial communities, which include methanogenic and/or methanotrophic Archaea, methane-oxidizing bacteria, and sulfur-oxidizing and sulfate-reducing bacteria (Delacour et al., 2008).

Since 1975, occurrences and processes of authigenic carbonate formation in

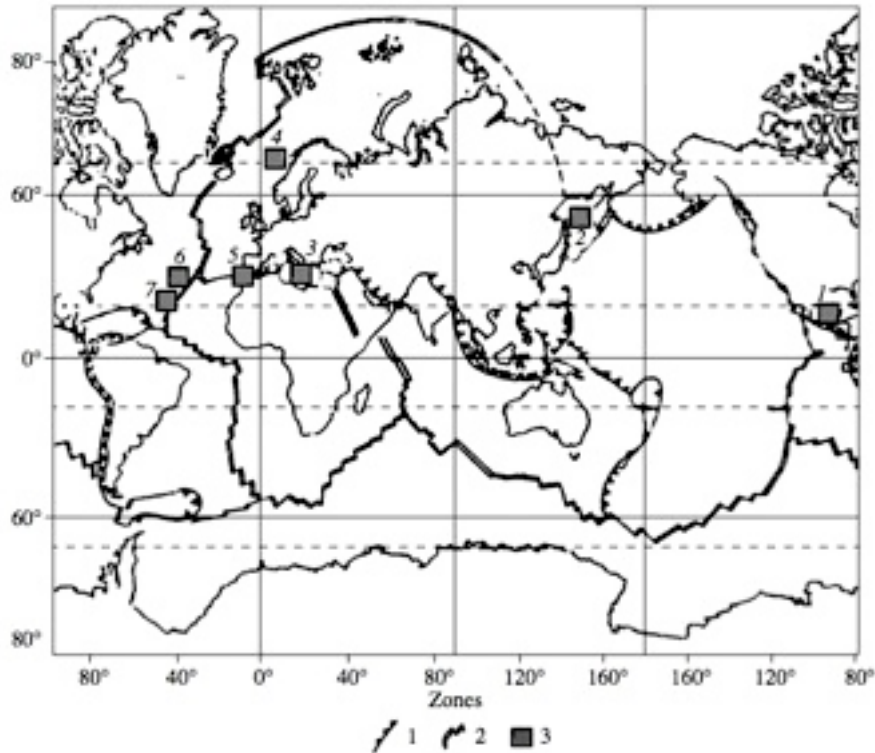


Figure 6: Location of the studied regions with authigenic carbonates in the ocean. (1) Subduction zones; (2) spreading zones; (3) study regions; (1) Gulf of California; (2) Sea of Okhotsk, Paramushir Isl. area; (3) Black Sea, Dnepr canyon; (4) Norwegian Sea, Haakon Mosby mud volcano (HMMV); (5) mud volcanoes of the Gulf of Cadiz; (6, 7) active hydrothermal fields of the Mid-Atlantic Ridge (MAR): (6) Lost City (30° N); (7) Logachev (14° N). (Lein, 2004)

sediments of the modern ocean had been investigated (see figure 6 and table 1). As shown in table 1, the authigenic carbonates are formed at different water depths, from shallow settings with just a few meters up to the deep ocean with water depths of more than 4500 m, and in different environments, from tropical zones to the polar-ones (Lein, 2004).

Their formation is a major process of interaction of organic and inorganic carbon cycles with the calcium cycle. The inorganic and the organic carbon cycles are connected by CO₂ assimilation (photosynthesis and chemosynthesis) and CO₂ extraction. It means that the Ca cycle governs via carbonates formation acidic-alkaline and redox conditions of the biosphere, particularly in the ocean.

Each type of carbonate described by Lein (2004) has particular formation conditions and characteristics.

- Lein (2004) Type I: decay of microbial organic matter in sediments

The formation conditions of the type I authigenic carbonates (Lein, 2004) include high content of labile C_{org} and enhanced heterotrophic microbial activity in the sediments. In this type, the organic matter decays in the sediments resulting in the precipitation of carbonates, that are depleted in heavy carbon isotope ^{13}C (up to 10-15per mil), relative to the normal marine carbonates produced by the input of seawater CO_2 that inherited the isotopic composition of the primary C_{org} . The $\delta^{18}O$ value in the carbonates depends mainly on the oxygen isotopic composition of the bicarbonate ion in the pore water or seawater and less on the water temperature. Mg-calcite predominates in carbonates of this type.

• *Lein (2004) Type II: Methane Derived Authigenic Carbonate (MDAC)*

Type II is formed as result of the migration of methane, of various origins, which his oxidation under anaerobic conditions induces the formation of carbonates. This type II corresponds to the so-called methane-derived authigenic carbonates (MDAC) (Lein, 2004). All the samples studied in this thesis belong of this type.

Methane seeps are related to specific tectonic and geomorphological processes of larger scale in the marine setting. Lein (2004) divide the formation processes of methane seeps authigenic carbonate on the following types and subtypes according to the source of the seepage methane: (IIa) diagenetic methane seeps; (IIb) thermogenic methane seeps; (IIc) the same as IIb, but with an assumed contribution of hydrothermal methane to the fluid (in the Gulf of Cadiz some studies suggest this case (Hensen et al., 2007; Scholz, F. et al., 2009) .

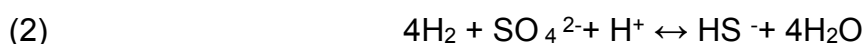
The methane seeps studied until now show that methane may be oxidized in both aerobic and anaerobic conditions, but the microbial activity is obligatory for methane oxidation in both situations. The group of the so-called methanotrophs microbes participate in the aerobic oxidation.

The mechanism of anaerobic methane oxidation and the role of different physiological groups of anaerobic microorganisms in this process are actively discussed since the first publications by Zehnder and Brock (1979, 1980). Based on laboratory experiments with pure methanogene cultures these authors demonstrated that if substrates (CO_2 , H_2) are exhausted and the methane content

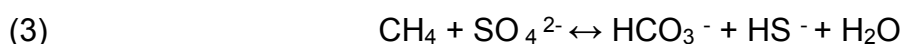
is high, methanogenes start to perform anaerobic methane oxidation, according to the reaction:



Since this process proceeds very slowly in pure cultures because of the hydrogen accumulation it is assumed (Reeburgh and Alperin, 1988; Valentine and Reeburgh, 2000) that the reaction (1) occurs in simultaneous with the sulfate-reduction reaction (2):



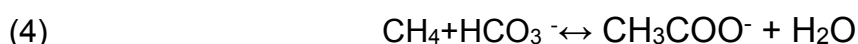
In natural anaerobic ecosystems this implies the involvement of sulfate-reducing bacteria (Reeburgh and Alperin, 1988; Valentine and Reeburgh, 2000). The formal summation of Equations (1) and (2) results in the net mechanism of sulfate-dependent methane oxidation (SDMO):



The hypothesis of direct methane oxidation by sulfate-reducing bacteria has been already proposed before (Barnes et al., 1976; Reebourgh, 1976; Reebourgh and Heggie, 1977). Microscopic study of bacterial mat samples from the surface of carbonate buildups and inoculation on elective nutrient media revealed abundant and diverse microflora, including sulfate reducers, aerobic methanotrophs, and large filamentous microorganisms morphologically similar to methanogenes (Pimenov et al., 1997). Results of molecular-biological studies, which revealed typical archaeal bacterial biomarkers, also indicate the presence of methanogenes in these bacterial mats (Pimenov et al., 1997; Turova et al., 2002).

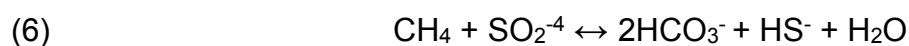
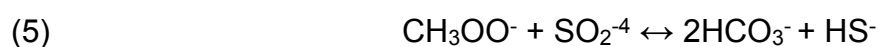
Lein (2004) used oxygen isotopes of authigenic carbonates to describe the nature of ultimate electron acceptor involved in the anaerobic methane oxidation. The $\delta^{18}\text{O}$ values of carbonates substantially differ from the $\delta^{18}\text{O}$ values of seawater and the sulfate dissolved therein, thus eliminating their participation as oxygen donors in the anaerobic methane oxidation according to Equations (1) and (3).

According to Valentine and Reeburgh (2000), such reactions proceed through methane oxidation to acetate and water, equation 4.



resulting in the acetoclastic methanogens activity, with the subsequent

participation of sulfate-reducing bacteria and anaerobic oxidation of acetate, resulting in the net Equation 5:



Equation 6, is the sum of reactions 4 and 5, mediated by methanogenes and sulfate reducers, as similar to the SDMO reaction 3. However, the oxygen source (HCO_3^-) and the intermediate oxidation product (CH_3COO^-) are substantially different. Lein asserts that the contribution of marine bicarbonate with a rather heavy carbon isotopic composition ($\delta^{13}\text{C} = -2.1\text{‰ VPDB}$) may explain the above considerable difference in $\delta^{13}\text{C}$ values between carbonates and organic carbon of authigenic carbonate buildups. The carbon isotopic composition of carbonate buildups is a mixture of isotopically light carbon formed during the methane oxidation and isotopically heavy bicarbonate carbon of seawater. Thus, anaerobic oxidation is mediated by a microbial consortium mainly including methanogene archae and sulfate reducers. According to the modern classification, a part of the sulfate reducers belongs to archae rather than to the bacteria Phylogenetic Domain (Michaelis et al., 2002; Pimenov et al., 1998).

- Lein (2004) Type III: Microbial oxidation of hydrothermal methane

Lein (2004) authigenic carbonate type III is characterized by the discharging onto the bottom surface as any other methane undergoes the microbial oxidation to form carbonate crusts. Carbon isotope of authigenic carbonates inherited from the hydrothermal methane is a geochemical evidence of the carbonate origin.

- Lein (2004) Type IV: Mixing of hydrothermal fluid with seawater

Lein (2004) authigenic carbonates of type IV are characterized by having seawater bicarbonate as the carbon and oxygen source for these carbonates, whereas calcium and partially strontium are derived from

hydrothermal sources. Carbonates of this recently discovered type are also related to microbial activity. A complicated microbial consortium impregnates the carbonate buildups and maintains the reduced ($E_h = -120$ mV) alkaline ($pH = 9.0-9.9$) environment in the hydrothermal fluid, which promotes the precipitation of carbonates. Microorganisms (more precisely, prokaryotes) with a specific calcite-forming function have not been found in nature up to date. However, it is these microbial communities that increase the pH value of seawater and create favorable conditions for calcium carbonate precipitation.

Carbon in authigenic carbonates of types I and II is depleted in the heavier isotope ^{13}C ($\delta^{13}C$ values vary from -15 to -50% (VPDB)). Unlike the carbonates found associated with mud (volcanoes) that have positive $\delta^{18}O$ values varying from 1.0 to 5.4% (VPDB), the authigenic carbonates of types I and II are characterized by negative $\delta^{18}O$ values ranging from -5.1 to -9.8% (VPDB). Microbial communities occur in all types of authigenic carbonates considered by Lein (2004). Various carbon sources can be considered: Organic matter, methane, bicarbonate ion of seawater and/or pore water, and even inorganic carbon compounds of hydrothermal solutions. The authigenic carbonate formation is a combination of biogeochemical (microbial) processes that ensure the interaction of calcium, organic carbon, and inorganic carbon cycles. In conclusion, as proposed by Lein (2004), the authigenic carbonates carbon sources can be divided in four major types: (I) organic carbon of bottom sediments; (II) methane carbon, including (IIa) diagenetic, (IIb) thermogenic, and (IIc) thermogenic + hydrothermal subtypes; (III) hydrothermal methane carbon; and (IV) carbon of ΣHCO_3^- in seawater and hydrothermal fluids. Authigenic carbonates of types I and II are the most widespread in the marine settings. All types of authigenic carbonates are formed with an obligatory participation of microorganisms, among which many groups of sulfate reducers and methanotrophs (archaea and bacteria) are most important. According to the first well-known model, microbial decay of organic matter in sediments to HCO_3^- results in an alkalinity increase due to H_2S formation during sulfate reduction in the pore water. The participation of microbial processes in the

carbonate formation under strongly anoxic conditions is controlled by the activity of different microbial groups, which produce intermediate products of methane oxidation. Bicarbonate of seawater and/or pore water participates in the process as a main oxygen source for carbonates. The third model is valid in the case of discharge of low-temperature hydrothermal fluids with a high concentration of H₂, which is a good substrate for the specific group of sulfate reducers stimulating the increase in alkalinity of solutions and lead to the formation of carbonate buildups at seepage sites. The whole variety of microorganism-mediated processes of the authigenic carbonate formation in ocean is not exhausted by these three models (Lein, 2004).

As results of the processes described before, Mg-calcite (+ protodolomite), calcite, and aragonite dominate among the authigenic carbonates. Holocene buildups (younger than 10 ka) at methane seepage sites on the seafloor mainly consist of mono-mineral aragonite (Lein, 2004). Sediments are commonly cemented by authigenic Mg-calcite, also the carbonate nodules are mainly composed of Mg-calcite. Carbonate buildups and nodules contain Sr and Ba. All authigenic carbonates are depleted in the heavy carbon isotope ¹³C and in general enriched in the heavy oxygen isotope ¹⁸O.

The growth rate of carbonate buildups ranges from 0.65 mm/yr to several millimeters per day under anaerobic conditions and from 0.02 to 0.37 mm/yr at the boundary between aerobic and anaerobic environments (Lein, 2004).

2.3 Fluid escape structures

2.3.1 Cold Seepages

In this thesis all the studied carbonate samples are from or associated with the cold seepage processes and are methane derived as discussed and shown in the following chapters. Submarine hydrocarbon seeps are geologically driven “hotspots” of increased biological activity on the seabed. A lot of sites of natural hydrocarbon seepage in the European margins were investigated in detail during the last years, including mud volcanoes and pockmarks, particularly important are

the Gulf of Cádiz and the Mediterranean sea. Individual seeps show ecosystem zonation related to the strength of the methane flux and distinct biogeochemical processes in surface sediments. A common feature to the seeps is the formation of authigenic carbonates. These, exhibit various morphologies ranging from large pavements and fragmented slabs to chimneys and mushroom-shaped mounds. These carbonates form hard substrates are colonized by benthic fauna. Gas hydrate dissociation could contribute to sustain seep chemosynthetic communities over several thousand years following large gas-release events.

Since the first discovery of a hydrocarbon-associated cold seep community off Louisiana (Kennicut et al., 1985), hydrocarbon seepage and its close association with “hotspots” of increased biological activity have been documented at a number of seafloor sites worldwide (Judd and Hovland, 2007). Geological structures associated with the expulsion of hydrocarbon-rich fluids, such as mud volcanoes and pockmarks, have been recognized all around the planet, the most famous examples are the ones on the margins of the Atlantic Ocean, the Mediterranean Sea, and the Black Sea, and new seepage sites continue to be discovered (Foucher, 2009).

The phenomenon of gas seeps is very important, is frequently associated with the growth of distinct chemosynthetic communities (Sibuet et al., 1998) and with the occurrence of authigenic carbonate mineralization as a consequence of the microbially mediated oxidation of methane (Boetius et al. 2000; Lein, 2004). Several of these features can occur on the seafloor above petroleum reservoirs. Examples of gas, and occasionally oil, leaking from reservoirs include seeps from the Gulf of Mexico (Sassen et al. 1993), the south-eastern Mediterranean (Coleman et al., 2001), the North Sea (Judd et al. 1994) and in a lot of other areas in the planet. Even at depth, fluid escape from hydrocarbon fields is one of the most frequent phenomena revealed by sub-surface investigation tools in hydrocarbon exploration and production (Mazzini et al., 2006).

Several different types of cold seeps can be distinguished, according to the depth, as shallow cold seeps and deep cold seeps. According to Judd et al., 2007, the different types of fluid escape structures that can be defined are as follows:

- **oil seeps**: are sites where liquid or gaseous hydrocarbons escape to the surface

or to the seafloor, through fractures and fissures or through pore permeable sediments or sedimentary discontinuities.

- **gas seeps** (usually methane seeps): are, like the oil seeps, sites in which gas, principally methane, escape to the surface through faults, fractures or other high permeability geological structure.
- **gas hydrate seeps**: A particular case of gas seeps occur when the pressure and temperature conditions promote the formation of gas hydrates and on these situations methane occurs also in the form of gas hydrates. Gas hydrates are ice-like minerals that form at low temperatures (usually at about 2-4 C) and high pressures in the deep sea. Hydrates contain gases, such as hydrocarbons, that glue themselves inside symmetrical cages of water molecules to form hydrate crystals. Research submarines are the ideal tool to study hydrates under natural conditions. Gas hydrate is a water clathrate of natural gas. Thus, gas hydrate is a naturally occurring solid comprised of water molecules forming a rigid lattice of cages, where most cages contain molecules of natural gas, mainly methane. Natural gas hydrates are therefore a subgroup of the clathrates. The term hydrate is applied to clathrates in which the structural molecules are water (H₂O) and the guest spaces are occupied by gas molecules (Judd et al., 2007).

The term natural is used to indicate gas hydrates that occur naturally on Earth, rather than being synthesized in laboratory or inadvertently created during industrial transportation of petroleum gas. The term natural also indicates that the gas that is incorporated on the hydrate is of natural origin, corresponds to natural gas, which corresponds to all gases derived from natural occurring chemical and biochemical processes. Natural gas hydrates occur wherever conditions are suitable. As water is ubiquitous on Earth and, after water, the second more ubiquitous compound in sediments is methane, the most widespread natural gas hydrate on Earth are methane hydrates. Methane occurs in nature often accompanied by higher molecular weight hydrocarbon gases and by non-hydrocarbon gases. So, natural gas hydrates can also occur with other relatively light molecular weight hydrocarbons such as C₂H₆, C₃H₈, C₄H₁₀, and non-hydrocarbons such as CO₂, N₂ and H₂S.

- **brine seeps** (usually form brine pools): Brine pools are sites of brine fluids

discharge into the seafloor. These pools are bodies of water that have salinity three to five times greater than the surrounding seawater. The brine often contains high concentrations of methane, providing energy to chemosynthetic animals that live near the pool. Deep sea brine pools often coincide with cold seeps. Methane released by the seep is processed by bacteria, which have a symbiotic relationship with seep mussels living at the edge of the pool (Judd et al., 2007).

- **pockmarks**: Pockmarks are crater-like structures in the seabed, formed by the expulsion of gas and/or water from sediments. These features occur world-wide, in the ocean at all depths (Judd et al., 2007).
- **mud volcanos**: Mud volcanoes are sedimentary structures formed by the emission of argillaceous material, water, brine, gas and oil (Milkov 2000). Such fluid venting structures occur in terrestrial and marine environments worldwide and are caused by tectonic stress (Milkov 2000, Pinheiro et al., 2003). These processes can lead to over-pressured pore fluids that promote the upward migration of over pressurized sediments and, finally, their extrusion at the surface or seabottom with the emissions of mud, water and gas that accumulate forming conical, volcanic edifices (Judd et al., 2007).

Various examples of authigenic carbonates from modern marine cold seeps have been described from continental margins worldwide (e.g., Campbell et al., 2002). They may or may not be associated with gas hydrates. The samples used in this thesis are found in close association with mud volcanoes and active and fossil cold seeps associated with faults (Luff et al., 2004; Judd et al., 2007).

Microbiological and geochemical studies proved that in marine cold seep environments, methane and other hydrocarbon compounds contained in the ascending fluids are anaerobically oxidized to CO₂ by a microbial consortium of sulfate-reducing bacteria and methanotrophic archaea (Boetius et al., 2000). Anaerobic oxidation of methane is the main microbial process driving the precipitation of authigenic carbonates within subsurface anoxic sediments. This process explains why the seafloor is often hardened by carbonate constructions at the sites of active methane seepage. The lateral and vertical extent of these

authigenic carbonate constructions is controlled by the balance between the intensity of the venting fluid flux and the ability of the microbial-archaea consortiums to oxidize methane and reduce the sulfate. However, the efficiency of this microbial-archaea consortiums can be counteracted by high methane flux, so that methane can escape into the water column and may eventually reach the atmosphere. Numerical modeling of carbonate crust formation has shown that bioturbation and sedimentation rates are also important factors in controlling the flow of water and methane, and thus carbonate precipitation at cold seep sites (Luff et al., 2004).

The authigenic carbonates observed at the seafloor exhibit various morphologies: (i) massive to porous crusts, centimeters to meters thick, that form large pavements or fragmented slabs; (ii) circular chimneys, and (iii) irregular concretions corresponding to cemented bioturbation casts. These hard substrates are often colonized by fixed organisms such as tubeworms and molluscs (bivalves and gastropods), as well as by abundant fauna (crustaceans, fishes) (Cunha, C. 2009 – PhD Thesis).

Authigenic carbonates can therefore provide a record of the history and evolution of cold seeps activity. Their mineralogy, geochemical and isotopic signatures depend on the composition of the fluids and thus provide information on the origin of these fluids and their evolution through time. It is noteworthy that carbonate mineral associations are generally dominated by aragonite and Mg-calcite, although dolomite and ankerite may become the dominant carbonate phase (Aloisi et al., 2000; Gontharet et al., 2007) as in some types of authigenic carbonates such as in the dolomite chimneys of the Gulf of Cádiz (Diaz-del-Rio et al., 2003; Magalhães et al., 2012). All cold-seep carbonates are characterized by very negative $\delta^{13}\text{C}$ values, as low as -54.7 (VPDB), clearly indicating that they are methane-derived products (Kulm et al., 1986; Hovland et al., 1988). Lipid biomarkers entrapped in the carbonate cements provide complementary information on the composition of the microbial communities that were involved during the formation processes, showing evidences of the presence of anaerobic oxidation of methane, sulfate reduction, and methanogenesis (Bouloubassi et al., 2006; Niemann et al., 2006).

2.3.2 Mud Volcanoes

Mud volcanoes are a manifestation of natural fluid migration and extrusion at the Earth's surface. They are geologic structures formed as result of the emission of mud, water and gas, usually CH₄, saturated to the surface or at the seafloor (Dimitrov, 2002). Often, included in the mud are rock clasts, ranging in size from a few millimeters to 10 m or more. These clasts may be of various lithological types and are derived from the walls of the conduits through which the over-pressurized fluid mixture has passed on its way to the surface. Mud volcanoes are morphologically diverse, ranging from semi-symmetrical mound shapes rising several hundred meters above the adjacent countryside to regular and irregular conical shapes. Mud volcanoes vary in size from small landforms of less than a meter in diameter to large structures occupying more than 100 km². Eruptions at mud volcanoes may be gentle or violent. In gentle eruptions, the mud volcanoes expand by gradual and progressive outflows of liquid mud. In violent eruptions,

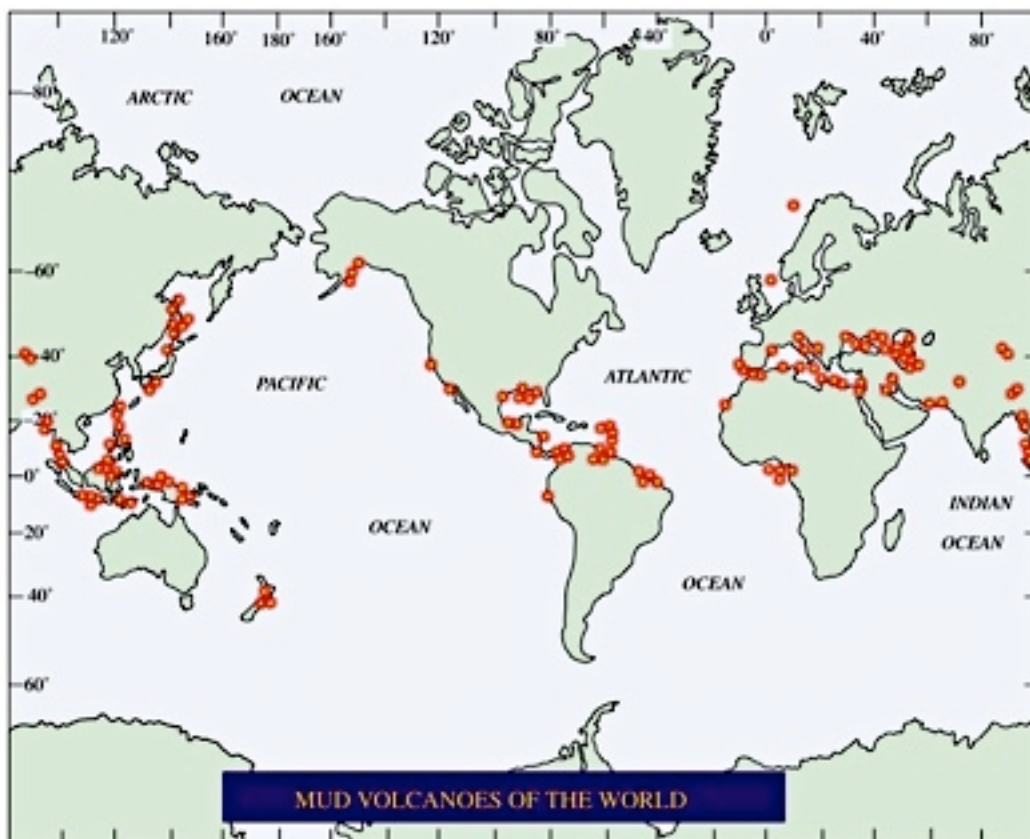


Figure 7: Map showing the global distribution of onshore and offshore oil seeps many of which also emit natural gas. Numbers indicate the count of seeps in a given region. Redrawn and modified from Wilson et al. (1973, 1974) (Kvenvolden et al, 2005).

mud and mud breccia may shoot up in the air to heights of a few kilometers. The emitted gas may ignite to produce spectacular flames. Mud volcanoes are globally distributed and occur in both the terrestrial and marine environments (figure 4). The number of prominent individual mud volcanoes totals 1950 (Dimitrov, 2003), although the count is continuously increasing as the knowledge, especially on the continental margins, increases. Mud volcanoes are irregularly clustered in belts that generally coincide with areas of active plate boundaries and zones of young orogenic activity (Dimitrov, 2002). More than half of the total number of mud volcanoes is located along the Alpine–Himalayan Active Belt where there are about 650 terrestrial and at least 470 offshore prominent examples. The largest and most active mud volcanoes can be found along this Belt (figure 7).

Interest in mud volcanoes has recently increased because, in part, their methane (a strong green house gas) emissions may have implications for global climate change. Dimitrov (2002) provides a comprehensive review of mud volcano occurrence, plumbing systems, and possible geologic consequences. In addition, there are recent reports of mud volcanoes in the Gulf of Mexico (MacDonald et al., 2000), offshore Nigeria (Graue, 2000), South Caspian Sea (Voitov, 2001), Southwest African continental margin (Ben-Avraham et al., 2002), northern Apennines of Italy (Capozzi and Picotti, 2002), Sicily (Etiope et al., 2002), western Mediterranean Sea (Sautkin et al., 2003), Gulf of Cadiz (Pinheiro et al., 2003, Somoza et al., 2003; (Van Rensbergen et al., 2005; Van Rensbergen et al., 2005), eastern Romania (Etiope et al., 2004), and East China Sea (Yin et al., 2003).

2.3.3 Pockmarks

Pockmarks are concave, crater-like features on the seafloor, generally up to several hundreds of meters in diameter and tens of meters in relief (Kelley et al. 1994). Mega pockmarks were also described and can have diameters of more than 1.5 km and depths exceeding 150 m (Pilcher et al, 2007). The formation of pockmarks is mostly caused by the seepage at the seafloor of thermogenic and biogenic origin gases, mainly methane (Rogers et al. 2006) and by the release of pore water . Pockmarks occur in lakes (Pickrill et al, 1993), shallow bays, estuaries and fjords (e.g. Hovland et al., 1988; Kelley et al. 1994; Plassen et al., 2003, Rogers et al. 2006; Forwick et al., 2009), on continental shelves, slopes and rises,

as well as in the deep sea (Piper et al. 1999; Paull et al. 2002; Loncke et al. 2004; Gay et al. 2007; Forwick et al., 2009).

The lateral distribution of pockmarks can be controlled by tectonic lineaments (e.g. Chand et al. 2008), underlying permeable bedrock and lithological boundaries (Paull et al. 2002; Forwick et al., 2009), as well as buried channels (Gay et al. 2003; Pilcher et al., 2007; Forwick et al., 2009). However, they also occur near slope failures (Hovland et al. 2002; Forwick et al., 2009) and in areas of rapid deposition (Pilcher et al., 2007; Forwick et al., 2009). Pockmarks are furthermore described from areas that have been affected by the up-drift of ice that detached from the sub-seafloor (Paull et al. 1999), decomposing gas hydrates and where gas is released due to melting permafrost (Long 1992). They can also be induced

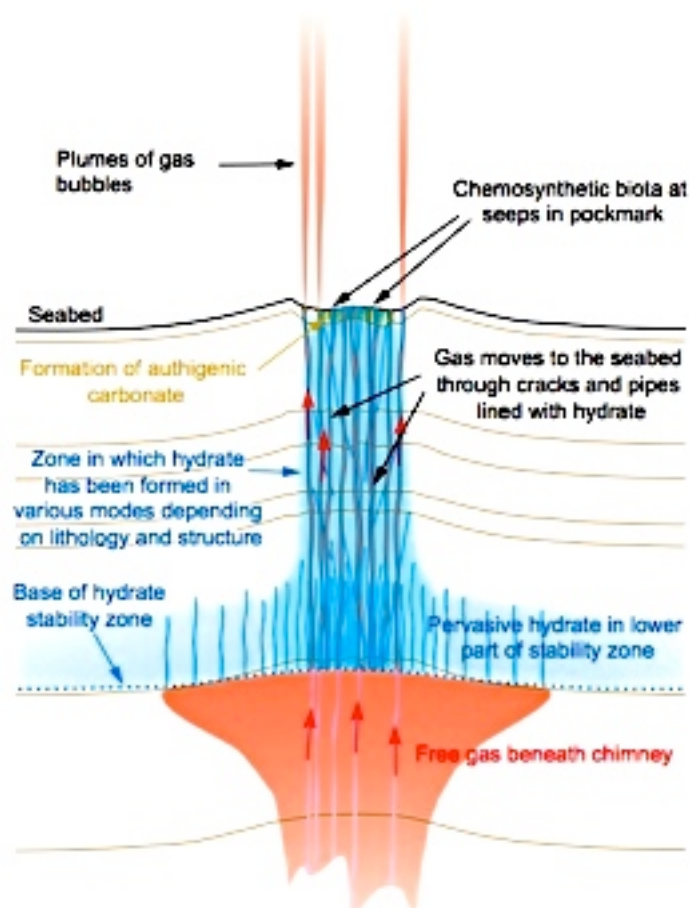


Figure 8: Illustration of a pockmark and underlying chimney during a phase of active expulsion of free gas. The passage of free gas through the hydrate stability zone is aided by the formation of hydrate around the pathways through which the gas is passing, inhibiting access of the gas to the pore water and preventing conversion of all the gas to hydrate. Progressive formation of hydrate and carbonate near the seabed seals pathways, causing an outward migration of the active gas vents. (Foucher et al, 2009)

by grounded moving icebergs or anthropogenic activities such as trawling and ship anchoring (Harrington 1985; Fader 1991; Forwick et al., 2009).

According to Judd et al., 2007, pockmarks are classified based on their morphology in:

- circular,
- elliptical,
- asymmetric,
- composite .

Pickrill (1993) classified the pockmarks as function on their state of development as:

- new,
- growing,
- decaying

Another classification proposed by Pilcher et al., (2007) based on their lateral distribution and formation mechanisms defines:

- fault- strike pockmarks,
- iceberg scour pockmarks,
- current-modified pockmarks.

The formation of pockmarks can occur catastrophically in a very short period of time (e.g. due to earthquakes, tsunamis, storms, melting of ground ice) or can be formed more continuously over longer periods (Kelley et al. 1994; Hovland et al. 2002; Forwick et al., 2009).

2.4 Chemiosynthetic Fauna

Chemosynthesis is the biological conversion of one or more carbon molecules (usually carbon dioxide or methane) and nutrients into organic matter using the oxidation of inorganic molecules (such as hydrogen gas, hydrogen sulfide) or methane as a source of energy, rather than sunlight, as in photosynthesis (Foucher et al, 2009). Chemoautotrophs, organisms that obtain carbon through chemosynthesis, are phylogenetically diverse, but groups that include conspicuous or biogeochemically important taxa include the sulfur-oxidizing gamma and epsilon proteobacteria, the Aquificaeles, the Methanogenic archaea and the neutrophilic iron-oxidizing bacteria (Foucher et al., 2009).

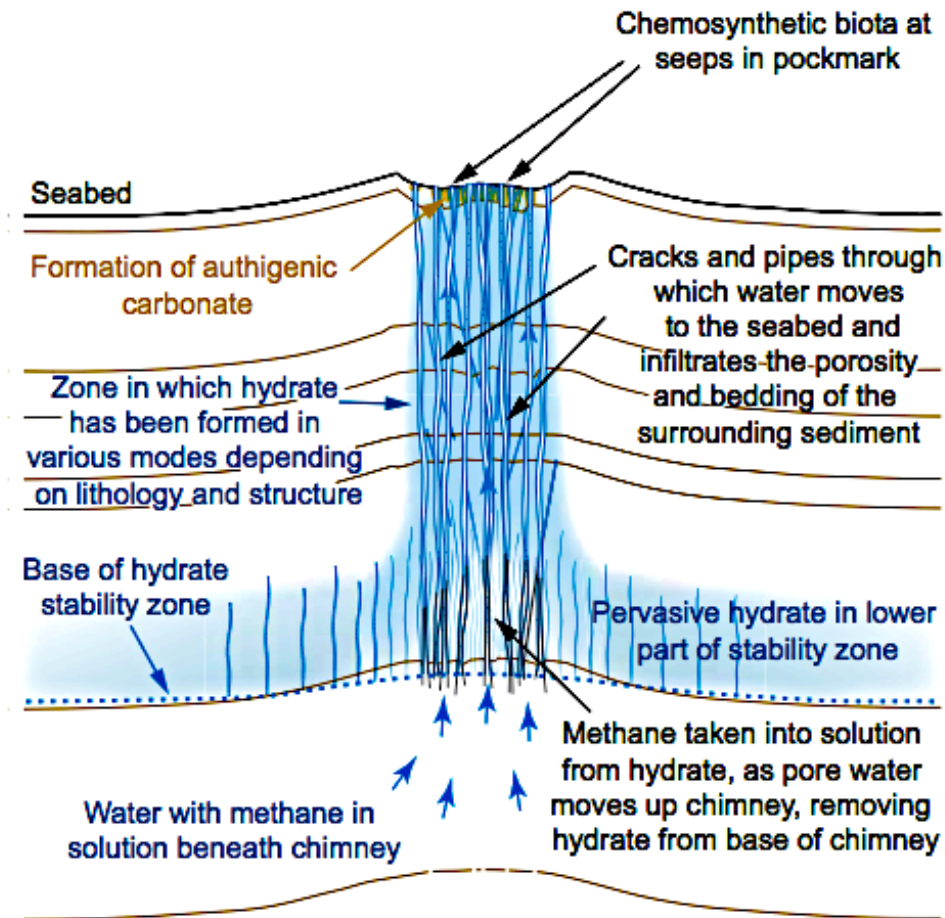


Figure 9: Illustration of a pockmark and underlying chimney when only pore water is migrating through the system. Methane from hydrate created during the free-gas expulsion phase keeps the methane in solution in the migrating pore water at saturation concentration, supporting chemosynthetic biota in the pockmark, until all the hydrate is removed in solution. This process may continue for thousands of years, with only moderate amounts of hydrate and concentration of methane in solution in the pore water entering the chimney from below. (Foucher et. al, 2009)

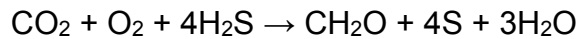
Many microorganisms in dark regions of the oceans also use chemosynthesis to produce biomass from single carbon molecules. Two categories can be distinguished. In the rare sites at which hydrogen molecules (H_2) are available, the energy available from the reaction between CO_2 and H_2 (leading to production of methane, CH_4) can be large enough to drive the production of biomass. Alternatively, in most oceanic environments, energy for chemosynthesis derives from reactions in which substances such as hydrogen sulfide or ammonia are oxidized. This may occur with or without the presence of oxygen.

Many chemosynthetic microorganisms are consumed by other organisms in the ocean, and symbiotic associations between chemosynthesizers and respiring

heterotrophs are quite common. Large populations of animals can be supported by chemosynthetic secondary production at hydrothermal vents, methane clathrates, cold seeps, and whale falls (Foucher et al., 2009).

Giant tube worms use bacteria in their trophosome to react hydrogen sulfide with oxygen as a source of energy. Some reactions produce sulfur, such as:

Hydrogen sulfide chemosynthesis:



(CH₂O is used to mean carbohydrate, not formaldehyde.)

Instead of releasing oxygen gas as in photosynthesis, solid globules of sulfur are produced (Kiel, 2010).

2.4.1 Methane hydrate and chemosynthetic biota at cold seeps

At seeps where methane is escaping into the water column as free gas it is evident that there is an abundant supply of subseabed methane for chemosynthetic biota (figure 8), but there are many seeps that support chemosynthetic biota where methane is only in solution in the pore water that flows through the seep. Methane hydrate beneath the seabed plays an important role where seeps lie within its stability field, generally in water depths greater than 400 m. Hydrate provides a metastable reservoir of methane, and it buffers the concentration of pore water methane in solution (figure 9).

Estimates of how long hydrate could provide a viable source of methane to chemosynthetic biota at the seabed under different conditions were made using a one-dimensional advection-diffusion model (Ivanov et al., 2007). The model assumes that, initially, hydrate lies 1 m beneath the seabed and the sulfate-methane transition (SMT) is at 30-cm depth. Above the SMT, methane is not present in the pore water, because it has been anaerobically oxidized with microbial mediation, taking the oxygen from sulfate that has diffused downward from the seawater to produce sulfide and bicarbonate (Boetius et al., 2000). If the SMT is much more than about 1-m deep, methane in pore water is out of reach of most of the biota living at or near the seabed.

Depletion of a layer containing 12.5% hydrate by chemical diffusion alone will

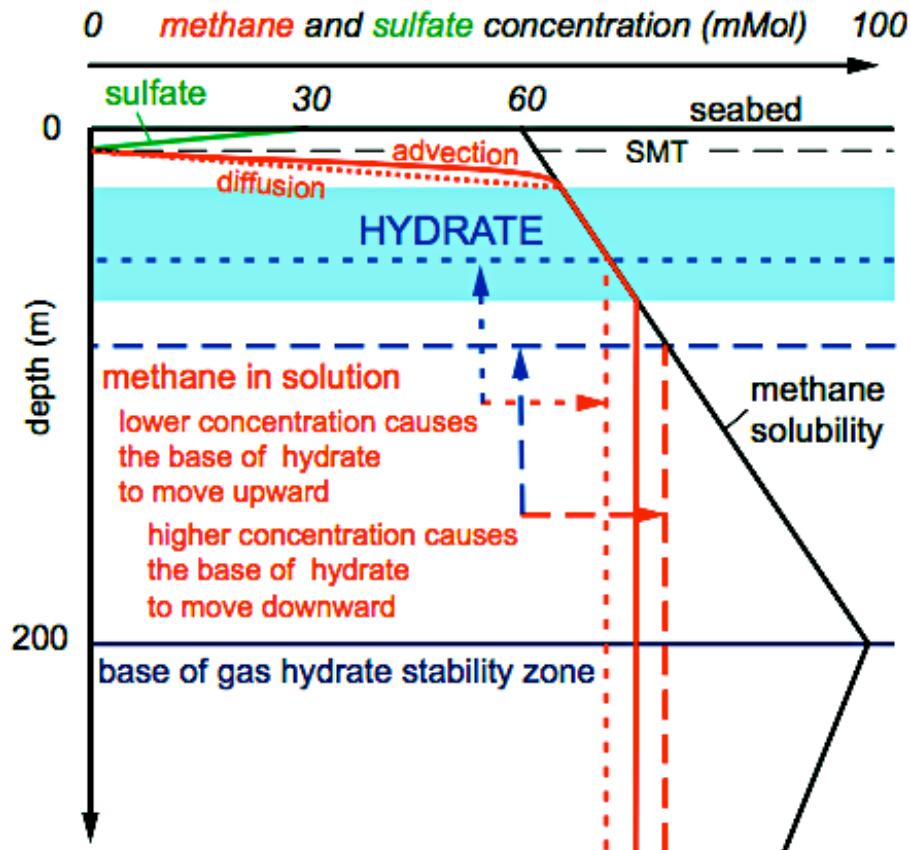


Fig 10: Schematic representation of the control of methane concentration beneath the seabed by the initial concentration of methane in solution in upwardly migrating pore water, the presence of hydrate, and sulfate in the seawater. The concentration of dissolved methane in the rising pore water controls the depth at which hydrate begins to form. If it is less than the lowest value of methane solubility, then all previously formed hydrate will be removed, but the rate of removal depends upon the degree to which the pore water is undersaturated and the rate of pore-water flow. (Foucher et. al, 2009)

cause the top to recede downward from 1m to 3m depth below the seabed after 1800 years (figure 10). The SMT will deepen from 0.3 to 1 m and the methane flux will decrease from 2.1–0.7 mol m⁻² yr⁻¹. Consumption rates of methane by in situ chemosynthetic biota vary greatly and are species dependent (Torres et al., 2002; Boetius and Suess, 2004), but a rate of a few tenths of a mol m⁻² yr⁻¹ appears to be sufficient for some species (Niemann et al., 2006a). So, although the methane flux would still appear to be sufficiently high, the increasing depth of the SMT below 1 m would progressively reduce the viability of chemosynthetic biota.

Upward advection of methane in solution in pore water can halt the downward movement of the top of the hydrate and the SMT. For the model case, this is produced by a fluid flow rate of 35 mm yr⁻¹ with the concentration of methane

buffered by the hydrate at 60 mol m^{-3} . The concentration of methane in solution in the pore water that enters the layer containing hydrate and the rate of flow of the water control how quickly the hydrate is removed. The layer would be diminished from beneath, where methane solubility is higher and the rising pore water first comes into contact with the hydrate. At one extreme, a 10-m-thick layer would be removed in 160 years if the concentration of methane in solution was zero and the fluid flow rate was 1 m yr^{-1} . For a near-saturation methane concentration of 55 mol m^{-3} and a fluid flux of 35 mm yr^{-1} , it would take 5500 years to reduce the thickness of the hydrate by one meter, while providing a methane flux of $2.1 \text{ mol m}^{-2} \text{ yr}^{-1}$ and maintaining the top of the hydrate and SMT at their initial depths.

In short, if hydrate had been produced at shallow depth by an event releasing a high volume of free gas in the past, an accumulation of methane hydrate of low-to-moderate concentration and a few meters thick near the seabed could sustain communities of chemosynthetic biota for periods of several thousands to a few tens of thousands of years at seep sites where methane concentration in pore water is high but not exceeding saturation. Such an event may have lasted only a few years or less, depending on the efficiency with which hydrate was formed from the escaping free gas. Consequently, short-lived, catastrophic gas venting at the beginning of the Holocene or earlier could, without subsequent reactivation, have provided the source of methane for active, present-day communities of chemosynthetic biota (Foucher et al., 2009)

Chapter 3: The Gulf of Cadiz

3.1 Study Area

The Gulf of Cádiz is located between 34°N and 37°15'N and 6°W to 9°45'W. It is the part of the Atlantic Ocean between Cape St. Vincent in Portugal and Cape Trafalgar at the western end of the Strait of Gibraltar. It corresponds to the southern Iberian and northern Moroccan margins at north and south, respectively. The Gibraltar Strait, at east, defines the connection to the Mediterranean Sea.

The geological history of the Gulf of Cádiz is closely related to the plate tectonic interaction between Southern Eurasia and North Africa and is driven by two main mechanisms: (1) subduction associated with the westward emplacement of the Gibraltar Arc, and (2) the formation of the Gulf of Cádiz accretionary wedge, probably not active at present (Maldonado et al., 1999).

The whole area is under compressive/transpressive deformation and events of mud volcanism and processes associated with the escape of hydrocarbon-rich fluids were discovered. These fluid migration and escape structures sustain a broad diversity of chemosynthetic assemblages (Cunha, 2007; Rodrigues, 2009). This extensive area encompasses more than 42 mud volcanoes, at depths ranging from 200 to 4600 m (confirmed by coring), and active methane seepage has been documented on several locations (Pinheiro et al., 2003, Magalhães et al., 2012).

3.2 Geological Setting

The Gulf of Cadiz is located at the front of the Betic-Rifian Arc. It has had a very complex geological history and undergone several episodes of extension, compression and strike-slip motion (Maldonado et al., 1999). The westward migration of the Gibraltar arc during the Late Miocene (5Myr) caused the formation of a fore-arc basin in the actual area of the Gulf of Cadiz (Maldonado et al., 1999). The emplacement of the thrusting units, gravitational sliding of the mobile shale and salt stocks formed a giant deposit-mass, called *Gibraltar Olistostrome*, that migrated west towards the Horseshoe and Seine abyssal plains (Maldonado et al., 1999). This olistostrome body consists of a chaotic mixture of Triassic, Cretaceous, Paleogene and Neogene sedimentary units, deposited on top of the Palaeozoic basement. These chaotic units involve a huge volume of Triassic mud

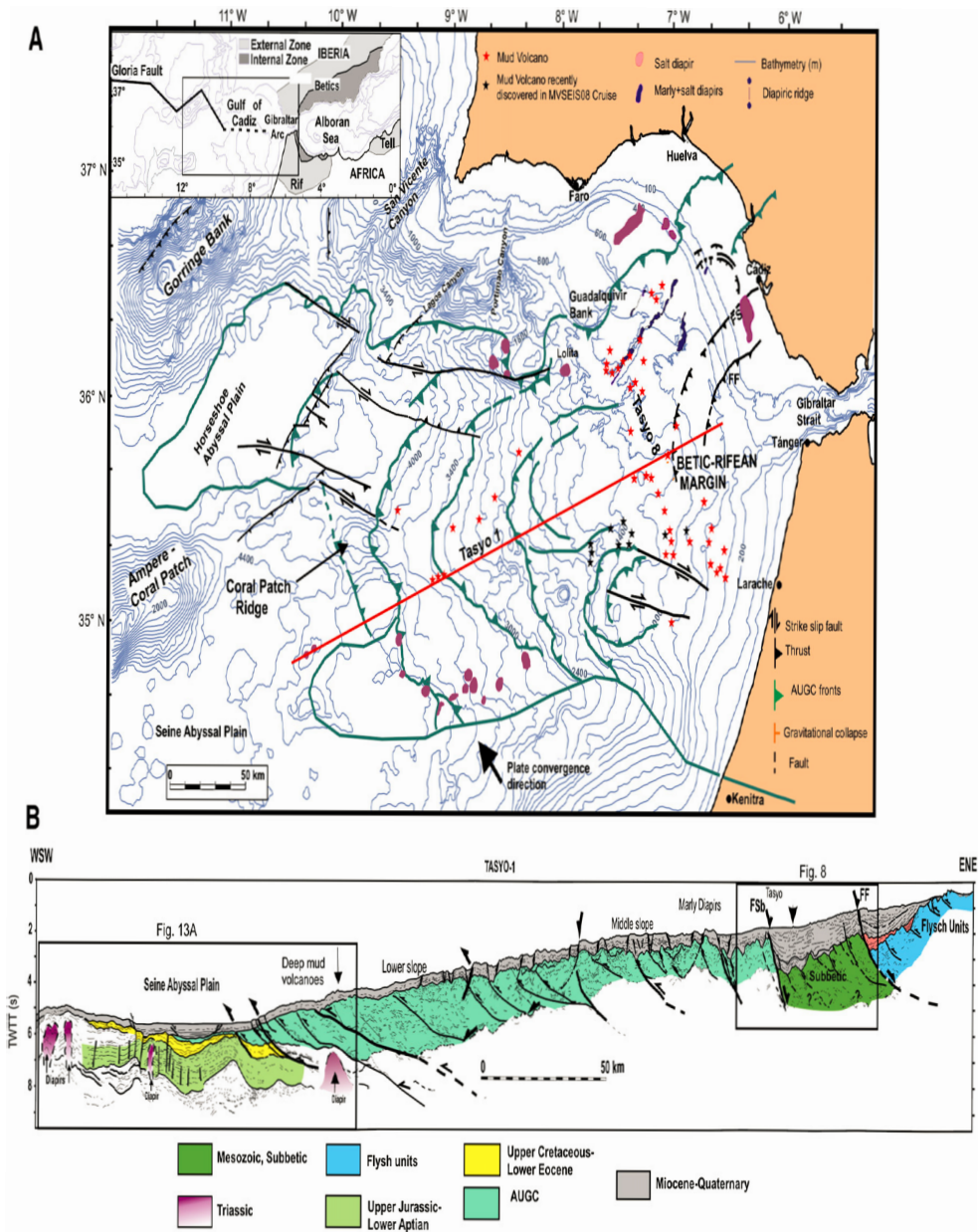


Figure 11: Tectonic map of the Gulf of Cádiz (Medialdea et al, 2009) showing the main outcropping and very shallow diapirs, faults, mud volcanoes and mud-carbonate mounds. FSb: Subbetic Front; FF: Flysch Front. Mud volcanoes recently discovered after Somoza et al. (2008). B) Line-drawing derived from the MCS profile TASYO 1 that crosses the Gulf of Cádiz.

and salt salt units and under-compacted Early-Middle Miocene plastic marls (Maldonado et al. 1999).

Throughout this area, pockmarks, extensive mud volcanism and mud diapirism, carbonate mounds and fields of high density chimneys, crusts and pavements related to hydrocarbon rich fluid venting are observed (Somoza et al., 2003; Pinheiro et al., 2003; Ivanov et al. 2007). In the south Iberia margin it is prominent

the presence of a large NE-SW diapiric ridge, the Guadalquivir Diapiric Ridge (GDR) that runs from the shelf break up to 1200 m water depth. This ridge is very important in the oceanography and the sedimentary dynamics of this margin because it controls the orientation of the main channel of the MOW (Mediterranean Outflow Water) undercurrent that have an important control on the erosion, sediment transport and deposition along the northern margin of the Gulf of Cadiz. The GDR is composed of a series of wide sub-circular conical mounds surrounded by ring-shaped seafloor depressions (Somoza et al., 2003; Diaz-del-Rio, et al., 2003; Leon et al., 2007).

In the Gulf of Cádiz area, the present-day convergence between the African and Eurasian plates is ~ 4 mm/y with a northwest–southeast trend, and it is being accommodated over a broad diffuse deformation zone (Stow et al, 2011). Nevertheless, different periods of crustal deformation, and plates movements are known to have controlled the evolution of this part of the Iberian Peninsula. The rifting phases that characterize the opening of the central and North Atlantic basin since the late Triassic to the Early Cretaceous had also constrained the deep structure of the Gulf of Cadiz (Pinheiro et al., 1996; Wilson et al., 1996; Borges et al., 2001) and its later deformation during the Cenozoic, especially in the Miocene (Zitellini et al., 2009). Those are the most important phases and the ones that give to the Gulf of Cadiz his present-day global configuration. The Gulf of Cádiz Cenozoic evolution was controlled by the Alpine tectonic phases that affected the southern part of the European plate. Since the late Miocene, the northwest–southeast compressional regime has been developed simultaneously with the extensional collapse of the Betic-Rif orogenic front, by westward emplacement of a giant "olistostrome," the Cádiz Allochthonous Unit (CAU), and by very high rates of basin subsidence coupled with strong diapiric activity (Maldonado et al., 1999). At the end of the Messinian, a transtensional regime caused the reopening of the connection between the Atlantic and the Mediterranean through the Strait of Gibraltar (Maldonado et al., 1999). By the end of the early Pliocene, subsidence decreased and the margin evolved toward its present shape (Maldonado et al., 1999; Medialdea et al., 2004). The tectonics structure and evolution represented a key long-term factor in affecting the seafloor morphology, which has then exerted a

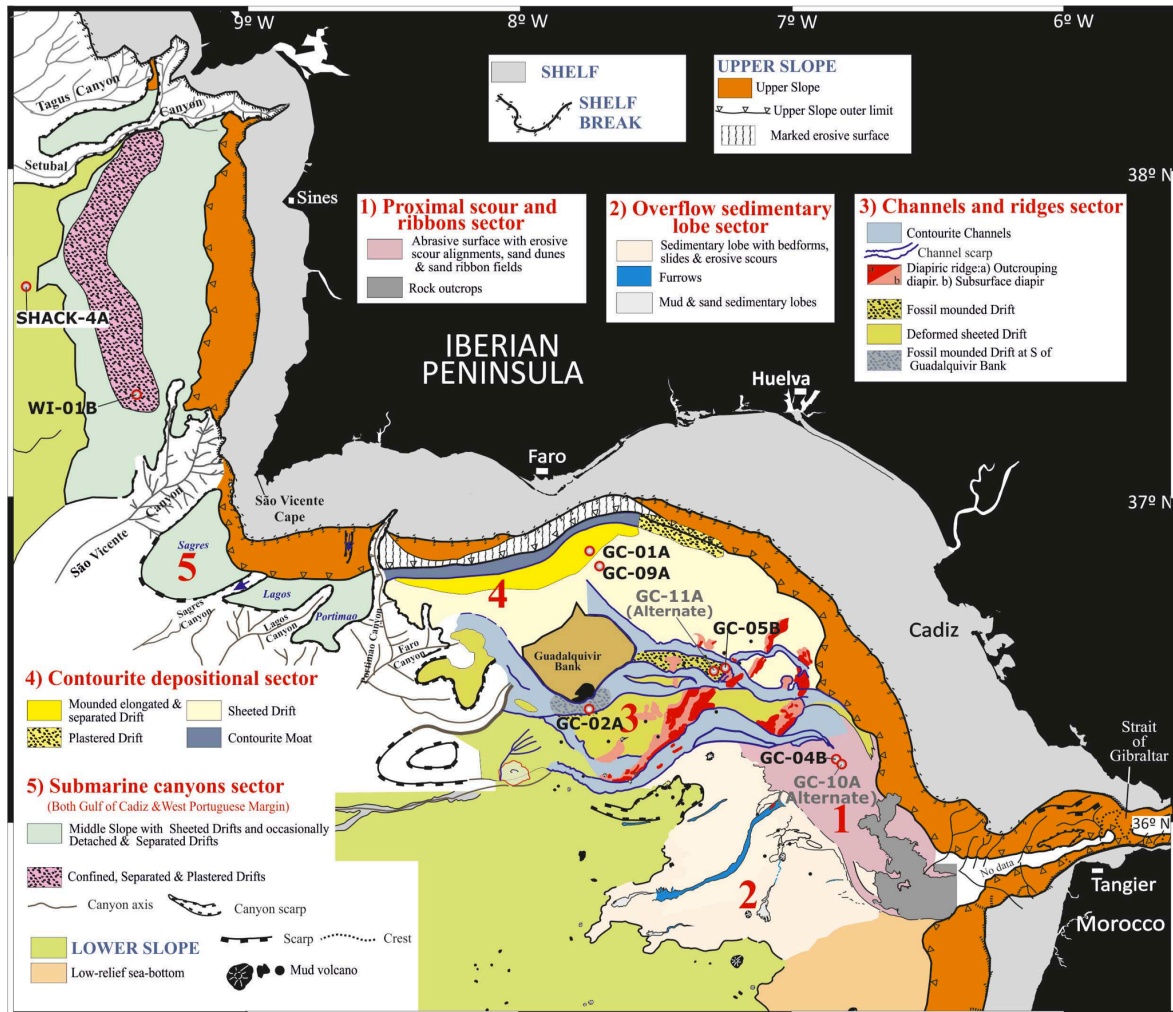


Figure 12: Regional map of the contourite depositional system on the middle slope of the Gulf of Cádiz and West Iberian margin with proposed site locations. Morphosedimentary sectors (1–5). (Hernandez-Molina et al., 2006)

strong control on the pathways of MOW, on the geomorphology and sedimentary architecture of the present-day Gulf of Cadiz. As a result of the complex geological evolution, the bathymetry of the continental shelf, slope and rise of the Gulf of Cadiz is quite irregular and exhibits widely varying gradients resulting from the interference of several different geomorphologic processes and structures. The shelf area can be divided into four morphological provinces; (a) the inner shelf, (b) the smooth mid-shelf, (c) the south-east shelf with bedforms, and (d) the outer shelf (Nelson et al., 1999).

The shelf break occurs at about 130 and 20 m water depth. In the continental slope it is possible to differentiate into four morphologic provinces: (a) a narrow belt between 130 and 400 m formed by the steeper (2–3°) upper slope, (b) two

gently dipping ($<1^\circ$) wide terraces located between 400 and 700 m water depth on both the southeast and northwest sides of the Gulf of Cadiz middle slope, (c) a central section between the terraces in which several, steep ($3\text{--}30^\circ$), narrow curvilinear ridges (3–10 km width) and valleys (1–3 km width) with general trends ranging from NE–SW to E–W, and (d) a smooth lower slope from 900 to 1500 m that is more steeply dipping ($2\text{--}4^\circ$) and incised by shallow valleys in a NE–SW direction (Nelson et al., 1999).

3.3 Oceanographic setting

The present-day circulation pattern is dominated by the exchange of water masses between the Atlantic Ocean and the Mediterranean Sea through the Strait of Gibraltar (figure 13). This exchange is driven by the influx into the Atlantic of the Mediterranean Outflow Water (MOW), highly saline and warm water mass, that flows near the bottom; and by the superficial influx of Atlantic water into the Mediterranean Sea, of less saline and cool-water and generates important sedimentary processes along the Atlantic margin (Serra et al., 2010a, 2010b).

The Mediterranean outflow as it comes out of the Gibraltar Sill it flows as a bottom current due to its high density and due to the Coriolis effect it turns to the right, flowing as a bottom current along the northern margin of the upper slope of the Gulf of Cadiz (Figure 13). In the Gulf of Cádiz, MOW flows between 500 and 1400 meters below sea level (mbsl) (Cherubin et al., 2000). Its distribution along the Margin is then conditioned by the complex morphology of the continental slope, in fact it generates two main sub currents, the upper-one, located between 500 and 700 mbsl, is called the Mediterranean upper water (MUW); and the lower-one, between 800 and 1400 mbsl, that is called Mediterranean lower water (MLW) (Borenäs et al., 2002). In the western sectors, the interaction of these branches with the seafloor generates big vortices, the so-called meddies, that are subsurface masses with anti-cyclonically rotation of warm salty water of the MO in the Atlantic Ocean water .

Between ~500 and 1500 mbsl, the water column along the West Iberian margin is dominated by the warm, salty MOW and its two sub-currents. Below MOW at

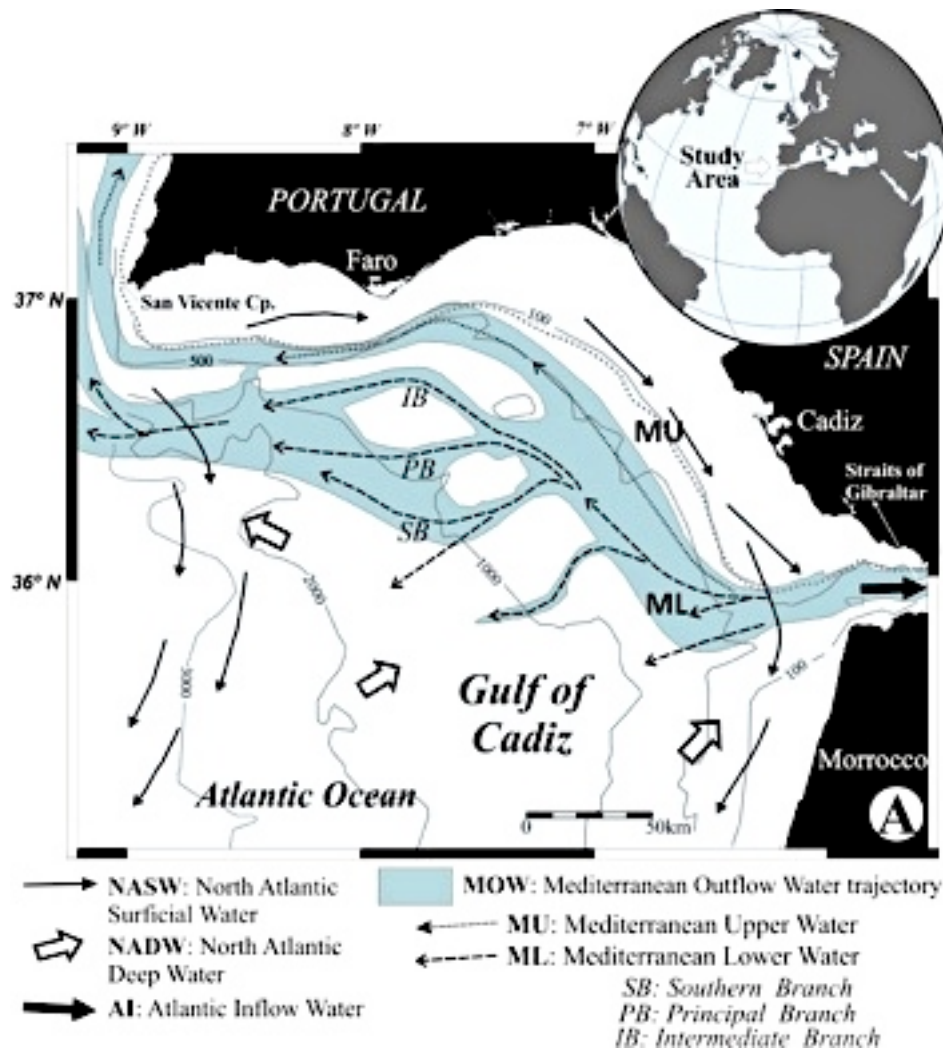


Figure 13 : Location sketch with main water-mass circulation along the margin (modified from Hernández-Molina et al., 2006) (Stow et al., 2011)

~1600 mbsl on the north margin is possible to find a water mass originated from the Labrador Sea Water (LSW). Below 2000 mbsl, recirculated Northeast Atlantic Deep Water (NEADW) prevails, which represents a mixture of LSW, Iceland Scotland Overflow Water (ISOW), Denmark Strait Overflow Water (DSOW), and to a lesser extent MOW and Lower Deep Water (LDW). Abyssal water in the region consists of a lower fringe of NEADW, with an increasing composition of southern-sourced LDW with depth until ~4000 mbsl, where LDW dominates (Stow et al., 2011).

3.4 Carbonate Chimneys

Dolomite chimneys are interpreted as cemented conduits formed as result of

methane-enriched fluid expulsion through the sediments. The abundant pseudopyrite framboids are related with the zone of shallow microbial sulphate reduction, a process fundamental to the nourishment of the chemosynthetic cold seep communities. In the last years, it has been considered the importance of carbonate cementation related with methane fluxes, both on submarine modern environments and on rocks of the fossil record (Orpin 1997; Somoza et al. 2002; Díaz-del-Río et al., 2003). Large fluxes of methane seem responsible for dolomite cementation, instead low and less intense fluxes involve the cementation of high-Mg calcite and aragonite. Recently, it has been proposed that extensive anaerobic microbial communities exist in sedimentary layers below (methane) vent fields (DeLong 2000). The sum of the syntrophy cooperation between methane-oxidisers (archaeobacterias domain) and sulphate-reducers microorganism produces carbonates and sulphides at the sulphate-methane interface, the depth below seafloor at this reaction occurs will depend on the methane flux rate (DeLong 2000).

Carbonate dolomite chimneys are found to be associated with hydrocarbon-rich fluid venting. They occur in several places on continental margins, such as in the Campos Basin of the Brazilian Margin (Miller, 2006), in the Krishna-Godavari Basin, eastern continental margin of India (Muralidhar et al., 2006); in the Otago continental slope, southern New Zealand (Orpin, 1997); Kuroshima Knoll, Ryukyu Islands, Japan, (Takeuchi et al., 2007); Denmark Margin (Jørgensen, 1989); and also in the Gulf of Cadiz (Díaz-del-Río et al., 2003; Magalhães, 2007; Magalhães et al., 2012). In the Gulf of Cadiz, dolomite chimneys were discovered in September 2000 during the cruise *Anastasya/2000* aboard of research vessel *Cornide de Saavedra* dredging a 870 m-deep and 120 m-tall carbonate mound called as the "Iberico". Here were collected more than 60 individual structures of chimneys with distinct pipe-like morphologies that varies from 1 to 0.40 m long (Díaz-del-Río et al., 2003).

The chimneys are dominated by Fe-riched dolomite (ankerite) forming aggregates with minor amounts of pyrite, iron oxide, Ta-enriched rutile, zircon and quartz. Abundant, well preserved remains of foraminifera (globigerinoids and milioids) composed of Mg-calcite are present within the matrix. Dolomite aggregates are

depleted in ^{13}C (-35 to -56‰ PDB) and are therefore interpreted being the result of methane oxidation by sulphate-reducing bacteria. Aggregates of single bacteria produces rounded to pentagonal shaped framboids of pyrite. Latter oxidation resulting from the contact with the sea bottom seawater resulted in the replacement of the major part of these bacterial-origin framboids by haematite. At same time, some of framboids have been found in the interior of the foraminifers, which could suggest some symbiotic association between foraminifer and chemosynthetic bacteria (Somoza et al., 2002 and Díaz-del-Río et al., 2003).

3.5 Carbonate Crusts

The authigenic carbonates can also precipitate in the form of carbonate crusts or pavements, that form thin (cm size) crusts up to massive crusts with up to 50 cm thick crusts or even several meters high mounds, at the sediment surface or within surface sediments. These carbonate crusts are built under a narrow range of physical, chemical and biological conditions. They are indicators of a relatively slow (20–90 cm a⁻¹) but pervasive (100–500 years) upwards flow of methane-charged (>50 mM CH₄) fluids (Pinheiro et al., 2003; Niemann et al., 2006). It is generally accepted that in the systems where the authigenic carbonate crusts are formed, the dominant fraction of the rising methane is anaerobically oxidized within the sediment and sequestered as carbonate, and as result only a very small amount methane can escape to the seabottom water column (Kvendolven et al., 2005). Carbonate crust formation has also the potential to affect the persistence and distribution of chemosynthesis-based benthic communities at cold seeps. By strongly inhibiting transport processes, the carbonate crusts separate sulfate from methane, decreasing the overall rates of the anaerobic oxidation of methane and of the consequent production of sulfide. Because most of the chemosynthesis supporting the development of macro-benthos at cold vents is based on the oxidation of sulfide produced through the anaerobic oxidation of methane, the potential of these systems, where active carbonate crust formation occurs, to harbor such organisms is severely decreased (Pinheiro et al., 2003; Kvendolven et al., 2005; Niemann et al., 2006).

The carbonate crusts also act as a fluid migration barrier, inhibiting or blocking the

upward flow of fluids through the sediments. Thus, sedimentary carbonate crusts may diverge and focus the fluid flow to adjacent areas not affected by crust formation. In the area of study, the Gulf of Cadiz, is possible to find two principal typology of carbonate crusts:

Dolomite crusts. This type of crust can be distinct from the dolomite chimneys by just by the difference in the morphology . Dolomite crusts have planar shapes, up to 10 cm thick and up to 70 cm across, they present no internal structure, low porosity, no macro-porosity or internal channels and neither shells nor biogenic components (except for foraminifera and coccoliths) (Somoza et al., 2003; Magalhães et al., 2007 and Magalhães et al., 2012).

Aragonite crusts. In all the aragonite crusts authigenic aragonite is the dominant mineral with subordinate authigenic calcite and high-Mg calcite (Magalhães et al., 2012), cementing a detrital fraction of quartz, feldspars, clays, mud volcano mud breccia clasts, shell fragments, foraminifera and calcareous nannofossils. The aragonite crusts present a significant macro-porosity (voids, fractures, tubular and irregular cavities some of them interconnected) and high percentages of open inter-granular pore space, indicating formation within very weakly compacted sediments (Somoza et al., 2003; Magalhães et al., 2007 and Magalhães et al., 2012).

3.6 Mud Volcanoes

The first discover and confirmation by ground-truthing of mud volcanoes in the Gulf of Cadiz was in 1999 during the TTR-9 cruise (Gardner, 2001). Since then, this area has been intensively investigated. Most of this work was carried out within the framework of the INGMAR (PLE/4/98), the Training Through Research program (IOC/UNESCO), and the MVSEIS - Euromargins (01-LEC-EMA24F http://www2.geo.ua.pt/mvseis/Mud_volcanoes.htm) projects, all of them leded (MVSEIS) or with the active involvement of researchers from the University of Aveiro. As result, 46 mud volcanoes were discovered and confirmed by coring in this area during several cruises.(Extensive hydrocarbon-rich fluid venting and mud diapirism were also observed throughout this area (Ivanov et al., 2000; Díaz-del-Río et al., 2003; Pinheiro et al., 2003; Somoza et al., 2003). These are related to

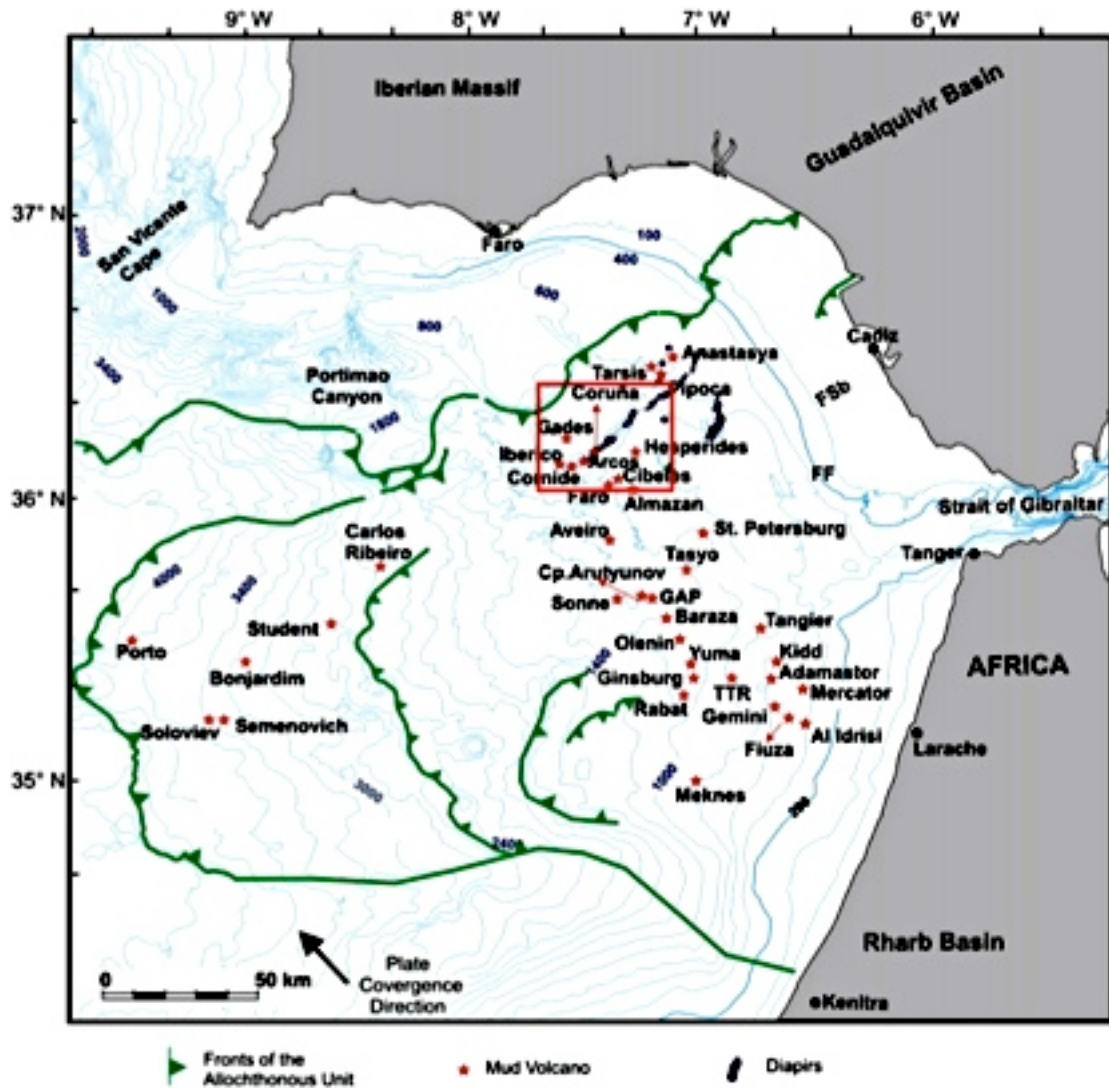


Figure 14: Map of the Mud Volcanoes discovered and confirmed in the Gulf of Cadiz until 2008. (González et al., 2009)

the lateral compression from Africa–Eurasia convergence, that promoted the fluid migration, from deeper parts of the basin, throughout faults, up to the seafloor. Several NE–SW oriented diapiric mud ridges have been found in the shallow NE sector of the Gulf of Cadiz. This area is characterized by abundant carbonate chimneys and crusts on top of these ridges (Gonzalez et al., 2009).

Most of the mud volcanoes in the eastern domain of the Gulf of Cádiz are found located between 350–2000 m water depth, parallel to the NE–SW and NW–SE main directions. Deeper mud volcanoes have also been recognized on the lower slope at 2300–4600 m depth (Madialdea et al., 2009, Magalhães et al., 2012). Most of those mud volcanoes are clearly controlled by the so-called SWIM lineaments (Hensen et al., 2007; Scholz et al., 2009) (see figure 14). These SWIM

lineaments correspond to the bathymetric expressions of strike slip faults, that most probably correspond to the reactivation of WNW-ESE pre-existing faults, and are segmented, of crustal-scale, extending from the Gorringe Bank to the Gibraltar area in the eastern Gulf of Cadiz (Zitellini et al., 2009; Magalhães et al., 2009). Zitellini et al. (2009) suggested that these faults mark a developing Eurasia-Africa plate boundary in the region. In particular, the lineaments passing through the study area consist of a network of shear structures that evokes the development of an incipient strike-slip fault system. These geological structures are known to provide fluid migration pathways (Moore and Vrolijk, 1992).

Geographically, the mud volcanoes are distributed in three main areas of the Gulf of Cádiz. Most of them are found on the upper and middle slope between 350 and 2000 m water depth, either on the northern Iberian margin, where they are found aligned along the regional compressive structures with a roughly NE-SW orientation (Somoza et al., 2003; Díaz-del-Río et al., 2003); or on the Moroccan margin, following an approximately regionally dominant NW–SE direction (Pinheiro et al., 2003; Madialdea et al., 2009).

Some of the most important and well-studied mud volcanoes in the Gulf of Cadiz are:

- Bonjardim mud volcano: It appears as an approximately circular, isolated feature, with a diameter of 1 km almost, it has a height of approximately 100 m with a seafloor depression at the rim of the cone.
- Carlos Ribeiro mud volcano: is located at a depth of 2200 m, with a height of approximately 80 m and a diameter of 1.5 km.
- Olenin mud volcano: it appears as a dome-like structure, located on a slope.
- Jesus Baraza mud volcano it has a circular feature . With a prominent high, maximum height above seafloor of about 150 m.
- Student mud volcano presents a sub-circular feature.

Three new mud volcanoes: Michael Ivanov, Absu and Tiamat mud volcanoes has been recently discovered during the RV Meteor M86/5 Cruise on march 2012. Some of the gravity cores recovered on the Michael Ivanov mud volcano are analyzed in this thesis.

Chapter 4: Materials

The samples studied in this Master thesis project correspond to carbonates crusts and chimneys collected from 5 different areas of Gulf of Cadiz (on small mounds on the MOW channel in front of Gibraltar Strait, on the Vernadsky Ridge, on the Pen Duick escarpment, on top of Mercator and Meknes mud volcanoes, and on Michael Ivanov mud volcano) as illustrated in the Figure 15 and reported in table 2. These samples were collected during four different cruises: TTR 14; TTR 15; TTR 16 and M86/5.

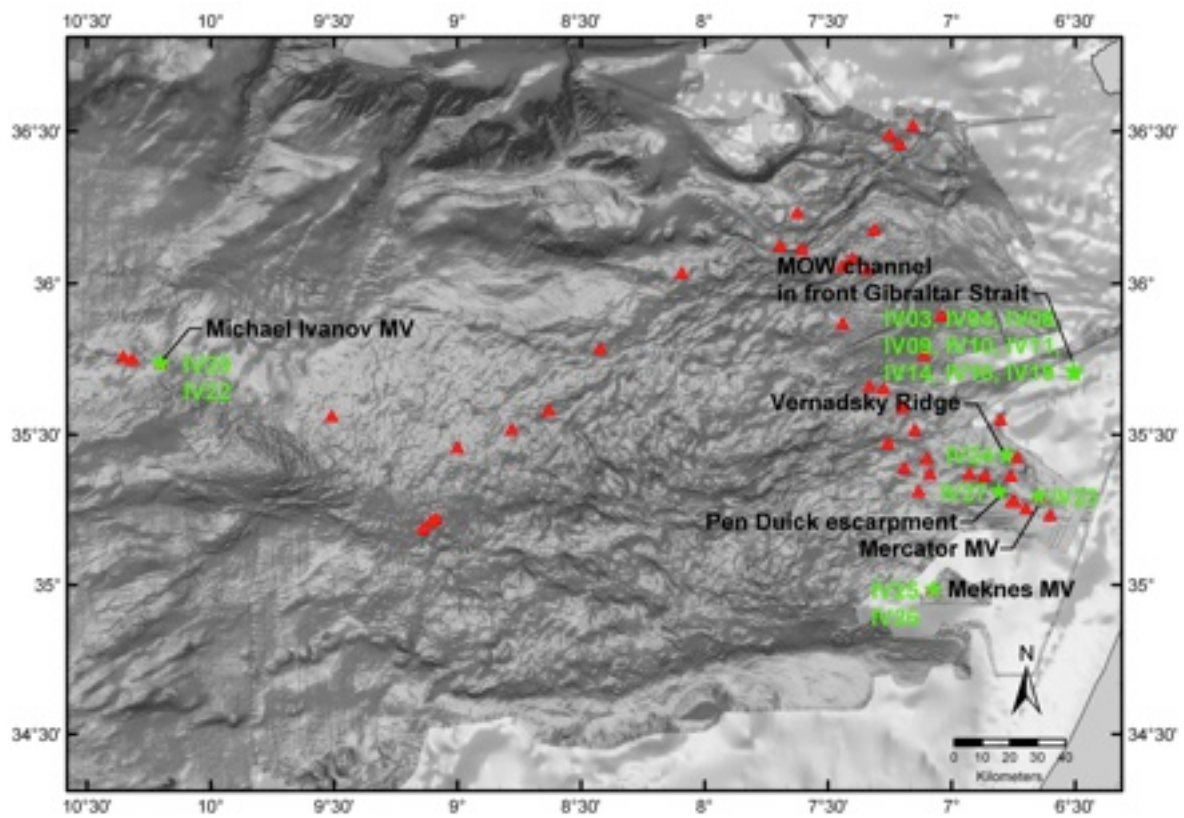


Figure 15: Map showing the location of the samples used in this Master thesis project (green stars). Red triangles indicate the location of the present-day confirmed mud volcanoes.

Table 2: List of samples used in this Master thesis project. Along this thesis, samples will be identified by her lab code

Cruise	STATION	Lab Code	Latitude (N)	Longitude (W)	Depth (m)	Sampling device	Sub samples	Structure
TTR-14	TTR14AT5 50D	IV03	35°42.105'	6°30.196'	368	Dredge	7 subsamples: IV03.01 to 07	small mounds on the MOW channel in front of Gibraltar Strait
TTR-14	TTR14AT5 50D	IV04	35°42.105'	6°30.196'	368	Dredge	6 subsamples: IV04.01 to 06	small mounds on the MOW channel in front of Gibraltar Strait
TTR-14	TTR14AT5 51D	IV08	35°42.597'	6°30.505'	445	Dredge	3 subsamples: IV08.01 to 03	small mounds on the MOW channel in front of Gibraltar Strait
TTR-14	TTR14AT5 51D	IV09	35°42.597'	6°30.505'	445	Dredge	3 subsamples: IV09.01 to 03	small mounds on the MOW channel in front of Gibraltar Strait
TTR-14	TTR14AT5 51D	IV10	35°42.597'	6°30.505'	445	Dredge	3 subsamples: IV10.01 to 03	small mounds on the MOW channel in front of Gibraltar Strait
TTR-14	TTR14AT5 52Gr	IV11	35°42.737'	6°30.333'	404	Grab	4 subsamples: IV11.01 to 04	small mounds on the MOW channel in front of Gibraltar Strait
TTR-14	TTR14AT5 52Gr	IV14	35°42.737'	6°30.333'	404	Grab	3 subsamples: IV14.01 to 03	small mounds on the MOW channel in front of Gibraltar Strait
TTR-14	TTR14AT5 52Gr	IV16	35°42.737'	6°30.333'	404	Grab	4 subsamples: IV16.01 to 04	small mounds on the MOW channel in front of Gibraltar Strait
TTR-14	TTR14AT5 52Gr	IV19	35°42.737'	6°30.333'	404	Grab	6 subsamples: IV19.01 to 06	small mounds on the MOW channel in front of Gibraltar Strait
TTR-15	TTR15AT5 69Gr	IV23	35°17.919'	6°38.718'	355	Grab	2 subsamples: IV23.01 to 02	top of Mercator mud volcano
TTR-15	TTR15AT5 74D	IV24	35°26.150'	6°46.915'	512	Dredge	4 subsamples: IV24.01 to 04	Vernadsky Ridge
TTR-15	TTR15AT5 81Gr	IV25	34°59.182'	7°04.344'	700	Grab	3 subsamples: IV25.01 to 03	top of Meknes mud volcano
TTR-15	TTR15AT5 83G	IV26	34°59.139'	7°04.400'	701	Gravity corer	1 subsample: IV26.01	top of Meknes mud volcano
TTR-16	TTR16AT6 00GR	IV27	35°18.779'	6°38.453'	610	Grab	9 subsamples: IV27.01 to 09	Pen Duick escarpment
M86/5	M86/5 - 24 GC04	IV20	35°44.335'	10°12.067'	4490	Gravity corer	7 subsamples: IV20.01 to 08	Michael Ivanov mud volcano
M86/5	M86/5 - 42 GC10	IV22	35°44.355'	10°12.179'	4481	Gravity corer	4 subsamples: IV22.01 to 07	Michael Ivanov mud volcano

4.1 Cruises

The carbonate samples considered in this thesis came from four different cruises that interested the Gulf of Cadiz in the passed years.

Cruise TTR 14

The TTR 14 cruise, Leg 1, was carried out in 2004, onboard the RV Professor Logachev, as part of the fourteenth Training-through-Research Cruise integrated in the framework of the MVSeis project and where researchers from the university of Aveiro had participate. The objectives of this leg were twofold: to conduct detailed investigations of geological and biological processes on the continental margins of the Gulf of Cadiz and to train students in how to conduct research in marine geoscience (Kenyon et al., 2006). Investigations were focused on mud volcanism,

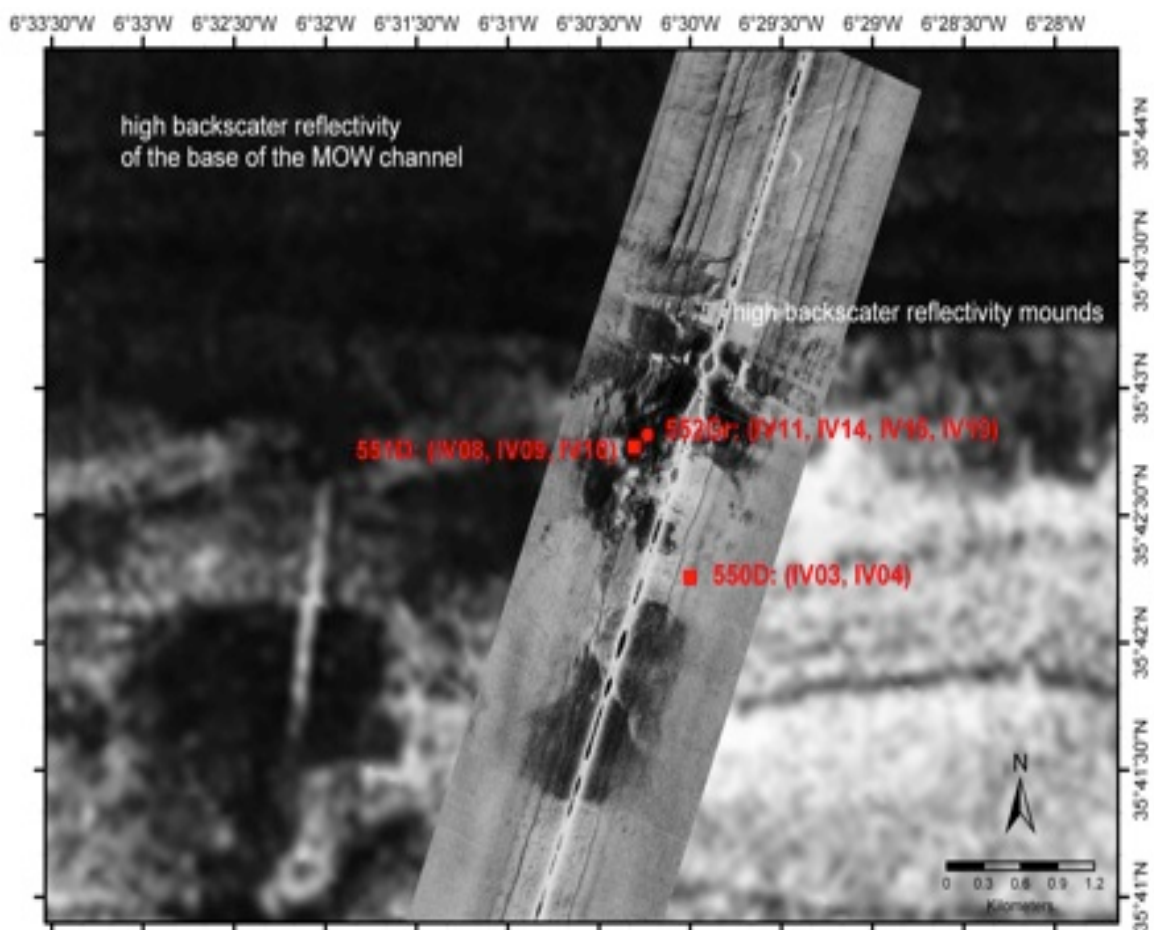


Figure 16: Location of the samples collected during the TTR 14 Cruise that were used in this project. On the background, low resolution NRL Seamap backscatter overlaid by the deep-towed high resolution MAK side-scan sonar acquired during the TTR 14 cruise. The location of the 3 sampling stations: 550D and 551D dredge samples are marked by the red squares and the TV-controlled grab sample 552Gr marked by the red hexagon.

fluid venting and related processes in the Gulf of Cadiz. Gas hydrates, carbonate crust and nodules, as well as benthic chemosynthetic communities were sampled from some of these structures (UNESCO, 2006). Large carbonate chimneys, related to fluid escape were sampled and recorded by a deep-towed video system on two small mounds on the main channel of the MOW in front of Gibraltar Strait (see figure 16). A selected set of samples, repre



Figure 17. Onboard pictures of the samples collected on the stations 550D, 551D and 552Gr.

ntative of the different lithologies collected in the stations 550D, 551D and 551Gr (Figure 17) have been studied in this work.

Cruise TTR 15

TTR 15 cruise, Leg 4, was carried out in 2005, onboard the RV Professor Logachev, as part of the fifteenth Training-through-Research Cruise integrated in the framework of the MVSeis Euromargins project and where researchers from the university of Aveiro had participate. The main objectives of the TTR-15 Leg 4 were to investigate the structural control of the fluid escape structures in the Gulf of Cadiz and the associated fauna, in particular to investigate several mud volcanoes in the Moroccan sector of the Gulf of Cadiz, and investigate the possible continuation to the east and west of the southernmost known mud volcano field in the NW Moroccan margin (UNESCO, 2007). Other main objective of this cruise was also the investigation, with geophysical methods and coring, of several high backscatter features observed in the available side-scan sonar imagery in the

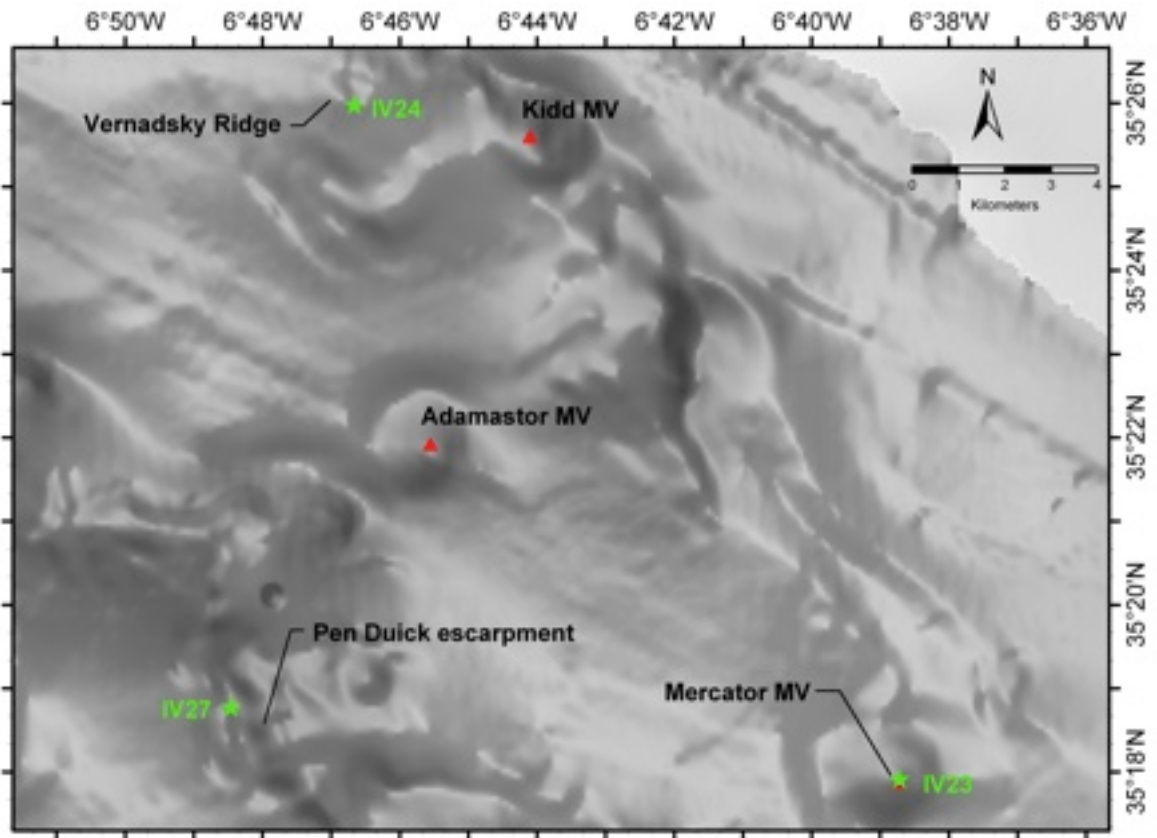


Figure 18: Location of the samples collected during the TTR 15 and TTR16 Cruises that were used in this project. A hillshade of the bathymetry is shown on the background

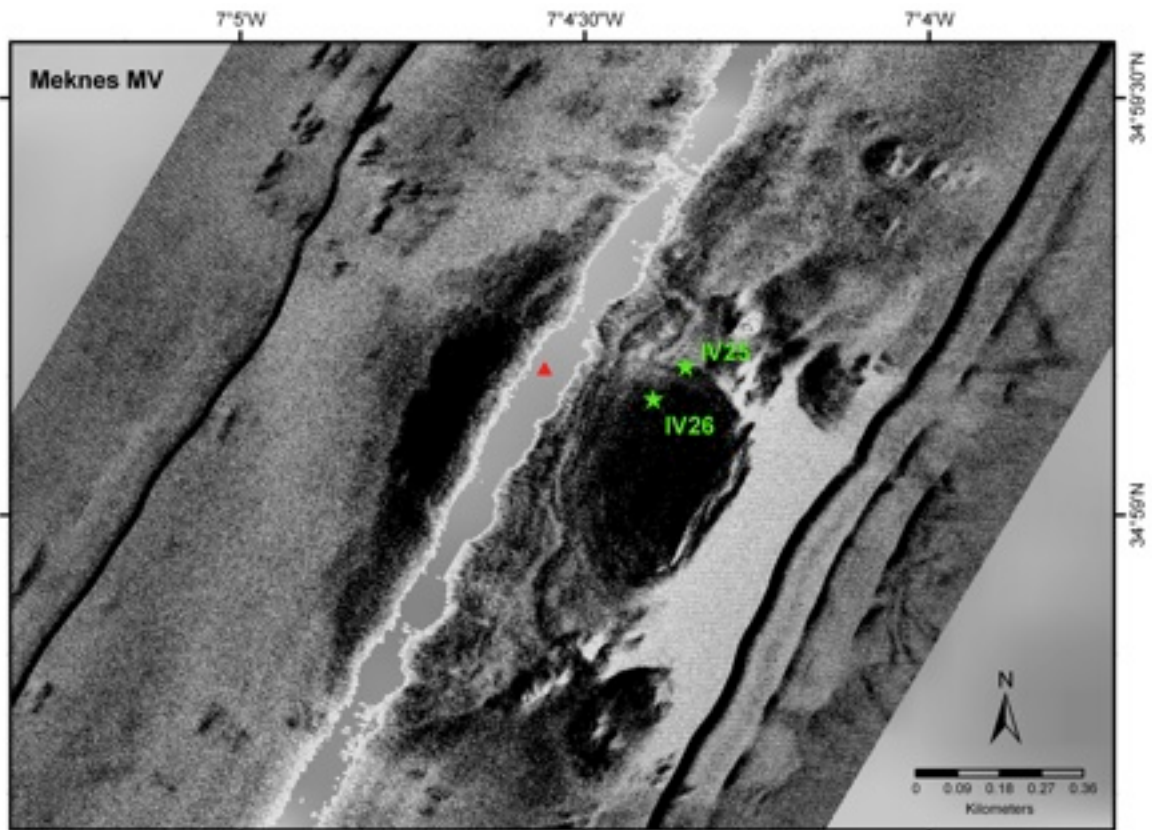


Figure 19: Location of the samples collected during the TTR 15 and TTR16 Cruises on the Meknes mud volcano, used in this project. on the background is shown a deep towed side-scan sonar backscatter imagery of the mud volcano with the crater and mud flows characterized by a strong backscatter intensity (corresponding to dark colors).

deep Portuguese sector of the Gulf of Cadiz. Some of these features have a corresponding bathymetric expression and need testing to ascertain if they are mud volcanoes (Akhmetzhanov et al., 2007).

A selected set of samples, representative of the different lithologies collected in the stations 569Gr, 574D, 581Gr and 583G, as reported in table 2.

Cruise TTR 16

The TTR 16 Leg 2, was part of the MVSEIS Euromargins Project, and was focused on two main areas: (1) the E. Moroccan Field, and (2) the Deep Portuguese Mud Volcano field. The main objectives of this cruise were: (1) To investigate the Pen Duick Escarpment to better understand this complex feature and associated ecosystems. (2) To re-visit the Yuma and Ginsburg mud volcanoes for detailed studies. (3) To carry out detailed studies in the deep Portuguese field (Akhmetzhanov et al., 2008). The TV controlled Grab TTR 16 – 600Gr was collected on the Pen Duick Escarpment and retrieved fragments of carbonate crusts together with coral and shell debris. From this sampling station, a representative authigenic carbonate sample was selected to this study (IV27). (UNESCO, 2008).

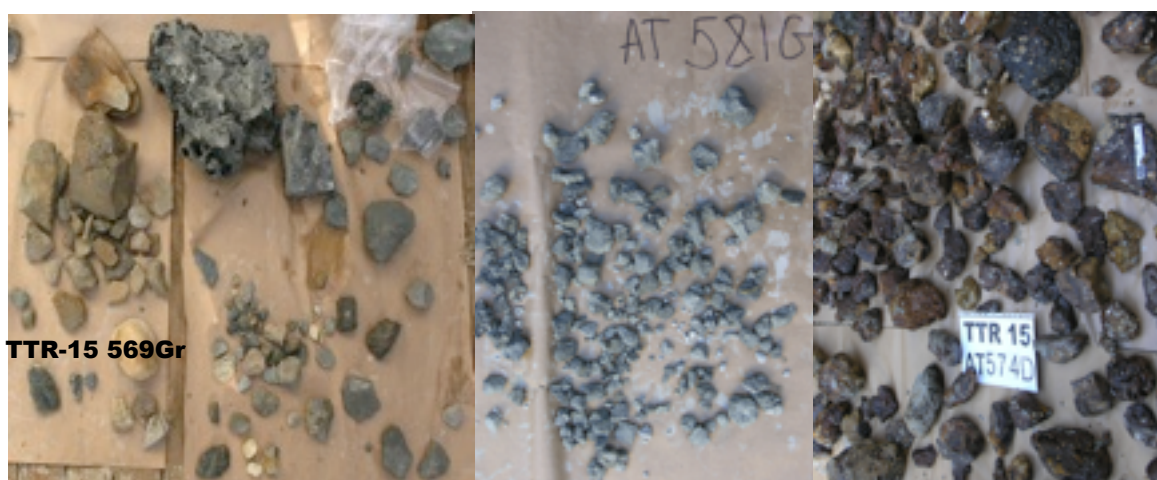



Figure 20: Onboard pictures of the samples collected on the stations 569Gr, 574D, and 581Gr, from which the representative samples IV23, IV24 and IV25, studied in this work, were collected from.

Cruise METEOR 86/5

METEOR 86/5 cruise, done onboard the RV Meteor in February and March 2012, had the objective of collect data from sites of fluid migration and escape to the

R/V Professor Logachev TTR-15		CORE AT583G							
Location:	Moroccan margin, top of Meknes mud volcano								
Latitude:	34°59,139	Date:	28.07.2005						
Longitude:	07°04,400	Recovery:	60 cm						
Water Depth:	701 m								
									
SUBSAMPLING CODES:									
<table border="1" style="width: 100%;"> <tr> <td>1- Express analysis</td> <td>3- Geochemistry</td> <td>5- Other</td> </tr> <tr> <td>2- Sedimentology</td> <td>4- Palaeontology</td> <td></td> </tr> </table>				1- Express analysis	3- Geochemistry	5- Other	2- Sedimentology	4- Palaeontology	
1- Express analysis	3- Geochemistry	5- Other							
2- Sedimentology	4- Palaeontology								

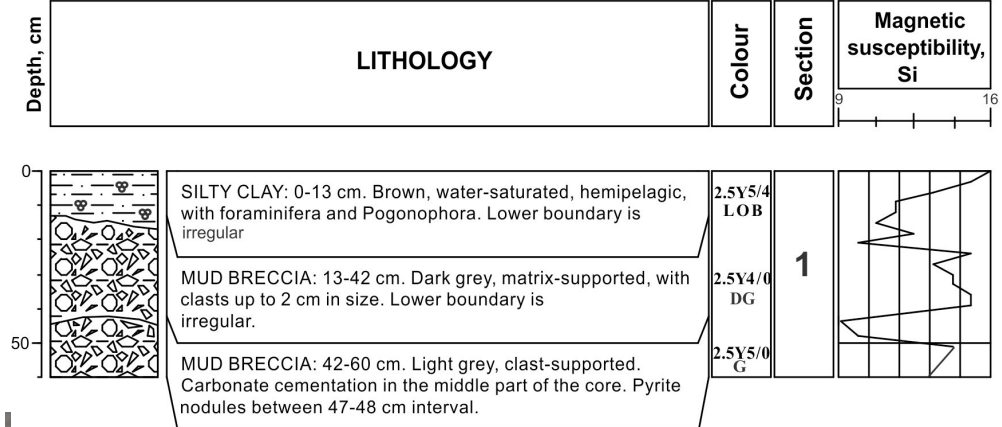


Figure 21: Core log and onboard picture of the gravity core TTR15 – 583G, from where the concretions sample IV26, that was studied in this work, was collected from

seafloor, located in the deep-sea region of the western Gulf of Cadiz and the adjacent abyssal plain. Geochemical pore water data from mud volcanoes (Porto, Bonjardim, Cap Arutyunov) which are aligned along the west-east trending



Figure 22: Onboard picture of the sample TTR 16 – 600Gr collected on Pen Duick escarpment, from which a representative samples IV27 was collected from and studied in this work.

transform faults (SWIM faults), showed that mud volcano fluids are sourced in several km depth below the seafloor. The geochemical composition of the mud volcano fluids indicates that they are affected by oceanic crust alteration, and hence implies that there is active flow connecting the oceanic basement and the seafloor. Such kind of hydrothermal circulation is only known for relatively young oceanic crust (<60 Ma). Because of the fact that “the existence of a hydrological connection between old, sedimented oceanic crust and the seafloor is a phenomenon, which essentially has not been investigated in the past, and may represent a (missing) link between hot vents at mid-ocean ridges and cold seeps at continental margins” this cruise had the objective of investigate sites along the westward trending transform faults (SWIM faults), mainly within the transition between the accretionary prism and the abyssal plain. As the sediment cover generally decreases to the west, the potential overprinting of the hydrothermal signal of seep fluids by sediment alteration processes is expected to be reduced

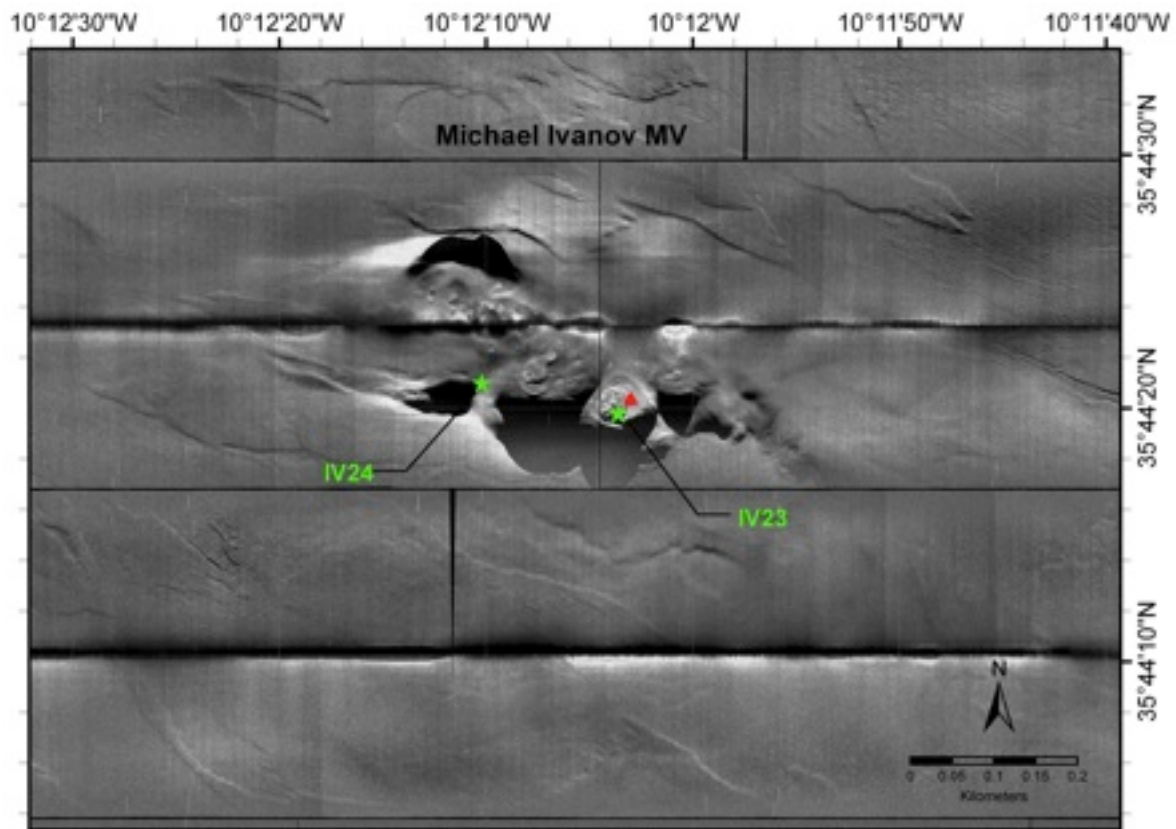


Figure 23: Location of the samples collected during the Meteor 86/5 Cruises on the Michael Ivanov mud volcano and used in this project. On the background is shown a autonomous underwater vehicle side-scan sonar backscatter imagery of the mud volcano, with multiple craters, mud flows and pockmarks.

likewise (Hensen and scientific cruise party, cruise report, in prep., Magalhães, pers.Comm.;<http://www.geomar.de/en/research/expeditionen/detail-view/exp//314699/>).

In this cruise had the participation of several researchers from the University of Aveiro and sediment samples were collected and two samples were selected and studied in the framework of this Master thesis. Authigenic carbonate samples IV20 and IV22 were collected from gravity cores: M86/5–24GC04 and M86/5–42GC10, respectively (ifigure 24). These gravity cores retrieved sequences of mud volcano mud breccia and hemipelagic sediments on the Michael Ivanov mud volcano. To be noted that on this mud volcano, another gravity core retrieved has hydrates, indicating the present-day active state of this structure with methane rich-fluids at the seafloor or very close to it.

Sediments from the top of the M.V. are formed by mud breccias, with clasts up to 4 cm in diameter (M86/5-24GC04), mainly of claystone but also including other

lithologies, such as authigenic carbonate concretions, some of which were studied in this Master project (sample IV20). They present intense H₂S smell, indicator of active anaerobic methane oxidation. The present-day active state of this structure is also reinforced by the presence of a 10x4x6 cm size gas hydrate chunk collected at shallow depth (65 to 76 cm depth) in a gravity corer. The gas hydrate chunk has a rounded shape, probably due to the melting of hydrate and subsequent formation of ice surrounding the hydrate, during the long time between recovery and sampling (Magalhães, pers. comm.). Core M86/5-42GC10, recovered at the northern crater of the mud volcano showed a sequence of silty clays and clays and an intercalation of mud breccias with very weak claystone clasts, partially dissolved into the matrix and several intervals of high authigenic carbonate content, with a carbonate concretion of 12 cm in diameter at 370-380 cm depth (sample IV22) that was studied in this Master project.

The samples analyzed in this thesis coming from the four cruises described before includes both carbonates crusts and chimneys coming from the different areas of interests of Gulf of Cadiz.

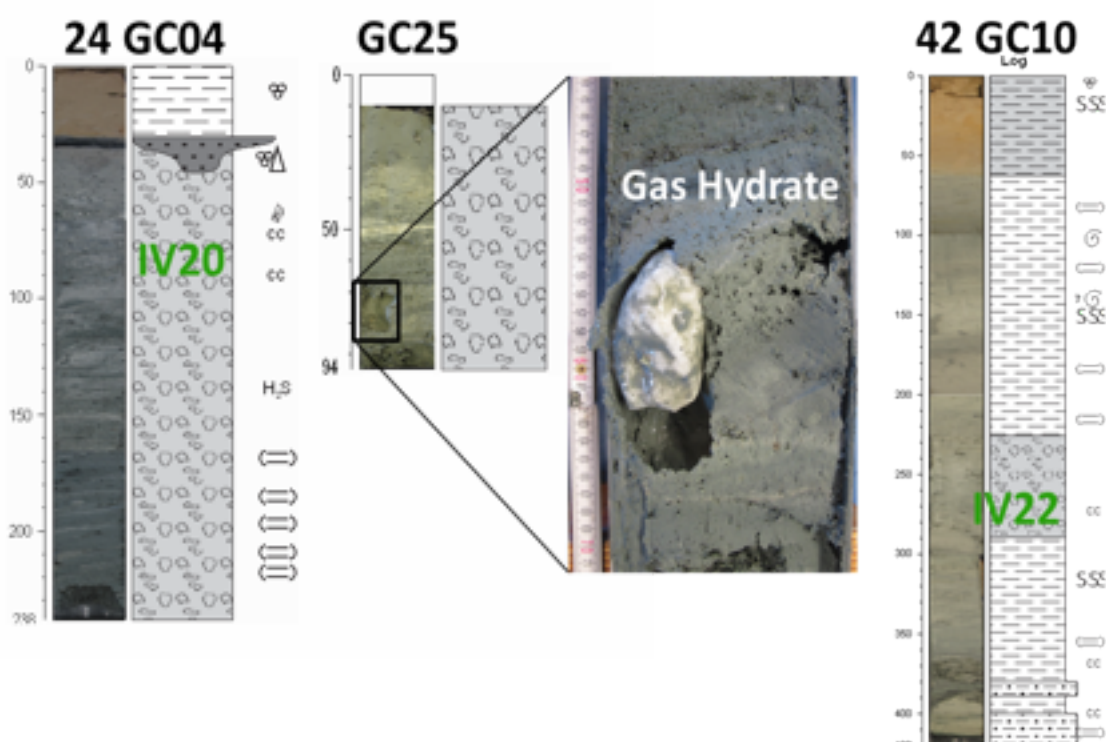


Figure 24: Gravity cores M86/5-24GC04 and M86/5-42GC10 and respective core logs from where the samples IV20 and IV22 were collected from. Gravity core M86/5-100GC25, where a gas hydrate chunk was observed, is also shown.

Chapter 5: Methods

For this work, were selected representative samples of the different lithologies collected from: the small mounds on the MOW channel in front of Gibraltar Strait, from the Vernadsky Ridge and the Pen Duick escarpment, and from the Meknes, Mercator and Michael Ivanov mud volcanoes. These samples were described macroscopically and cutted along transversal and longitudinal sections. Thin sections of the representative lithologies were prepared and their petrography described. On the concretions samples, the preparation of thin sections was not possible to be done due to the low cohesion of the samples.

Powdered sub-samples were then collected by hand micro-drill along radial and longitudinal profiles on the transversal and longitudinal cuts of the samples, and the collected powdered was used for the x-ray diffraction mineralogy, total organic carbon, carbonate content, carbon and oxygen stable isotope analysis.

All the data obtained from the different analysis have been interpreted and plots produced using three different programs: Microsoft Excel, R statistics(see Annex I) and GCDkit (GeoChemical Data kit) (see Annex II) that runs on the R platform.

5.1 Thin Sections

5.1.1 What is a geological thin section?

In many areas of geological studies such as mineralogy, petrography and sedimentology thin section preparation is the most adequate mean to examine microscopically samples of sediments, soil or rock samples. This analysis is normally carried out using transmitted polarized light of thin sections (of known and exact thickness) of the samples. Reflected light microscopy is also widely used for certain applications, in particular in the study of opaque minerals. This technique requires the surface of the sample to be flat and highly polished for the best results to be achieved. The increasing use of electron microscopes is also contributing to the need for top quality thin sections of a wide range of materials.

5.1.2 Thin Section Preparation Systems

Traditionally, this time consuming and highly skilled process was done by hand.

Recently developed automatized mechanic methods have revolutionized the process by introducing technology that automates and simplifies the preparation of thin sections - all with improved quality results, and have the following advantages:

- consistently produces high quality thin sections;
- substantially increases thin section preparation output;
- virtually eliminate the need for hand lapping & polishing;
- allows the production of thin sections of variable dimensions.

Different types of thin sections and different protocols and instruments to prepare thin sections are available. In this work, standard rock thin sections not recovered by a glass cover were produced. This type of thin section allows the standard transmitted-light petrographic observation, and allows posterior analyses of the samples by scanning electron microscopy (SEM), cathodoluminescence microscopy and ion microprobe analyses.

5.2 X-ray diffraction

X-ray diffraction (XRD) is a versatile, non-destructive technique that reveals detailed information about the chemical composition and crystallographic structure of natural and manufactured materials. On this master project, the bulk mineralogy and the relative abundance of different carbonate mineralogies was determined through X-ray diffraction (XRD) on 68 powdered sub-samples (table 3). X-ray diffraction patterns were obtained at the Laboratório de Raios-X of the Geosciences Department, using a Scintag X-ray diffractometer with CuK α radiation (1.5405 Å wavelength). Scans were done from 5° to 60° 2 θ at 0.02°/sec, using 40 kV accelerating voltage and 30 mA current. As the intensity of the diffraction pattern of a mineral in a mixture is proportional to its concentration, estimates of the relative proportions of the minerals in a sample were made by measuring their relative peak areas. Peak identification and minerals relative abundance estimation were performed using the MacDiff software package, as described above. The peak areas were measured for the main peaks of the

carbonate minerals aragonite (3.40 Å), calcite (< 8 mol% MgCO₃, 3.036 to 3.012 Å), high-Mg calcite (8 to 30 mol% MgCO₃, 3.012 to 2.946 Å), protodolomite (30 to 40 mol% MgCO₃, 2.946 to 2.916 Å) and dolomite (40 to 55 mol% MgCO₃, 2.916 to 2.871 Å). The Mg:Ca ratio of the carbonate minerals was calculated from the shift of the d-spacing of the (104) reflection peak of calcite and dolomite from the stoichiometric peaks positions in the diffraction spectra (Goldsmith and Graf, 1958; Lumsden, 1979).

5.2.1 X-ray Generation and Properties

X-rays are electromagnetic radiation with typical photon energies in the range of 100 eV - 100 keV. For diffraction applications, only short wavelength x-rays (hard x-rays) in the range of a few angstroms to 0.1 angstrom (1 keV - 120 keV) are used. Because the wavelength of x-rays is comparable to the size of atoms, they are ideally suited for probing the structural arrangement of atoms and molecules in a wide range of materials. The energetic x-rays can penetrate deep into the materials and provide information about the bulk structure.

X-rays are produced by either x-ray tubes or synchrotron radiation. In a x-ray tube, source used in x-ray diffraction instruments, x-rays are generated when a focused electron beam, accelerated across a high voltage field, bombards a stationary or a rotating solid target. As electrons collide with atoms in the target and slow down, a continuous spectrum of x-rays are emitted, which are termed Bremsstrahlung radiation. The high energy electrons also eject inner shell electrons in atoms through the ionization process. When a free electron fills the shell, an x-ray photon with energy characteristic of the target material is emitted. Common targets used in x-ray tubes include Cu and Mo. In recent years synchrotron facilities have become widely used as preferred sources for x-ray diffraction measurements. Synchrotron radiation is emitted by electrons or positrons traveling at near light speed in a circular storage ring (Youli Li, 2002).

5.2.2 Lattice Planes and Bragg's Law

When x-ray photons collide with electrons in atoms, some photons from the incident beam will be deflected away from the direction where they originally

travel. If the wavelength of these scattered x-rays do not change in energy level, the process is called *elastic scattering* (Thompson Scattering) in that only momentum has been transferred in the scattering process. These are the x-rays that we measure in diffraction experiments, as the scattered x-rays carry information about the electron distribution in materials. On the other hand, in the *inelastic scattering* process (Compton Scattering), x-rays transfer some of their energy to the electrons and the scattered x-rays will have a different wavelength than the incident x-rays. Diffracted waves from different atoms can interfere with each other and the resultant intensity distribution is strongly modulated by this interaction. If the atoms are arranged in crystals, the diffracted waves will consist of sharp interference maxima (peaks) with the same symmetry as in the distribution of atoms. Measuring the diffraction pattern therefore allows us to deduce the distribution of atoms in a material.

The peaks in a x-ray diffraction pattern are directly related to the atomic distances. For a given set of lattice planes with an inter-plane distance of d , the condition for a diffraction (peak) to occur can be simply written as $2 d \sin \theta = n \lambda$ which is known as the Bragg's law. In the equation, λ is the wavelength of the x-ray, θ the scattering angle, and n an integer representing the order of the diffraction peak. The Bragg's Law is one of most important laws used for interpreting x-ray diffraction data.

It is important to point out that although we have used atoms as scattering points in this example, Bragg's Law applies to scattering centers consisting of any periodic distribution of electron density.

5.2.3 Powder Diffraction

Powder X-ray Diffraction (XRD) is perhaps the most widely used x-ray diffraction technique for characterizing materials. The sample is usually in a powdery form, consisting of fine grains of the crystalline material to be studied. The technique is used also widely for studying particles in liquid suspensions or polycrystalline solids (bulk or thin film materials). The term 'powder' really means that the crystalline domains are randomly oriented in the sample. The positions and the

intensities of the peaks are used for identifying the underlying structure (or phase) of the material. Powder diffraction data can be collected using either transmission or reflection geometry. The peak positions, intensities, widths and shapes all provide important information about the structure of the material.

5.2.4 X-ray Crystallography

In particular in this thesis is used the X-ray crystallography that is a standard technique for solving crystal structures. In recent years, the advent of synchrotron radiation sources, area detector based data collection instruments, and high speed computers has dramatically enhanced the efficiency of crystallographic structural determination. In x-ray crystallography, integrated intensities of the diffraction peaks are used to reconstruct the electron density map within the unit cell in the crystal. To achieve high accuracy in the reconstruction, which is done by Fourier transforming the diffraction intensities with appropriate phase assignment, a high degree of completeness as well as redundancy in diffraction data is necessary, meaning that all possible reflections are measured multiple times to reduce systematic and statistical error (Youli Li, 2002).

5.2.5 MacDiff 4.2.6

In this work, the diffractograms obtained for each sample have been interpreted using the MacDiff 4.2.6 interpretation software. It is a program for the analysis and display of X-ray powder diffractograms running on Apple Macintosh platforms. It offers conventional XRD profile-correction processes (e.g. outliers, smoothing, divergence, alpha²-stripping) and supports qualitative and quantitative mineral composition. MacDiff also supports methods of peak fits and peak decomposition of coinciding lines. The user has at his disposal the capability of continuous measurement checks and the possibility to perform corrections as well (e.g. by manual or computed back- ground adaptations). For peak indication the user has the option to employ variable peak data sets. High resolution hardcopies of the diffractograms can be produced. Data and plots can be exported to most of the available table-processing or vector-graphics programs. The applications of MacDiff range from routine analysis in sedimentology, especially clay minerals, over analysis of X-ray diffractograms of all types of rocks and minerals all the way

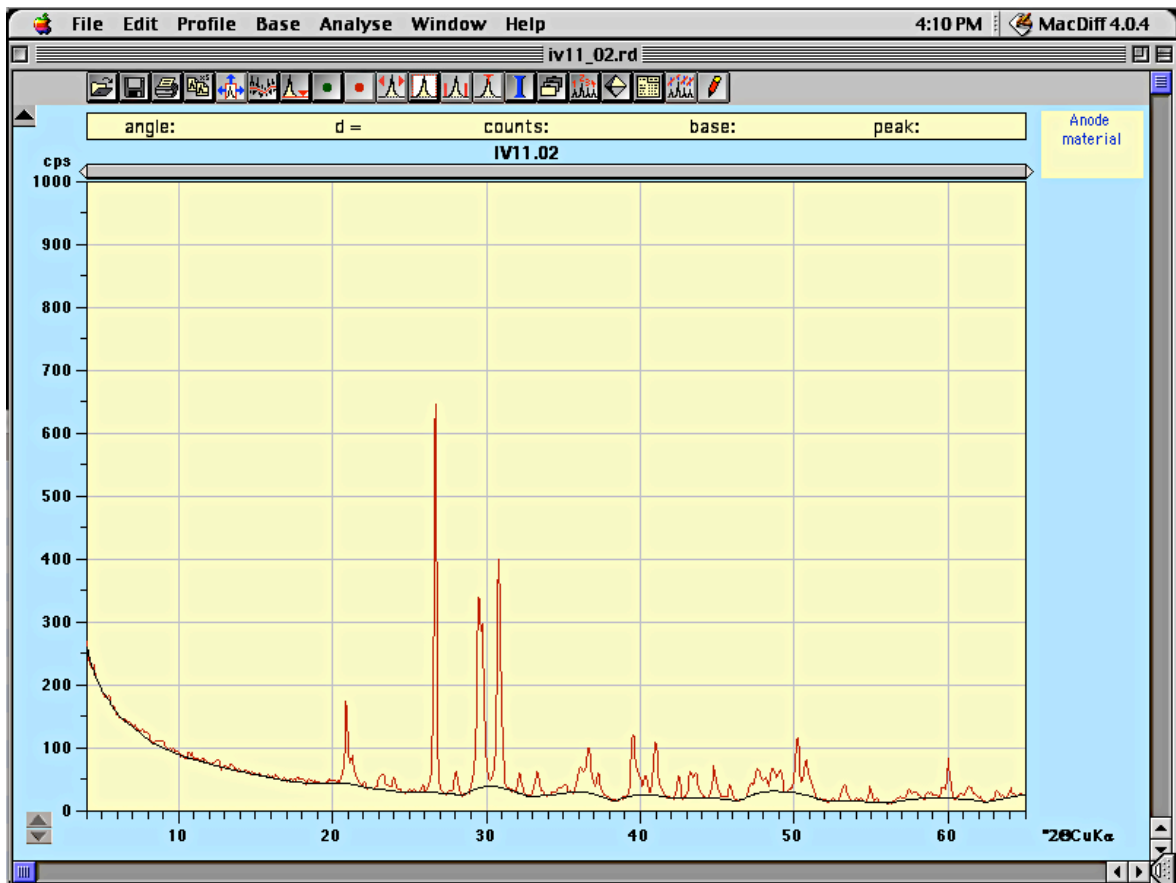


Figure 25: MacDiff 4.0.4 screenshot. Example of visualization.

to phase analysis of various crystalline substances.

MacDiff is a freeware software and is available together with the most minerals PDF databases, free of charge. It may be copied and distributed without restrictions for non-profit and non-commercial use. (<http://www.geol-pal.uni-frankfurt.de/Staff/Homepages/Petschick/PDFs/MacDiff%20Manual%20E.pdf>).

In this Master project, MacDiff was employed for the analysis of all the 60 diffractograms on a Apple Macintosh platforms.

Interpretation steps

To have a correct interpretation of the diffractograms, in this work, I followed the sequence of processing and interpretation steps as described below.

After opening the file (on the top menu *File*--->*Open*) the raw diffraction profile was smoothed, using the *smooth counts* function. It cleans the diffractograms from the high frequency instrument noise and produces clear and well defined the peaks. Then I computed the baseline through the *show baseline* command, it will calculates the baseline of the diffractogram that define the base of the peaks for

further area calculations.

After this step, I corrected the peaks position using has standard the Quartz, syn $d=3.343$. To do this, we plot the quartz profile using the Quartz (syn $d=3.343$) *peak that naturally occurs in all the analyzed samples, as a standard*. For this step, we have to search on the minerals database the quartz mineral record and plotted his profile on the diffractogram using the *Draw* command. Then identifying and selecting the diffractograms main peak of Quartz, we use the function “*peak correction*” in the menu *Profile*, it opens a selection windows with the different options of correction, where we select “*quartz, d=3.343*” peak correction. The program, based on the standard data selected, shift the entire diffractogram in order to adjust the selected quartz peak with his theoretical position. After his step, we start with the interpretation of all the main peaks present, sequentially following their relative intensity importance. When all of the main peaks have been interpreted and all the minerals identified, we saved the interpreted file as new file.rd and saved the interpretation and quantification report. This report stores all the relevant information: mineral phase, main peak position, peak area, peak intensity and width at half of the high of the peak. This data was then imported into a spreadsheet table and used to calculate the relative abundance of the different minerals, the magnesium content on calcite, Mg-calcite, protodolomite and dolomite minerals, as will be showed later.

5.3 Geochemistry

5.3.1 LECO C, O, N and S elemental analysis

The carbonate and the organic carbon were determined using a LECO CHNS-932 elemental analyzer. Three replicates of powdered and homogenized bulk material (2 mg), collected with a micro-drill, were analyzed per sub-sample. The same set of sub-samples was later subjected to combustion for 8 h through a predefined stepwise increase in temperature up to 400°C, to remove organic carbon, and re-analyzed for inorganic carbon. The organic carbon content (C_{org}) was determined by the difference between total carbon and the inorganic carbon concentration. Results are presented in weight percent (wt%). The relative precision of repeated measurements of both samples and standards was 0.03 wt%.

5.3.2 Carbon and Oxygen Isotopes

The study of the isotopes of carbon ($^{13}\text{C}/^{12}\text{C}$) and oxygen ($^{18}\text{O}/^{16}\text{O}$) permit to have important informations about the paleoenvironmental conditions of the formation of the rocks. It can give information about the temperature, the conditions of formation and the different origins of the chemicals and elements that are being precipitated and form the rocks. Based on those informations and on the results of the isotopic ratios, it is possible to classify the different carbonates components and to correlate the different carbonate minerals with their formation conditions. The variations in the ratio of the isotopes, $^{18}\text{O}/^{16}\text{O}$ e $^{13}\text{C}/^{12}\text{C}$, are calculated using an high precision mass spectrometer. The results are reported in the conventional δ ‰ notation with reference to VPDB (Vienna Peedee Belemnite). The δ value is defined as the per mil proportion of the isotopic ratio measurement of a sample over the isotopic ratio of a standard sample, according to the equation:

$$\delta A = \left(\frac{R_{\text{sample}} - R_{\text{standard}}}{R_{\text{standard}}} \right) \frac{1}{A} * 1000$$

A decrease of the δ values of the samples corresponds to an increase in the amount of light isotopes (^{16}O and ^{12}C) in relation to the standard. Otherwise an increase of the δ values of the samples means an increase in heavy isotopes (^{18}O and ^{13}C) in respect to the standard (Hudson 1977; Anderson & Arthur 1983; Marshall 1992; Corfield 1995, Fairchild et al. 1988). For example, a $\delta^{18}\text{O}$ value of +15‰ indicates that the sample is enriched in ^{18}O by 15 parts per thousand relative to the standard.

The $\delta^{18}\text{O}$ of a water carbonic precipitate depends from the composition of the carbonate and on the temperature of formation. Usually, negative $\delta^{18}\text{O}$ values are associated with precipitation from low salinity fluids and with formation temperatures (Hudson 1977).

The composition of $\delta^{13}\text{C}$ of carbonate precipitates reflect the different sources of bicarbonate dissolved in the water. These sources can include: sea water ($\delta^{13}\text{C}$

around 0 ‰), dissolution of carbonate skeletons ($\delta^{13}\text{C}$ around 0 ‰), alteration and dissolution processes of the soil ($\delta^{13}\text{C}$ around -10 ‰), bacteria oxidation and sulfate reduction in organic matter ($\delta^{13}\text{C}$ around -25 ‰), bacteria methanogenic fermentation ($\delta^{13}\text{C}$ around +15 ‰), methane oxidation ($\delta^{13}\text{C}$ between -50 and -80 ‰), and abiotic reactions associated with thermic fracturation and decarboxylation ($\delta^{13}\text{C}$ between -10 and -25 ‰) (Hudson, 1977; Irwin et al., 1977; Coleman, 1993; Mozley & Buns, 1993).

Therefore, carbonates that precipitates in isotopic equilibrium (or almost in equilibrium) with their formation fluids show characteristic ^{18}O and ^{13}C compositions that reflect, in a reasonable way, their formation environment. However for skeleton types of carbonates there are two potential problems that have to be considered present: the *vital effects* and the possibility of a state of isotopic disequilibrium in the precipitation (Hudson 1977; Swart 1983).

In this work, Carbon and Oxygen isotopic composition of the samples were measured on the same powdered sub-samples that were used for XRD and LECO analysis. The samples were analyzed at the MARUM Centre of the University of Bremen, in Germany. Samples for carbon and oxygen stable isotopic analyses were prepared by reacting at 90°C with 100% phosphoric acid on an automated carbonate device connected to a VG-PRISM mass spectrometer calibrated with NBS19, NBS 18 and NBS 20. The results are reported in the conventional δ ‰-notation with reference to VPDB (Vienna Peedee Belemnite). Analytical reproducibility of the method, based on repeated standards is better than $\pm 0.1\%$ for both carbon and oxygen. For temperature calculations of the dolomite samples, dolomite $\delta^{18}\text{O}$ values were corrected for the analytical offset of +1.63‰, consequence of the unequal oxygen fractionation during the reaction to CO_2 (Rosenbaum and Sheppard, 1986).

5.4 Scanning Electron Microscopy (SEM)

The scanning electron microscope (SEM) uses a focused beam of high-energy electrons to generate a variety of signals at the surface of solid specimens. The signals that derive from electron-sample interactions reveal information about the

sample including external morphology (texture), chemical composition, and crystalline structure and orientation of materials making up the sample. In most applications, data are collected over a selected area of the surface of the sample, and a 2-dimensional image is generated that displays spatial variations in these properties. Areas ranging from approximately 1 cm to 5 microns in width can be imaged in a scanning mode using conventional SEM techniques (magnification ranging from 20X to approximately 30,000X, spatial resolution of 50 to 100 nm). The SEM is also capable of performing analyses of selected point locations on the sample; this approach is especially useful in qualitatively or semi-quantitatively determining chemical compositions, crystalline structure, and crystal orientations.

5.4.1 Fundamental Principles of Scanning Electron Microscopy (SEM)

Accelerated electrons in an SEM carry significant amounts of kinetic energy, and this energy is dissipated as a variety of signals produced by electron-sample interactions when the incident electrons are decelerated in the solid sample. These signals include secondary electrons (that produce SEM images), backscattered electrons (BSE), diffracted backscattered electrons (EBSD that are used to determine crystal structures and orientations of minerals), photons (characteristic X-rays that are used for elemental analysis and continuum X-rays), visible light (cathodoluminescence or CL), and heat. Secondary electrons and backscattered electrons are commonly used for imaging samples: secondary electrons are most valuable for showing morphology and topography on samples and backscattered electrons are most valuable for illustrating contrasts in composition in multiphase samples (i.e. for rapid phase discrimination). X-ray generation is produced by inelastic collisions of the incident electrons with electrons in discrete orbitals (shells) of atoms in the sample. As the excited electrons return to lower energy states, they yield X-rays that are of a fixed wavelength (that is related to the difference in energy levels of electrons in different shells for a given element). Thus, characteristic X-rays are produced for each element in a mineral that is "excited" by the electron beam. SEM analysis is considered to be "non-destructive"; that is, x-rays generated by electron interactions do not lead to volume loss of the sample, so it is possible to analyze

the same materials repeatedly.

5.4.2 Applications

The SEM is routinely used to generate high-resolution images of shapes of objects (SEI) and to show spatial variations in chemical compositions:

1. acquiring elemental maps or spot chemical analyses using EDS,
2. discrimination of phases based on mean atomic number (commonly related to relative density) using BSE,
3. compositional maps based on differences in trace element "activators" using CL.

The SEM is also widely used to identify phases based on qualitative chemical analysis and/or crystalline structure. Precise measurement of very small features and objects down to 50 nm in size is also accomplished using the SEM. Backscattered electron images (BSE) can be used for rapid discrimination of phases in multiphase samples. SEMs equipped with diffracted backscattered electron detectors (EBSD) can be used to examine microfabric and crystallographic orientation in many materials.

In our case the SEM analysis should be performed on the thin sections.

Chapter 6: Results

6.1 Samples description

Based on the morphology, the macroscopic characteristics and the mineralogy, the following three different types of authigenic carbonates have been defined for the studied samples from the Gulf of Cadiz: chimneys, crusts and concretions.

6.1.1 Chimneys

The chimneys have been characterized on their color, dimensions, morphologies, cohesion and bioturbation (Figure 26). Based on these parameters the samples have been divided in two main groups.



Figure 26: Examples of chimneys samples from TTR-14.

One group is composed of chimney fragments, usually of brown-yellow-okra colors and more rarely with grayish colors. Those chimney fragments of grayish colors present, in general, a low or mean cohesion level and at the touch are “sandy”, very porous and have irregular morphologies. On these samples the bioturbation is low or inexistent.

The second group is composed by pipe-like chimneys. The samples of this group show very dark-reddish colors on the samples exterior and have interiors of very light and yellowish colors. These color variations is interpreted as resulting from the oxidation of minerals (such as pyrite) due to the oxygenated seawater contact of the samples. This process is evident in some samples that exhibit oxidation fronts spreading out from the exterior of the sample and from the open holes of burrows where seawater was in contact with. The morphology of the chimneys is in general very constant and regular with pipe-like shape, in some of the cases. They are very well cemented, very consolidated and hard, also in the inner part.

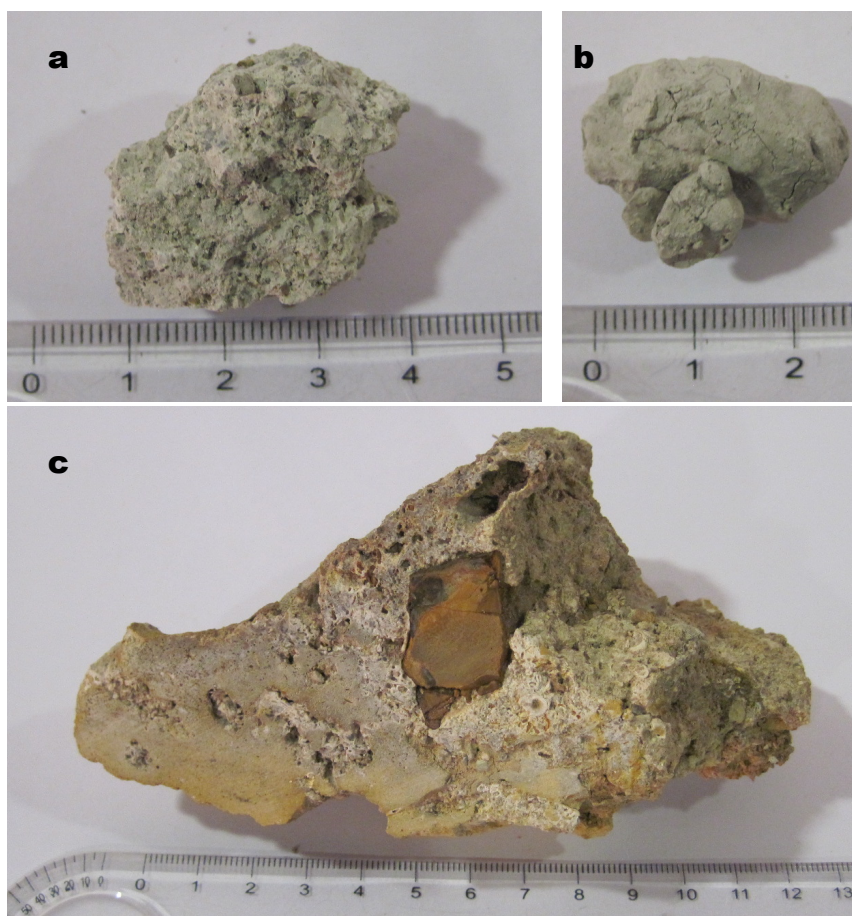


Figure 27: Examples of two crusts (a and c) and a concretion (b).

On this type of samples the levels of bioturbation are very high, when compared with the chimney fragments type. In some of the chimneys colonization of the exterior part of the chimney by different types of benthic fauna, is frequent and sometimes, very densely colonized.

The dimensions of the chimneys are very variable, ranging from a few centimeters up to 30-40 cm long and with diameters up to 30 cm.

6.1.2 Concretions

The concretions have all been collected from mud volcanoes. They consist in a semi consolidated mud volcano mud breccias, cemented by carbonate minerals. They have a grey color, in general a lighter grey. The concretions are not well consolidated and are in general very friable and are easily desegregated by hand or with a spatula. Concretions have in general irregular or nodular shapes (Figure 27b).

6.1.3 Crusts

Carbonate crust samples are very similar between them. They are grayish, very porous, and frequently show reddish intrusions or darker spots (Figure 27a and 27c).

Once all the different samples were described and all the typologies defined, selected specimens representative of all the different lithologies were further analyzed. Sub-samples of the selected samples were collected whenever changes in the composition, color, structure or texture were identified. Sub-samples were collected along transversal or radial cuts on the samples where slices were collected for thin section preparation and petrographic microscopy observations and powdered sub-samples were collected with a hand micro-drill and further analyzed for x-ray diffraction mineralogy, total organic carbon and carbonate content, carbon and oxygen stable isotopic composition.

In the photos of Figure 28 is showed the location of the sub-samples drilling points of the chimneys samples. The concretions are homogeneous so all the sub-samples of each sample are representative of the entire sample.



Figure 28: Scans of the sample 600 G and the cutted surface of the chimneys samples. On that have been identify the sub sampling point.

6.2 Petrography

The petrographic observation and interpretation was done on thin sections of the chimneys samples. The preparation of thin sections of the concretions and crusts was technically very difficult, due to the low cohesion of the samples that were not able to be efficiently polish, and therefore these samples were not described under the petrographic microscope.

Petrographic characterization of chimneys

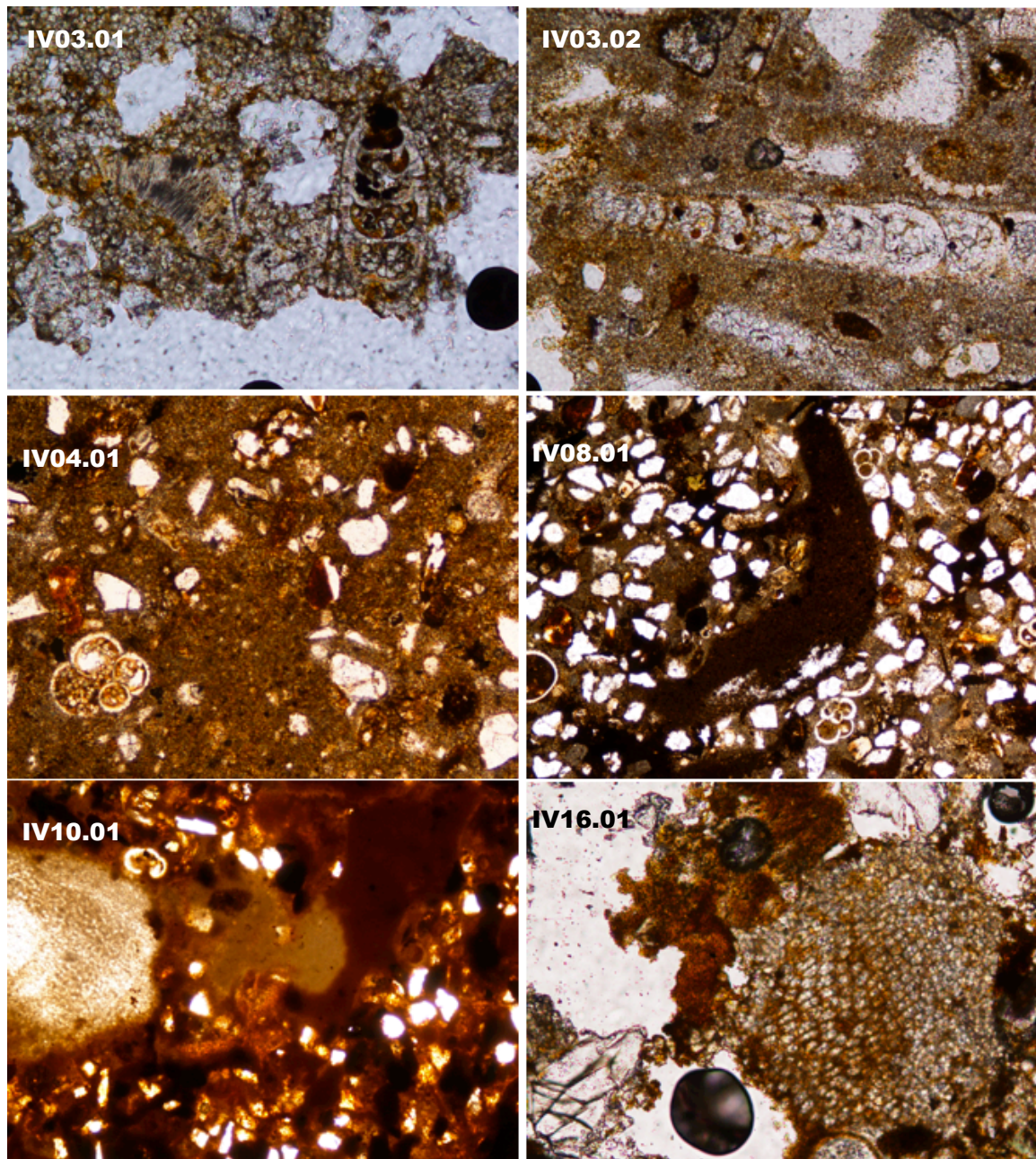


Figure 29: Microscope photos show examples of different textures of the thin sections. From the top: IV03.01, IV03.02, IV04.01, IV08.01, IV11.01 and IV16.01.

- *IV03_01*: intramicrite, very homogeneous texture, with a sandy matrix and very rare organic clasts of shell fragments. The cement is micritic. Bioclasts of foraminifera and shell fragments (gastropods) are rare.
- *IV03_02*: Very different texture than the observed in sample *IV03_01*, the matrix is very dark, difficult to light penetration. It corresponds to a sparse biomicrite, with abundant foraminifera bioclasts, higher than sample *IV03_01*, but not enough to define it as a packed biomicrite. Detrital quartz grains were identified as also some green and others yellow-reddish detrital grains. The bioclasts consist of foraminifera, gastropods and mollusk shell fragments.
- *IV04_01*: Texture corresponds to a wachestone with abundant detrital grains and some bio-clasts inside a homogeneous micritic matrix, with slightly changes in color, from orange to gray. Bioclasts are composed of foraminifera, shell fragments, gastropod, calcispheres and coccolitophoridae.

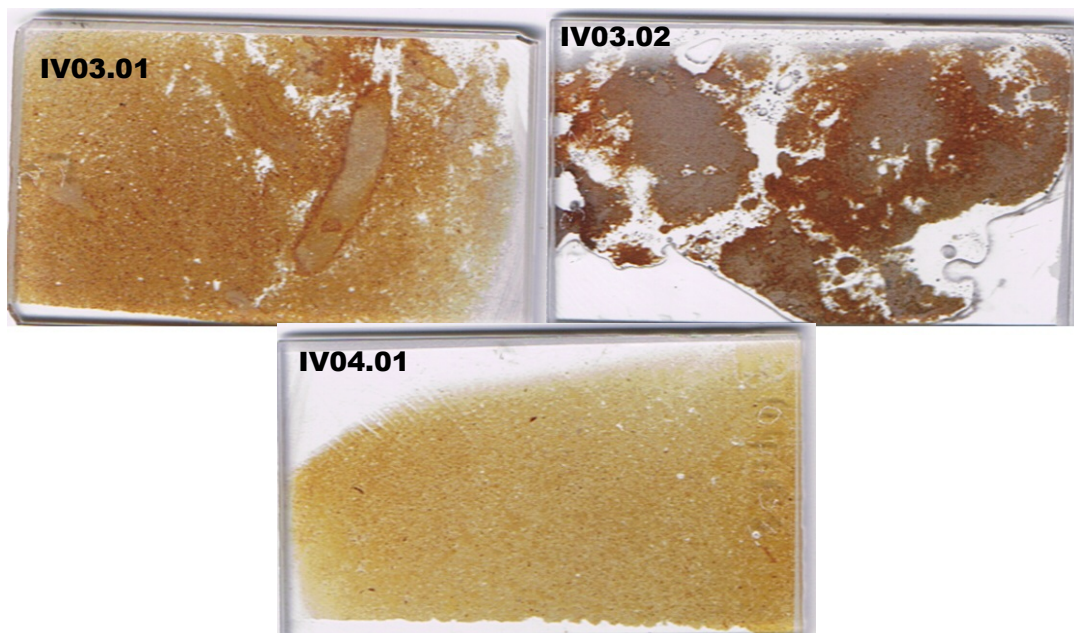


Figure 30: Scans of the thin section IV03.01, IV03.02 and IV04.01.

- *IV04_02*: Intramicrite to packed biomicrite texture with a lot of bioclasts, with some pellets. High variety of detrital grains of variable mineralogy. Bioclasts

include foraminifera, shell fragments, gastropod, coccolitophoridae, calcispheres and radiolarian.

- *IV08_01*: This sample has non homogeneous texture, ranging from fossiliferous micrite to packed bio-micrite. Bioclasts, detrital grains are very abundant. The matrix is very fine and of dark brown color. Is possible to recognize changes in color and composition along the thin section, the matrix became gray and the texture became more uniform; probably those areas result from intrusions of clayish material or result from sediment bioturbation. Considering the detrital grains, they are both single minerals and poly-mineral rocks fragments. Several different crystalline detritals are observed. The bioclasts observed in this thin section are foraminifera, coccolitophoridae, gastropods, shell fragments (bivalve), echinoderms.
- *IV09_01*: The texture of this sample is very similar to sample *IV08_01*. Has a variable texture, ranging from fossiliferous micrite to packed bio-micrite. It is possible to distinguish high amount and largely variable bioclasts, rock clasts, detrital minerals, in a brown-beige micritic matrix with sparse pelets. Speaking about the detrital minerals and rocks fragments, is possible to observe in this sample several different grains of variable forms and colors: yellow, semi transparent, reddish, greenish, darkish particles with homogeneous structures pellets and probably remains of organic matter, “filamentous” structure or crystalline polygonal structure. The observed bioclasts include foraminifera, coccolitophoridae, gastropods, shell fragments (bivalve), calcispheres, radiolarians.
- *IV10_01*: Has a packed bio-micrite texture, with detrital grains, rock fragments and abundant bioclasts in a micritic matrix. Different detrital grains with variable forms and colors can be observed: yellow, semitransparent, reddish, greenish, darkish particles with homogeneous structures, “filamentous” structure or crystalline polygonal grains. The bioclasts are of foraminifera, coccolithophores, gastropods, shell fragments and radiolarian.

- *IV11_01*: The texture is very variable, not uniform along the thin section, ranging from packed bio-micrite to fossiliferous micrite and intramicrite. The detrital grains are variable in composition and abundance, such as the bioclasts. The matrix is very fine (micritic) with a dark brown color. It is possible to see in various parts of the thin section that the matrix changes in color and composition, locally becoming grayish; probably those areas are the result of clay intrusions or from bioturbation. Considering the detrital grains and the rock fragments, it is possible to observe in this sample several distinct grain shapes and compositions: yellow, semi-transparent, greenish, darkish grains with homogeneous structures, “filamentous” structure or very angular shapes. The bioclasts are composed of foraminifera, coccolithophoridae, gastropods, shell fragments (bivalve).

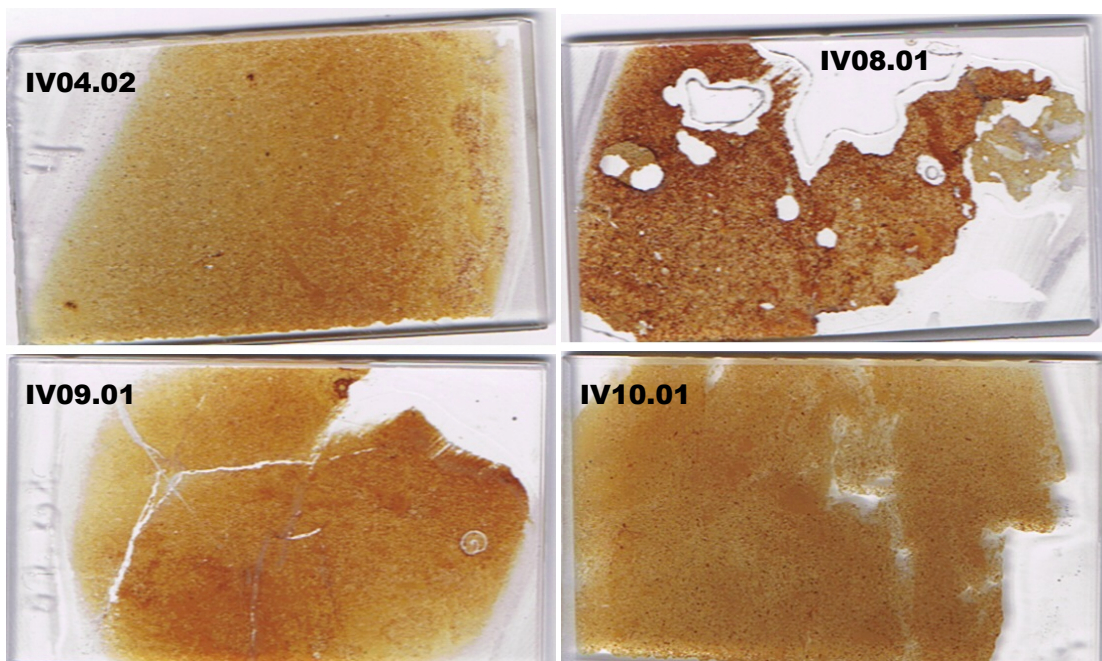


Figure 31: Scans of the thin sections IV04.02, IV08.01, IV09.01 and IV10.01.

- *IV14_01*: This sample has a packed bio-micritic texture, and the detrital grains are composed predominantly by rock fragments and mono-mineral detrital grains. The clasts have a high grain size than the previous samples. The matrix is micritic, of dark color, with some pellets and probably remains of organic

matter. Bioclasts are predominantly foraminifera tests but are very scarce.

- *IV16_01*: This sample has a packed bio-micrite texture; clasts are almost entirely composed of bioclasts. The matrix of this sample is micritic, variable in color, ranging from grayish to brownish and dark colors. Bioclasts are composed of foraminifera tests, coccolitophoridae, gastropods, shell fragments (bivalve), radiolarian, algae residuals, spicules, Bryozoa.
- *IV19_01*: The texture is ranges from intramicrite up to a packed bio-micrite texture. In most area of the thin section predominates the presence of angular detrital grains of rocks fragments and mono-mineral detrital clasts. In other areas of the thin section bioclasts, mainly foraminifera tests, predominate. The matrix is micritic and of brownish-dark color.

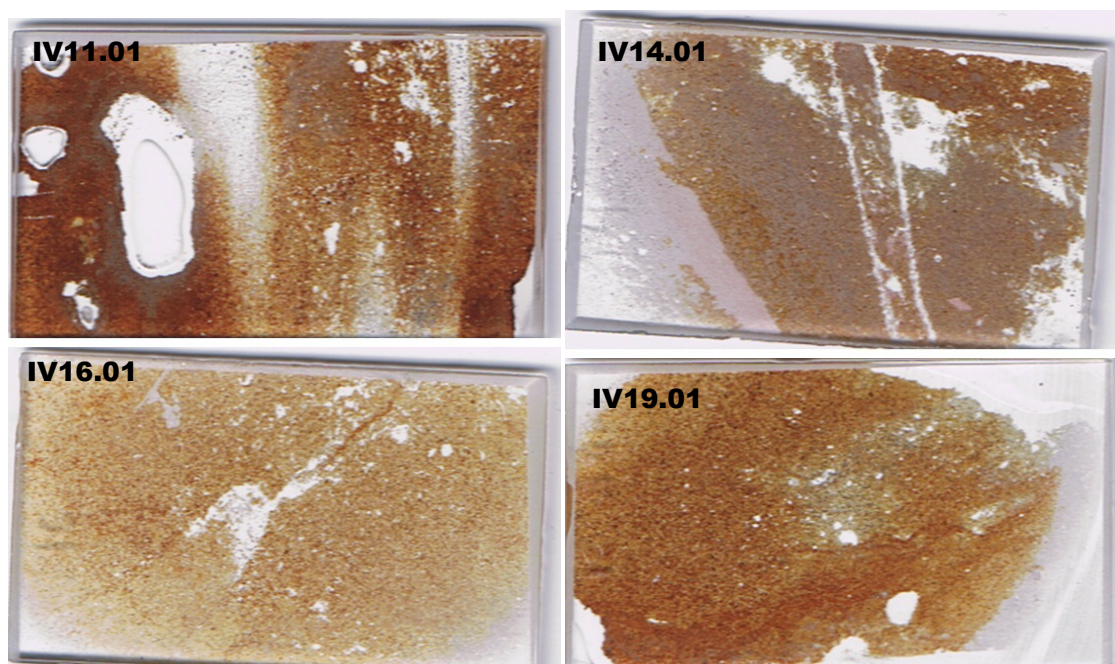


Figure 32: Scans of the thin sections for the sampels *IV11.01*, *IV14.01*, *IV16.01* and *IV19.01*

All the samples have a significant porosity. Different types of porosity can be distinguished, from intra granular to inter granular porosity.

Most of the samples exhibit evidences of the initial phases of typical diagenesis process such as grain compaction, the recrystallization of foraminifera tests in the

inside chambers walls, cementation, chemical compaction and fracturing.

6.3 XRD

6.3.1 Total Mineral Composition

All the results of XRD has been elaborated and interpreted using the software MacDiff. In figure 33 is possible illustrated to see an example of the MacDiff interpretation window of the diffractograms that has been done to have the results illustrated. The data obtained from MacDiff has been elaborated imported and analyzed with Excel spreadsheet and plotted in R to obtain comparative data.

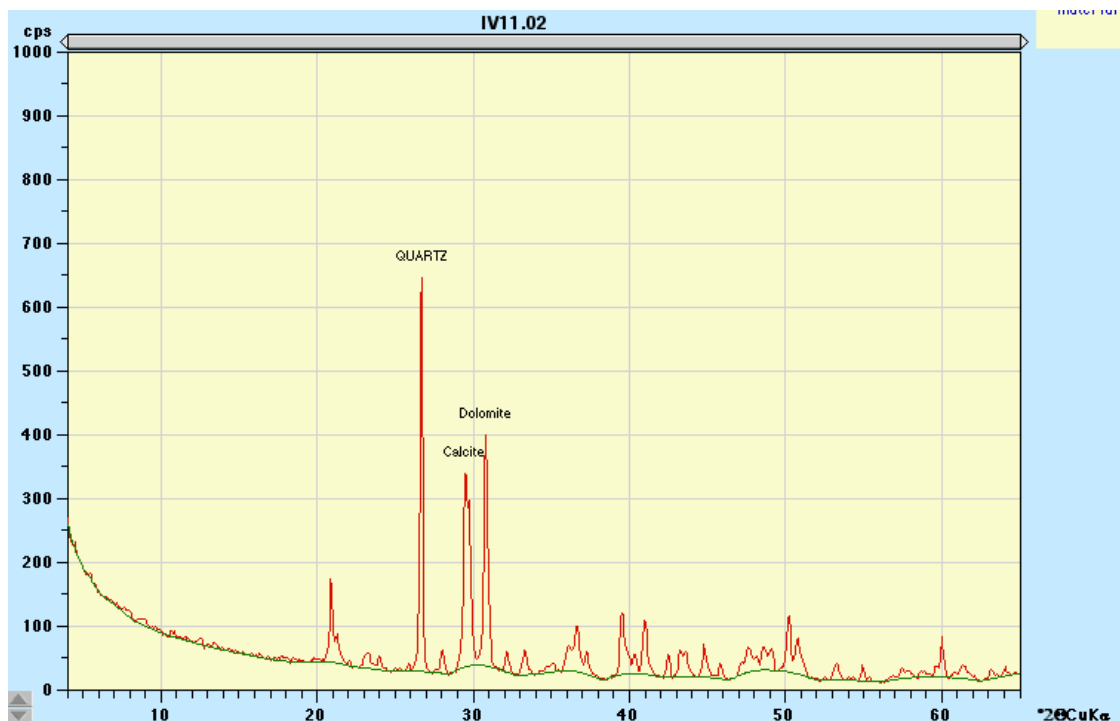


Figure 33: Example of diffractogram in Macdiff showing the peaks for calcite, dolomite and quartz

6.3.1.1 Chimneys

From the mineralogy analyzed with the XRD is possible to notice that, the three types of carbonates defined based on their morphology and macroscopic characterization are also well recognizable characterized by a distinct mineralogy. As show in figure 34 with the box plots graphs, the chimneys show, in the major part in general, high level abundance of dolomite with a range between 20% and

Table 3: Resume of results analysis from XRD, LECO and isotopes for all the samples

Sample ID	Arag _(XRD) (wt%)		Calc _(XRD) (wt%)		Dol _(XRD) (wt%)		Detr _(XRD) (wt%)		CaCO _{3(XRD)} (wt%)		CaCO _{3(LECO)} (wt%)		TOC _(LECO) (wt%)		d(104)		CaCO ₃ fraction (wt%)				δ ¹³ C _‰ (VPDB)	δ ¹⁸ O _‰ (VPDB)		
															Calc	Dol	Calc	Dol	Calc	Arag	Dol			
IV03.03			11.37	59.15	29.48	70.52	67.18	0.08	3.03	2.90	1.01	45.64	16.12	83.88	-9.00	4.66								
IV03.04			12.44	56.79	30.77	69.23	67.15	0.08	3.03	2.90	1.68	45.64	17.96	82.04	-9.04	4.62								
IV03.05			13.61	49.32	37.07	62.93	60.75	0.07	3.03	2.90	0.34	44.97	21.63	78.37	-8.21	4.07								
IV03.06			13.61	49.32	37.07	62.93	67.18	0.08	3.03	2.90	0.34	44.97	21.63	78.37	-9.64	4.85								
IV03.07			12.18	45.82	42.00	58.00	61.96	0.07	3.03	2.90	1.01	44.97	20.99	79.01	-8.16	3.67								
IV04.02	3.49		17.19	52.50	26.82	73.18	67.64	0.08	3.03	2.90	2.35	45.64	4.77	23.49	-9.13	4.39								
IV04.03			17.65	44.83	37.52	62.48	73.43	0.09	3.03	2.90	1.68	45.97	28.25	71.75	-11.47	4.90								
IV04.04				72.70	27.30	77.78	77.78	0.09		2.90		45.97	100.00		-21.92	5.44								
IV04.05			6.82	59.29	33.88	66.12	72.98	0.09	3.03	2.90	1.01	45.97	10.32	89.68	-21.34	5.30								
IV04.06				7.11	92.89	7.11	54.42	0.07		2.90		45.64	100.00		-0.60	2.48								
IV08.02	9.89		48.54	41.58	58.42	60.37	0.07	3.03	0.34			16.92	83.08		-3.92	4.19								
IV08.03	3.16		23.38	23.03	50.43	49.57	62.79	0.08	3.03	2.90	1.01	44.30	47.17	46.46	-2.71	3.56								
IV09.02	4.31		11.51	46.45	40.46	62.26	68.51	0.08	3.03	2.90	0.34	45.64	6.92	18.48	-20.54	4.41								
IV09.03	3.75		13.87	41.92	40.46	59.54	69.92	0.08	3.03	2.90	1.01	45.64	6.31	23.29	-19.06	4.35								
IV10.02				60.08	39.92	60.08	71.49	0.09		2.90		45.64	100.00		-21.31	5.97								
IV10.03				53.20	46.80	53.20	68.68	0.08		2.90		44.97	100.00		-21.84	5.89								
IV11.02			29.18	21.71	49.12	50.88	59.98	0.07	3.03	2.91	1.68	42.95	57.34	42.66	-10.00	3.13								
IV11.03			30.92	22.20	46.88	53.12	63.99	0.08	3.03	2.91	2.35	42.95	58.20	41.80	-11.67	3.49								
IV11.04			30.19	20.49	49.31	50.69	64.75	0.08	3.01	2.91	8.39	42.95	59.57	40.43	-9.70	3.30								
IV14.02			14.34	40.44	45.21	54.79	62.51	0.08	3.03	2.91	1.01	41.95	26.18	73.82	-12.18	3.99								
IV14.03			27.63	28.03	44.33	55.67	61.66	0.08	3.03	2.91	1.68	41.95	49.64	50.36	-7.80	3.19								
IV16.02	6.47		50.09	43.43	56.57	60.37	0.07	3.01	8.39			11.44	88.56		1.46	2.55								
IV16.03			9.62	44.67	45.71	54.29	58.63	0.07	3.03	2.90	1.01	44.30	17.72	82.28	-8.73	4.30								
IV16.04			23.95	42.39	33.66	66.34	74.24	0.09	3.03	2.90	1.01	44.30	36.10	63.90	-8.61	4.18								
IV19.02	1.49		21.47	33.85	43.19	56.81	68.01	0.08	3.01	2.90	8.39	45.64	2.63	37.79	-13.77	4.07								
IV19.03			14.78	54.74	30.48	69.52	68.35	0.08	3.02	2.90	4.36	45.97	21.27	78.73	-18.41	5.01								
IV19.04	2.91		5.73	50.67	40.68	59.32	63.84	0.08	3.03	2.90	1.68	45.64	4.91	9.66	85.42									
IV19.05			8.89	46.05	45.06	54.94	61.97	0.07	3.03	2.90	1.01	45.97	16.19	83.81	-18.31	4.99								
IV19.06			9.83	42.25	47.92	52.08	59.63	0.07	3.03	2.90	2.35	45.97	18.88	81.12	-15.63	4.93								
IV20.02			62.41	0.45	36.95	62.86	59.54	0.07	3.03	2.90	1.68	45.30	99.28	0.72	-30.88	4.16								
IV20.03			69.74	30.26	69.74	62.79	62.79	0.08	3.03	3.03	1.68	45.30	100.00		-29.72	3.95								
IV20.04			69.17	0.88	29.96	70.04	61.42	0.08	3.03	2.89	1.68	49.66	98.75	1.25	-30.18	4.12								
IV20.05			73.38	26.62	26.62	73.38	67.92	0.08	3.03	3.03	1.68	100.00	100.00		-29.54	4.16								
IV20.06	0.32		50.81	0.57	25.62	51.70	50.19	0.06	3.03	2.92	1.68	38.59	0.62	98.27	1.10	-31.76	4.17							

Table 3: Resume of results analysis from XRD, LECO and isotopes for all the samples

Sample ID	Arag _(XRD) (wt%)		Calc _(XRD) (wt%)		Dol _(XRD) (wt%)		Detr _(XRD) (wt%)		CaCO _{3(XRD)} (wt%)		CaCO _{3(LECO)} (wt%)		TOC _(LECO) (wt%)		d(104)		Mole Mg(%)		CaCO ₃ fraction (wt%)		δ ¹³ C‰ (VPDB)		δ ¹⁸ O‰ (VPDB)			
IV20.07			59.03	0.90	32.59	59.94	53.12	0.07	3.03	2.89	1.68	48.66	98.49	1.51												
IV20.08			55.29	0.90	32.59	56.20	59.47	0.07	3.03		1.68	48.66	98.39	1.61												
IV22.04			23.53	0.73	75.74	24.26	17.64	0.03	3.03	2.87	0.34	55.37	96.99	3.01												
IV22.05			60.21		39.41	60.21	65.61	0.08	3.03		1.68	100.00														
IV22.06			63.04		36.96	63.04	73.67	0.09	3.03		2.35	100.00														
IV22.07	0.40		67.05	0.62	31.93	68.07	68.42	0.08	3.03	2.90	2.35	46.64	0.59	98.50	0.91											
IV23.01	9.86		29.81	22.55	37.78	62.22	56.24	0.08	3.03	2.89	1.68	49.33	15.85	47.91	36.24											
IV23.02	23.65		17.22	20.64	38.48	61.52	64.51	0.08	3.03	2.89	1.01	50.34	28.00	33.55	33.55											
IV24.01	22.40		26.54	14.43	36.63	63.37	74.68	0.09	3.03	2.90	2.35	46.64	35.35	41.88	22.77											
IV24.02	27.20		25.11	10.18	37.18	62.50	78.87	0.10	3.03	2.91	0.34	41.95	43.53	40.18	16.29											
IV24.03	12.25		11.31	25.73	50.71	49.29	57.91	0.07	3.03	2.90	0.34	44.97	24.85	22.95	52.20											
IV25.01	15.53		74.58	75.08	9.07	90.61	82.22	0.10	3.03		2.91	43.29	17.14	82.86												
IV25.02	6.01		74.58	80.59	19.41	80.59	77.34	0.10	3.03		1.01	7.46	92.54													
IV25.03			80.59	80.59	19.41	80.59	78.57	0.10	3.03		2.91	42.62	100.00													
IV26.01	0.57		76.89	22.54	27.73	77.46	74.78	0.09	3.03		1.68	0.74	99.26													
IV27.01	21.99		50.28	27.73	28.88	72.27	83.29	0.10	3.03		1.01	30.43	69.57													
IV27.02	36.65		34.47	28.88	30.04	71.12	89.74	0.11	3.03		0.34	51.54	48.46													
IV27.03	27.91		42.05	30.04	21.88	69.96	85.49	0.12	3.03		0.34	39.89	60.11													
IV27.04	10.52		56.16	11.44	21.88	78.12	73.14	0.09	3.03	2.92	3.02	38.59	13.46	71.89	14.65											
IV27.05	0.98		58.41	15.82	24.62	75.20	74.98	0.09	3.03	2.92	1.01	38.59	1.30	77.67	21.03											
IV27.06	3.77		57.29	38.95	28.46	61.05	75.74	0.09	3.03		1.68	6.17	93.83													
IV27.07	8.93		49.05	13.55	28.46	71.54	72.31	0.09	3.03	2.93	0.34	36.91	12.49	68.56	18.95											
IV27.08			68.05	31.95	31.95	68.05	73.11	0.09	3.03		1.01	100.00														
IV27.09	23.45		40.54	10.36	25.65	74.35	88.19	0.11	3.03	2.92	1.01	38.59	31.54	54.53	13.93											

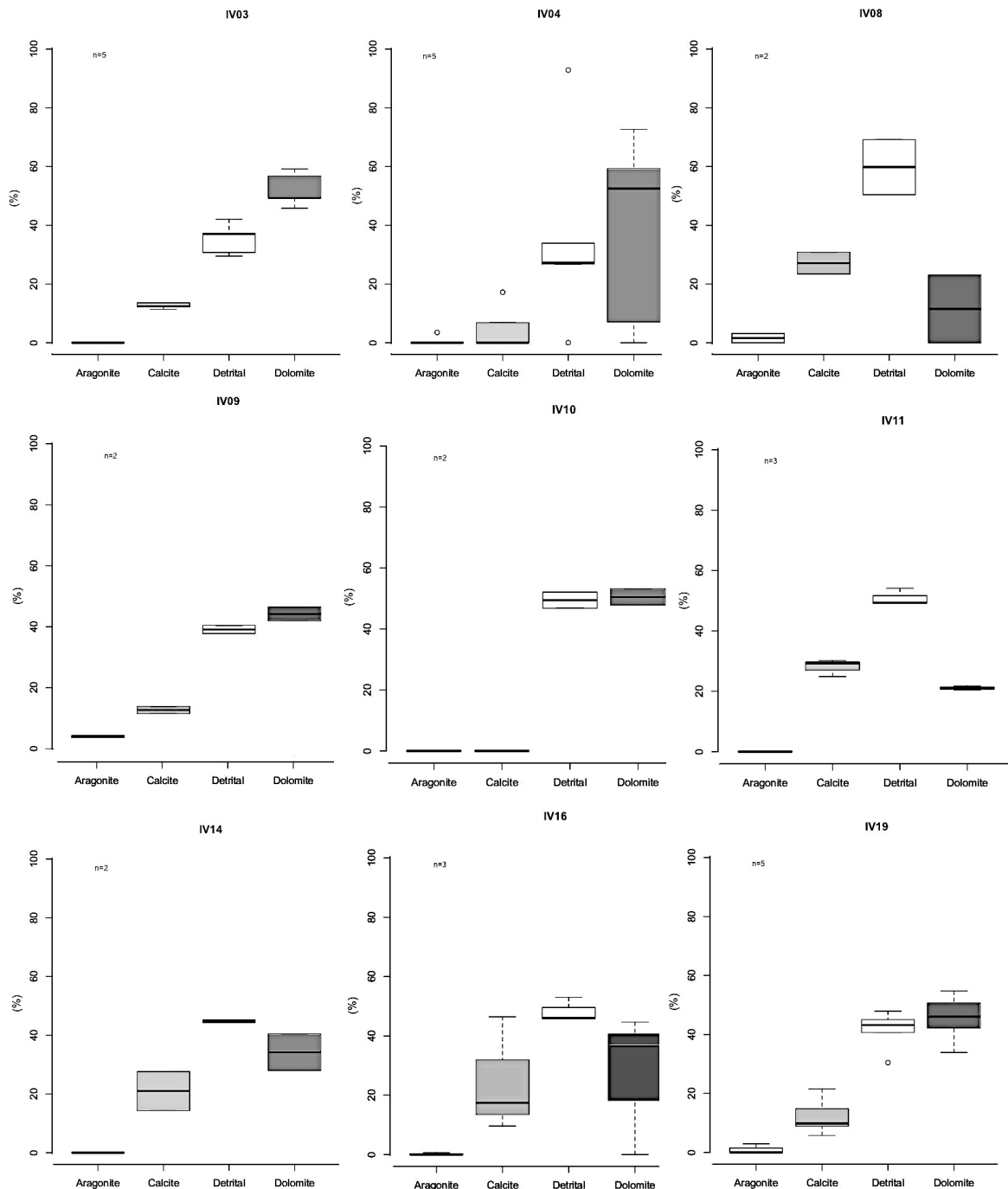


Figure 34: Box-plot of mineral composition for TTR 14 chimney samples. Box-plots indicate the minimum, maximum median and lower and upper quartiles for a variable. The box represents the interquartile range that contains 50% of values. The whiskers are lines or points that extend from the box to the highest and lowest values. A line across the box indicate the median. The number of sub samples used in the statistic elaboration is reported as *n* and calcite and dolomite are indicated by light and dark gray respectively.

72.70%, just one sub-sample has a value that is very low: IV04.06 measures 7.11% (table 3 and figure 34). The calcite percentage has a bigger larger variability range than the dolomite, in fact it goes from 5.73 to 50.09% (table 3 and figure 34).

For aragonite the chimneys doesn't seem to follow rules, we have only minor (< 10%) amounts of aragonite on 8 samples, with aragonite ranging between 1.49 and 9.8%. is always lower than the other two carbonate minerals in the chimneys (table 3 and figure 34). The detrital fraction are of course, depending from the carbonate content; the and it ranges is between 90% and 26.82% (table 3 and figure 34). The sample with 90%, IV04.06, is the one that has just a very low amount of carbonate (7.11%) and is the lower value. Instead the higher value of carbonates amount is 73%.

The detrital fraction in the chimneys is composed mainly by quartz. Other minerals present often in this type of carbonates are include clay minerals, feldspar, plagioclase, illite and phyllosilicates.

The anomaly low carbonate content of represent by the samples IV04.06, can be hypothesized is interpreted as resulting from the nature of this sample. S it corresponds to material that is infilling a borrow channel it does not correspond to the normal carbonate lithology but instead it corresponds to material that resulted from the metabolic activity of the borrowing organism and from sedimentary and digested material of the carbonate rock itself. Moreover, the LECO carbon content of this sub-sample (figure 34) shows higher inorganic carbon content that has not a crystallographic structure, indicating most probably an organic origin. A are due to the instrument: in fact, as explained in the previous chapter, the XRD read the crystalline formation of carbonate, so probably this sub-sample (that is an intrusion, as you can see in figure 28) has carbon inside but not in a an crystallized organized form.

6.3.1.2 Concretions

The concretions have a different type of composition: the carbonate fraction is always composed by aragonite, calcite and dolomite, but the percentage composition is different. In these samples, the aragonite is almost not present: just two sub-samples, IV20.06 and IV22.07, present it and only in a very low percentages, 0.32% and 0.40% respectively.

The dolomite is more present but only in vestigial amounts than calcite but however the range is very small, just ranging between 0.45% and 0.90%. The major carbonate mineral present in the concretion is calcite, with the values that

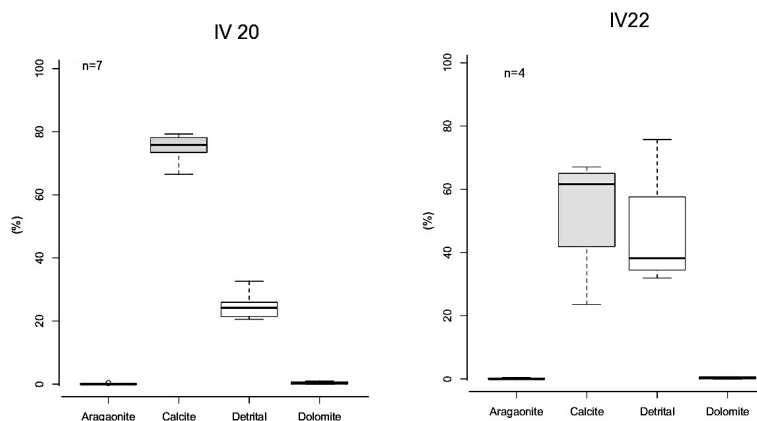


Figure 35: Box-plot of mineral composition for M86/5 concretion samples. Box-plots indicate the minimum, maximum median and lower and upper quartiles for a variable. The box represents the interquartile range that contains 50% of values. The whiskers are lines or points that extend from the box to the highest and lowest values. A line across the box indicate the median. The number of sub samples used in the statistic elaboration is reported as *n* and calcite and dolomite are indicated by light and dark gray respectively.

range for this mineral are between 23% and 73%.

Four sub-samples (IV20.03 IV20.04 IV22.05 and IV22.06) have only they show just calcite as in the carbonate fraction, IV20.03 IV20.04 IV22.05 and IV22.06. The detrital fraction is related with the carbonate fraction and the ranges between values are 25.62% and 75.74%. This fraction is composed mainly by quartz and clay minerals, but also pyroxens and phyllosilicates.

6.3.1.3 Crusts

The particularity distinctive feature of the crusts composition is the presence of aragonite presence, as is possible to see in figure 36. This mineral is present in almost all the sub-samples, the values are very variables between 36.56% and 0.57%. The range of the calcite abundance varies are between 76.89% and 11.31%, the sub-sample IV27.08 is composed, in the carbonate fraction, only by this mineral. The dolomite fraction has a range of values between 10.18% and 80.59%; there is a sub-sample, the IV25.03, that is totally composed by this carbonate mineral.

The detrital fraction also has a similar range of values, between 9.07% and 50.71%. This fraction is mainly composed by quartz clay and in almost all the samples is present pyrite or simile other similar sulphur minerals or their correspondent oxidized minerals composed such as by iron oxides. Are also

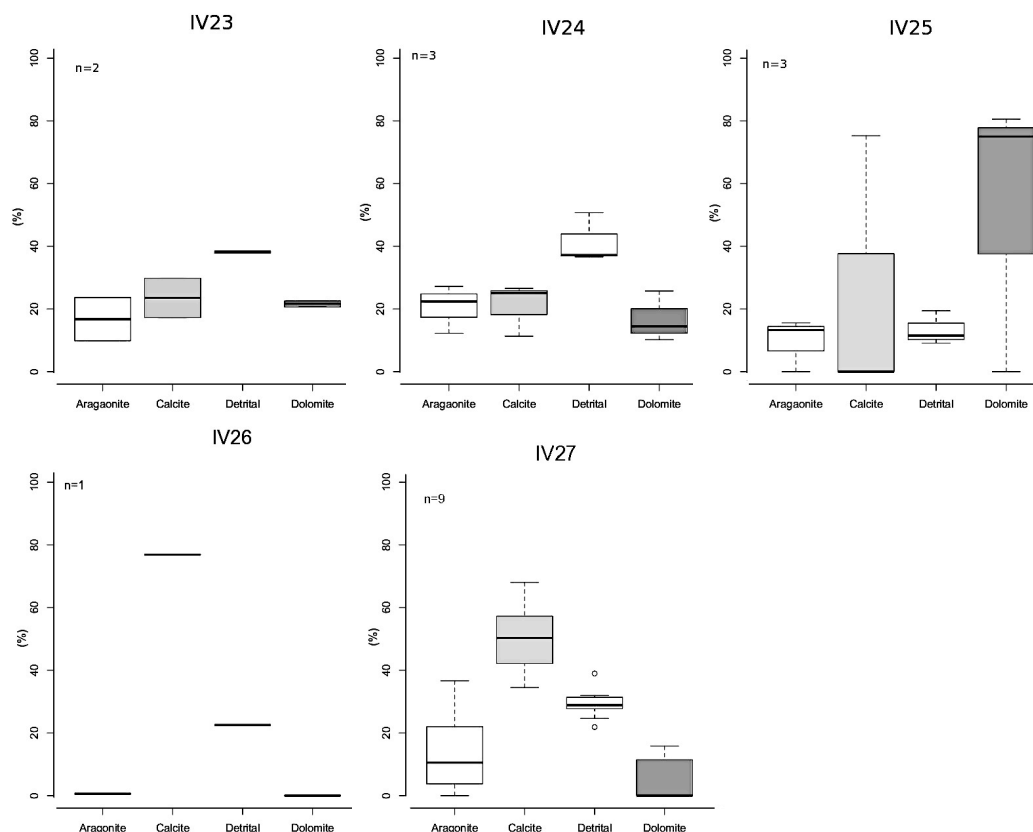


Figure 36: Box-plot of mineral composition for TTR 15 and 16 crust samples. Box-plots indicate the minimum, maximum median and lower and upper quartiles for a variable. The box represents the interquartile range that contains 50% of values. The whiskers are lines or points that extend from the box to the highest and lowest values. A line across the box indicate the median. The number of sub samples used in the statistic elaboration is reported as *n* and calcite and dolomite are indicated by light and dark gray respectively.

presents pyroxens in some sub samples.

6.3.2 Carbonate Content

The carbonate content can be estimated by XRD but the precision of on the mineral quantification by XRD is in the order of 10%, therefore to quantify the carbonate content and to evaluate the precision of the XRD minerals quantification the samples were quantified by chemical analysis by LECO. Results (table 3 and figure 38) show normal or expected differences between the LECO and the XRD quantifications. These differences result from the different precision of these analysis but also due to the fact that the XRD measures the carbonate or mineral content by the crystallinity of their structure, while the LECO measures the chemical abundance of elements such as carbon. The difference accepted usually between the methods is lower than 15%. In the samples analyzed in this thesis,

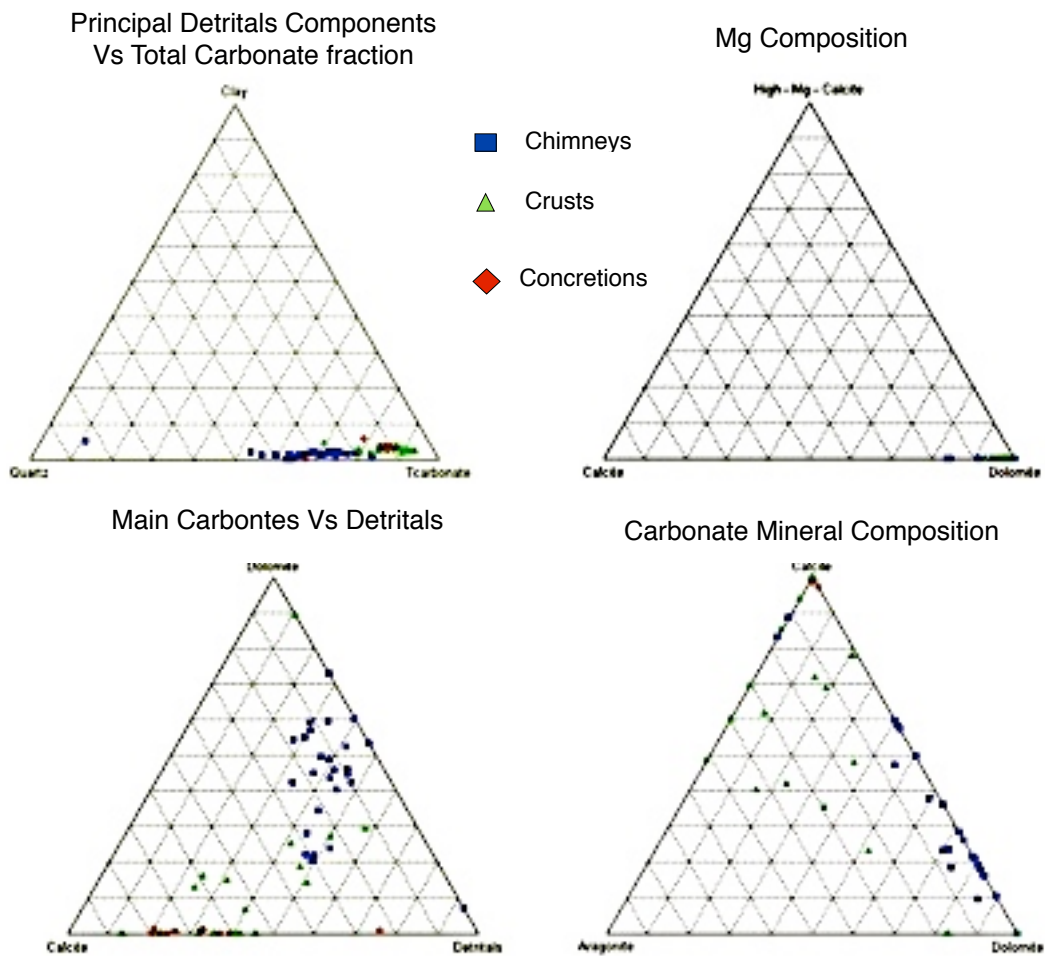


Figure 37: Ternary mineral and compositional plots.

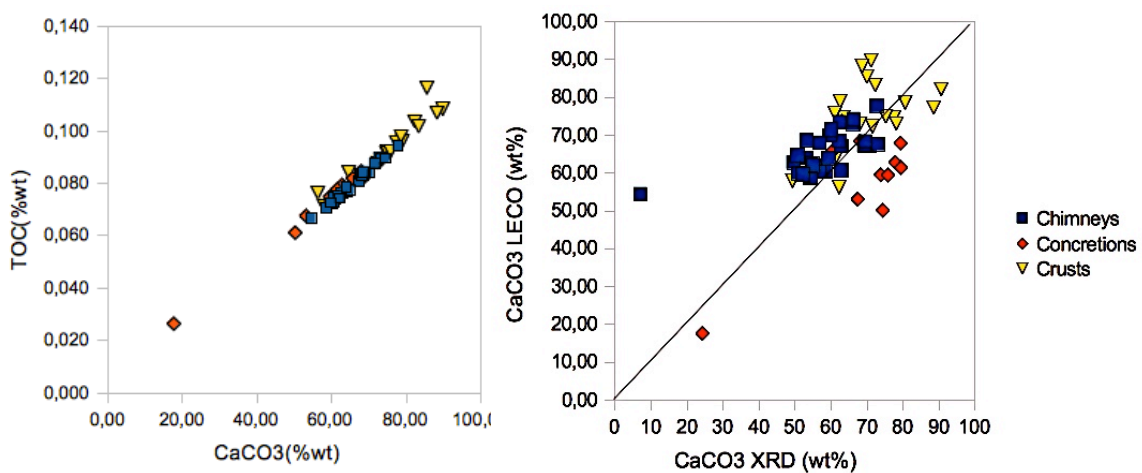


Figure 38: Total Organic Carbon and total carbonate fraction (measured by LECO) show a linear direct and very good correlation; and the total carbonate fraction correlation measured with XRD and LECO show also a good correlation.

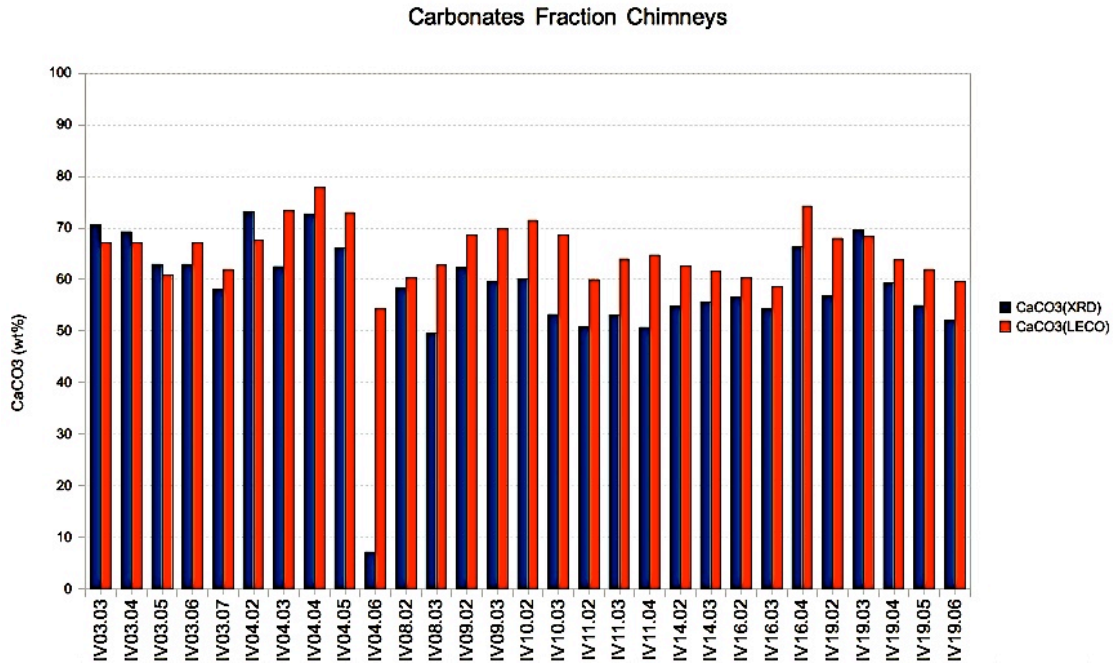


Figure 39: Column graph between quantification of carbonate fractions by XRD and LECO for TTR 14 chimneys samples.

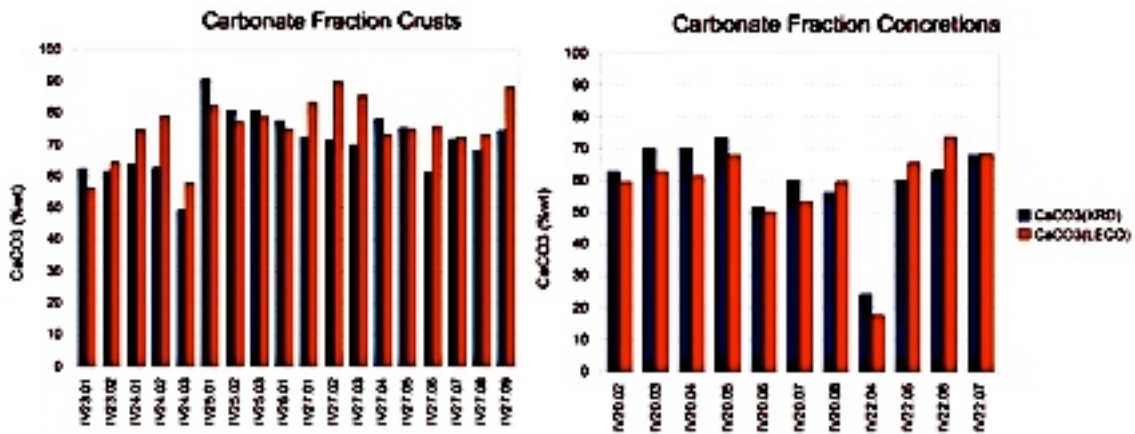


Figure 40: Column graph between quantification of carbonate fractions by XRD and LECO for TTR 15, TTR 16 crust and M86/5 concretion samples.

we have noticed that usually the quantifications with XRD give lower values than the quantifications with LECO (figures 39 and 40).

The samples are almost all in the range of tolerance of 10 to 15%. Only the sub-sample IV04.06 has a very large difference between the two methods: the carbonate in XRD is 7.11% and 54.42% with LECO. This difference can be explained by the methods himself. In fact looking at the figure 28 this sub-sample coincide to the white intrusion, this can be formed by carbon and carbonate content that are not in a crystalline form, so it is measured by LECO but not by

XRD.

The total carbonate fraction of the chimneys determined with XRD have values ranging from 49.57% to 73.18%, not considering the sample IV04.06, as described before. The total carbonate fraction determined by LECO show values between 54.42% and 77.78%. In the concretions the carbonate content determined with XRD range between 24.26% and 73.38% while for LECO shows a variation between 17.64% and 73.67%.

The crusts also have similar variations in the total carbonate content: for XRD values range from 49.29% up to 90.61% and for LECO ranges between 57.91% and 89.74%.

In figure 38, that describe the correlations between TOC (Total Organic Carbon) and the total carbonate fraction in the LECO measurement, in possible to see that all the samples follow a linear correlation and that only one sample seems to be very different from the others. This abnormal sub-sample (IV22.04) corresponds to a concretion that has a very low value of total carbonate content when compared with the other samples and an abnormal high detrital and clay fraction, indicating a very low cementation degree and therefore a very low amount of authigenic carbonate phases and for this reason has a very low content of carbon.

As shown in figure 38, the correlation between the XRD and LECO total carbonate fraction quantifications, it is possible to notice that two samples deviate from the linear correlation of these variables. These two abnormal sub-samples correspond to the concretion IV22.04 described above and the chimney sub-sample IV04.06 that corresponds to the burrow channel infill, described above in this section.

6.4 Isotopes

Carbon ($\delta^{13}\text{C}$) and oxygen ($\delta^{18}\text{O}$) isotopic compositions of the samples (For the isotopes results, table 3 and figure 41) shows the correlation between $\delta^{18}\text{O}$ and $\delta^{13}\text{C}$ for of the three groups of samples (chimneys, crusts and concretions) show a significant variability. While the is possible to notice that, for $\delta^{18}\text{O}$ values show a constancy of the values, there aren't big anomalies, all the samples are in a range between 2.482‰ (VPDB) and 5.976‰ (VPDB). Looking at the $\delta^{13}\text{C}$ values show

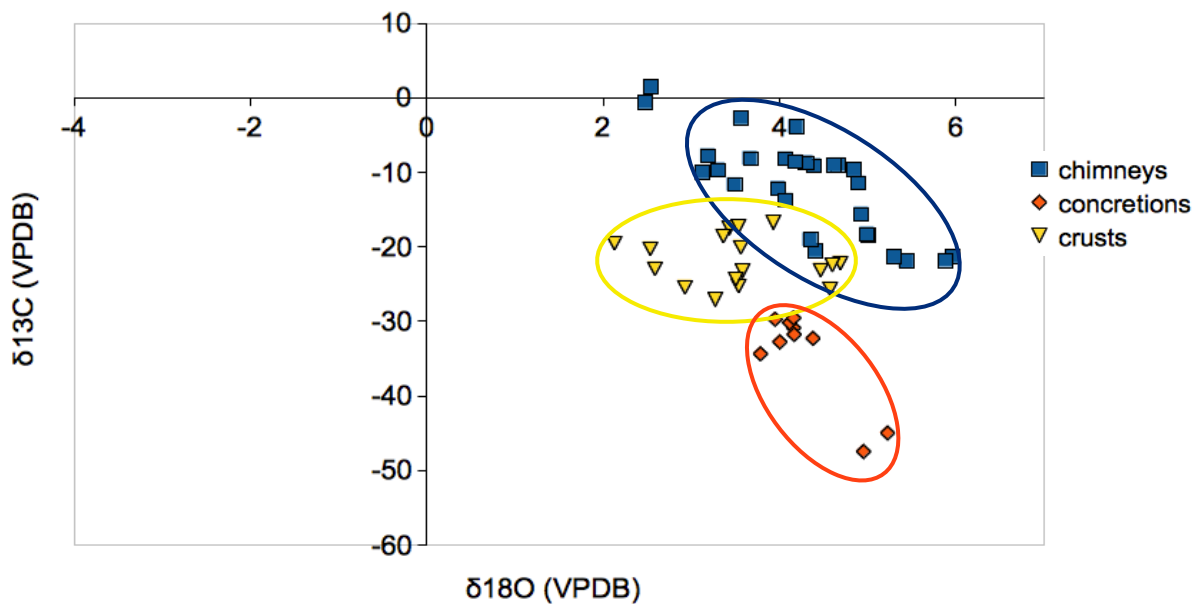


Figure 41: $\delta^{18}\text{O}$ vs $\delta^{13}\text{C}$ for the three types of samples. The values of the isotopes (VPDB) are expressed in ‰.

is possible to see a very large high variability, from -47.47 up to + 1.46‰ VPDB. To be noted that the different carbonate types show partly overlapping but distinctive compositional domains. The concretions show the more negative $\delta^{13}\text{C}$ values ranging between -29.54 and -47‰ VPDB and $\delta^{18}\text{O}$ values with low variability (of about 4‰ VPDB). The crusts have intermediate $\delta^{13}\text{C}$ values (when compared with the other carbonate types) varying from -16.75 and -27.08‰ VPDB, corresponding to a narrow variability. Considering the oxygen isotopes composition, the crusts have a larger range of values, varying from 2.13 and 5.23‰ VPDB. The chimneys show highly variable $\delta^{13}\text{C}$ values, from about -21.92‰ VPDB up to +1.46‰ VPDB. The oxygen isotopic composition of the chimneys also show a significant variability, ranging from 2.48‰ up to 5.97‰ VPDB. On the $\delta^{13}\text{C}$ - $\delta^{18}\text{O}$ domain the chimneys indicate a linear compositional trend resembles a system with a mixture of two end members: one corresponding to negative carbon isotopic values and the second end-member with isotopic compositions with close to zero $\delta^{13}\text{C}$ values and about 2‰ $\delta^{18}\text{O}$ values. These two compositional end-members would correspond to methane rich fluids and the normal seawater. Therefore it can be interpreted that the chimneys would indicate a formation from pore waters representing a mixture of methane rich fluids and

normal seawater. The concretions would represent a formation from fluids clearly enriched in methane while the crusts point to methane enriched source fluids but with an intermediate composition. Some chimneys sub-samples show abnormal compositions, corresponding to a non-methane-derived source: there are, at list, four anomaly samples. Two of these sub-samples are from the chimneys group and are the (IV04.06 with a $\delta^{13}\text{C}$ value of -0.60‰ (VPDB) and IV16.02 with a $\delta^{13}\text{C}$ value of 1.46‰ (VPDB), that already resulted out of the ranges for the other analysis, and IV16.02 that measure 1.46‰ (VPDB) correspond to a normal seawater source. This is strange because, usually the methane derived authigenic carbonates values for $\delta^{13}\text{C}$ are negatives. As shown in figure 28, these two sub-samples correspond to the infillings of borrowings and therefor is normal that this material have a non methane-derived formation process and are instead composed by normal sediments and material resultant from the organic activity of the burrowing organism, as already observed on the mineral content of these sub-samples.

The other two sub-samples with close to normal seawater $\delta^{13}\text{C}$ values (IV08.02 and IV08.03) are interpreted as being the result of a high detrital and a high bioclasts (that have seawater carbon isotopic values) contents.

Other seems outside of the area of major concentration, are concretions: IV22.06 with a value of $\delta^{13}\text{C}$ of -47.47‰ (VPDB) and IV22.07 that measure -44.98‰ (VPDB). Otherwise, also if those two are particularly negatives, all the concretions shows levels of $\delta^{13}\text{C}$ lower than chimneys and crusts. Also is possible to notice that the graph show three distinct groups of samples that coincide with the three types of carbonates considered in this master thesis. Looking at table 3 the range of values for the three types of carbonates seem to be ordered in three groups on the basis of $\delta^{13}\text{C}$. Otherwise the ranges values of $\delta^{18}\text{O}$ for the three types of carbonates are similar: between 2.48‰ (VPDB) and 5.97‰ (VPDB) for chimneys, between 3.78‰ (VPDB) and 5.23‰ (VPDB) for concretions and between 2.13‰ (VPDB) and 5.23‰ (VPDB) for crusts. For $\delta^{13}\text{C}$, instead, the ranges are very different. The values in chimneys goes from 1.46‰ (VPDB) to -21.92‰ (VPDB), in concretions maximum and minimum levels are -29.54‰ (VPDB) and -47.47‰ (VPDB) and, in the end, for crusts the interval is between -16.75‰ (VPDB) and

-27.08‰ (VPDB).

Looking at the figure 42, that shows the oxygen isotope and the total carbonate fraction, is possible to see that only one sample (IV22.04) seems to be different from the others; this difference is not for on the isotopic values but is just for the carbonate content. This sample, that as said described before, in section 6.3, shows an abnormally low content of carbonate content fraction. All the other

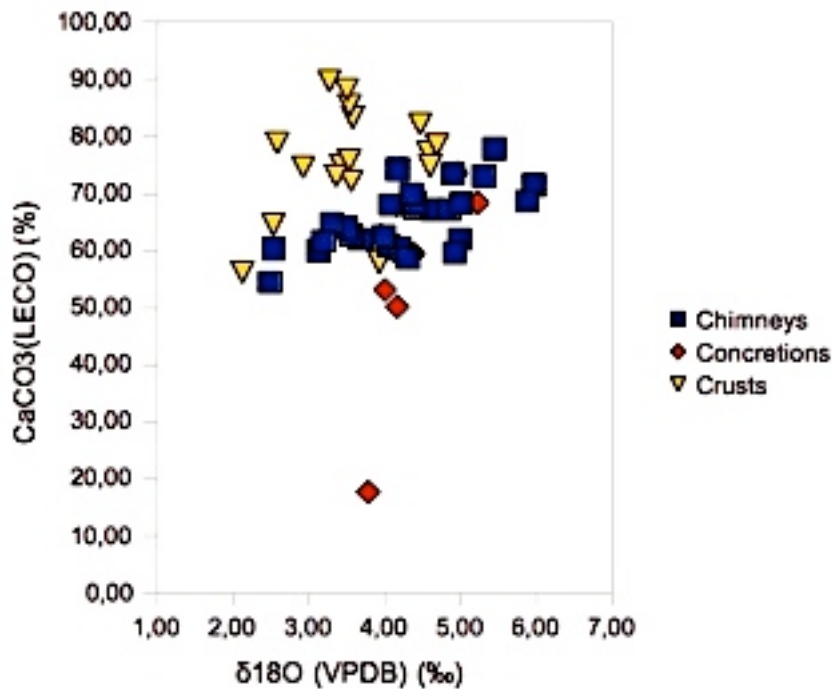


Figure 42: Correlation between total carbonate fraction from LECO and the $\delta^{18}\text{O}$ isotope for the three type of samples.

samples form a homogeneous big group divided in two parts: one with concretions and chimneys samples and another (yellow triangles) with corresponding to the crusts. This division is only mainly resultant of the distinctive imposed by the carbonate content.

In the figure 43 is showed the relationship between the main carbonate fractions mineralogy (such as calcite, on the left, and dolomite, on in the graph on the right), and the $\delta^{18}\text{O}$. For Dolomite, the crusts and the chimneys are mixed and it seems that the samples of this two types follow a linear correlation trend. Otherwise the concretions are almost all near the X-axes as the dolomite content because the trend of dolomite is very low.

For the calcite graph, things are most confused and is not possible to recognize

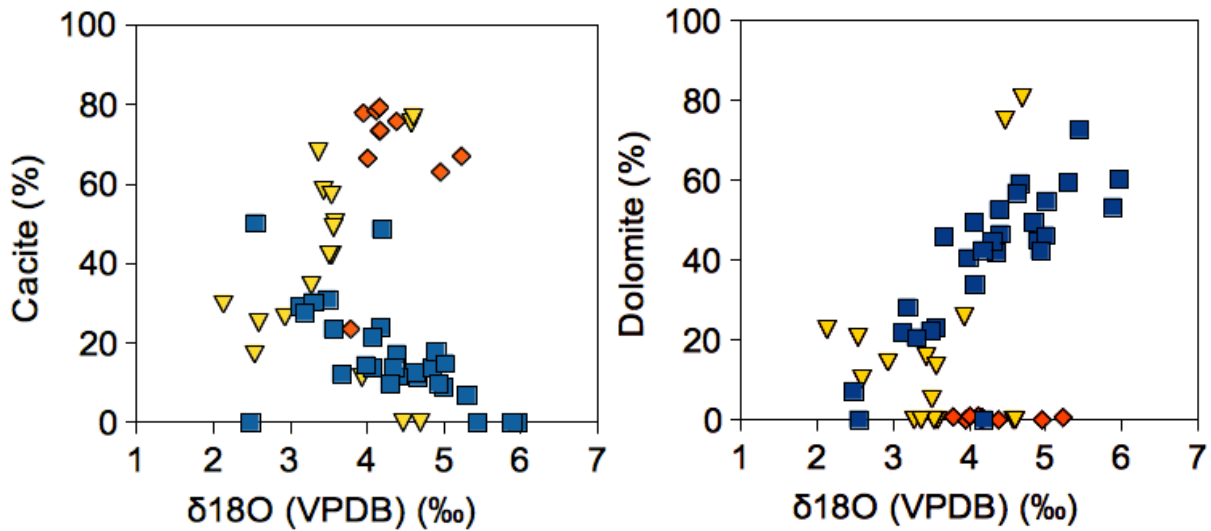


Figure 43: Correlation between the two main carbonate fractions, Calcite and Dolomite, from XRD and the $\delta^{18}\text{O}$ isotope for the three type of samples.

any clear trend in it. The $\delta^{13}\text{C}$ isotopic compositions show a larger variability and seem to better illustrate any changes in fluids compositions from which the carbonate minerals were formed from. Unlike the $\delta^{18}\text{O}$, the carbon isotope is more discriminating and, considering figure 44, the three groups are well defined along the axis X based on the C isotopic composition. The concretions are well divided from the crusts and the chimneys than have overlapping compositional domains and, in part, mix.

This picture shows also that the crusts have a higher quantity amount of total carbonate fraction content when compared with respect to the other two carbonate types of carbonates. Only one sample (IV22.04), a concretion, seems to be different from the others, in relation respect to the total CaCO_3 content. The other two samples that are divided from the others are (IV22.06 and IV22.07), are also concretions, but they are discriminated by the values of $\delta^{13}\text{C}$ values that are the more negative (-47.47‰ (VPDB) and -44.98‰ (VPDB) respectively).

The concretions seems to have more negative values of $\delta^{13}\text{C}$ when compared with the crusts and the chimneys. In fact, it is possible to distinguish the three groups considering $\delta^{13}\text{C}$ variation, independently from the carbonate content, on the horizontal curve: the more negatives values correspond to the concretions. Than the crusts, even observing an overlapping with the chimneys, have intermediate $\delta^{13}\text{C}$ values also if the higher values of them mix a bit with the lower ones for the

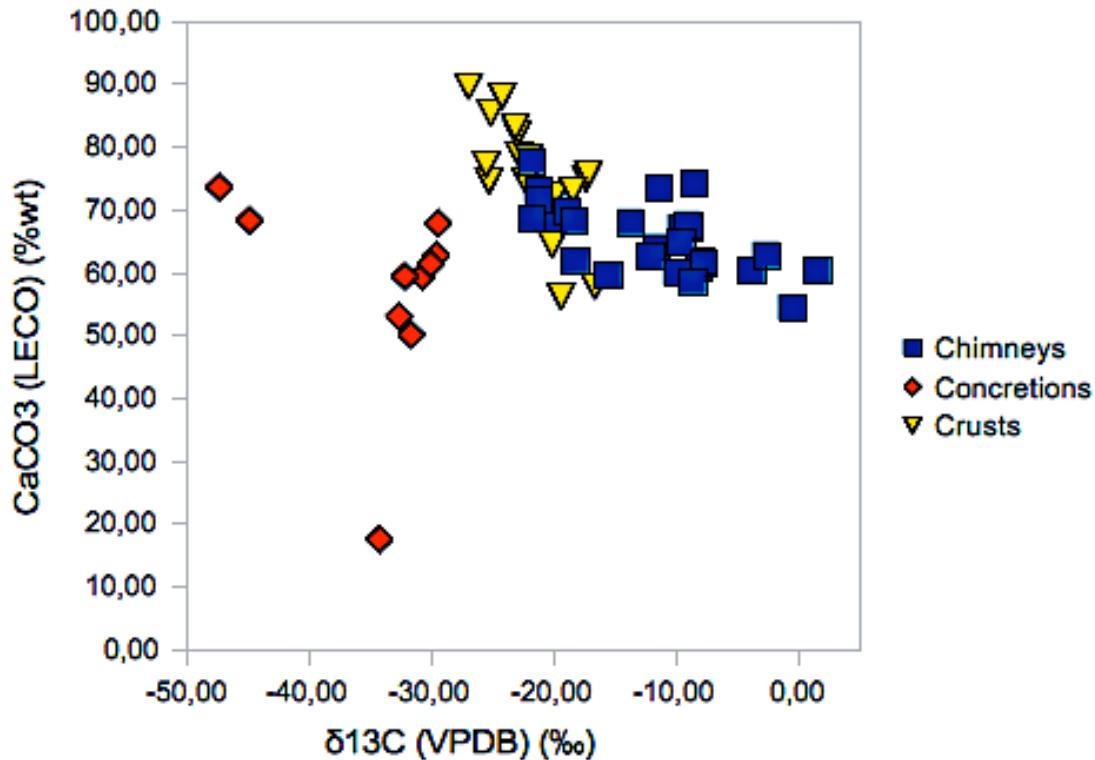


Figure 44: Correlation between total carbonate fraction from LECO and the $\delta^{13}\text{C}$ isotope for the three type of samples.

chimneys; and in the end there are the chimneys that have heavier $\delta^{13}\text{C}$ compositions. Those samples have one positive value for this isotope: 1.46‰ (VPDB) for the sub-sample IV16.02, as said before.

On figure 45, on the left side, is shown the relationship between calcite content and $\delta^{13}\text{C}$. Also in this picture the three groups are divided and clearly identifiable. The concretions show a dispersed pattern domain, than the crusts and in the chimneys, also if mix a bit, the patterns seem to indicate preferably distinct trends. The concretions are also well defined in a “vertical way”: in fact they show a high content of calcite and more negative of $\delta^{13}\text{C}$ values.

The chimneys, on the contrary, show the lower contents of calcite and the higher values of $\delta^{13}\text{C}$. The crusts are in the middle between them and represent an intermediary behavior. Again, is notable IV22.04 with the lower levels content of carbonate, and therefore the lower level content of calcite. There are five sub-samples that don't have calcite and they are: IV04.06, IV10.02 and IV10.03 for the chimneys; and sub-samples IV25.01 and IV25.03, for the crusts.

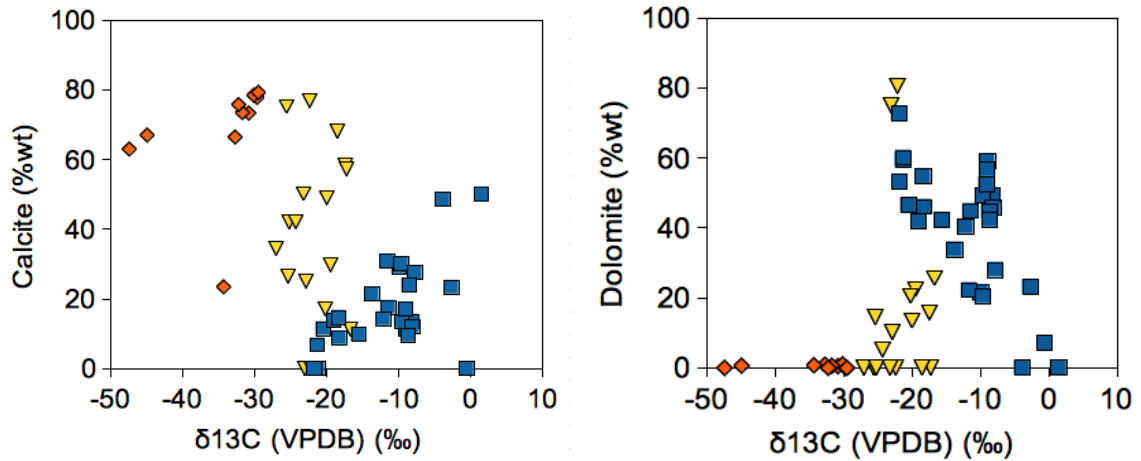


Figure 45: Correlation between the two main carbonate fractions, Calcite and Dolomite, from XRD and the $\delta^{13}\text{C}$ isotope for the three type of samples.

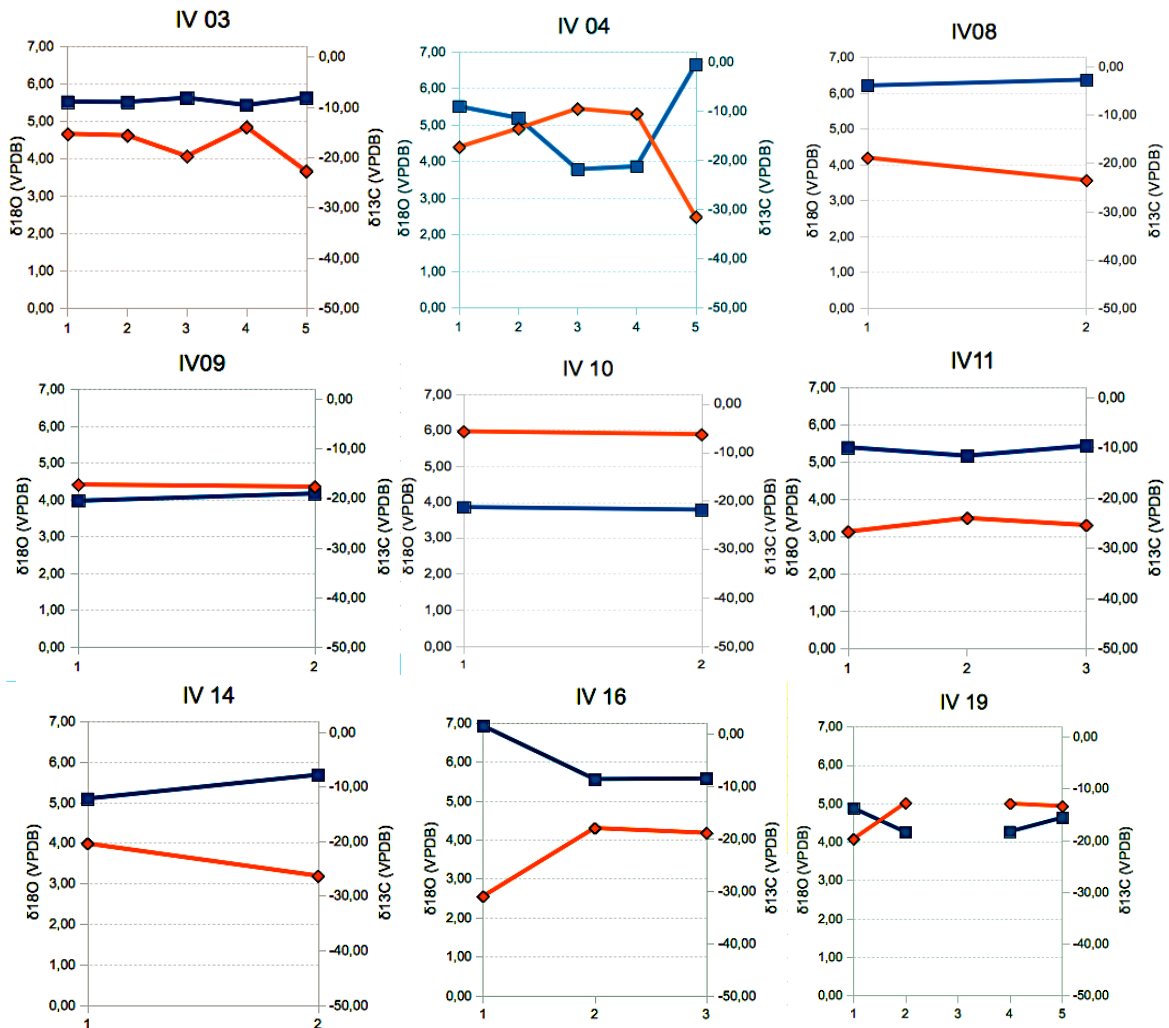


Figure 46: isotopes profiles for chimneys samples of TTR-14. In blue the $\delta^{13}\text{C}$, in red the $\delta^{18}\text{O}$. The values of both the isotopes are expressed in (VPDB).

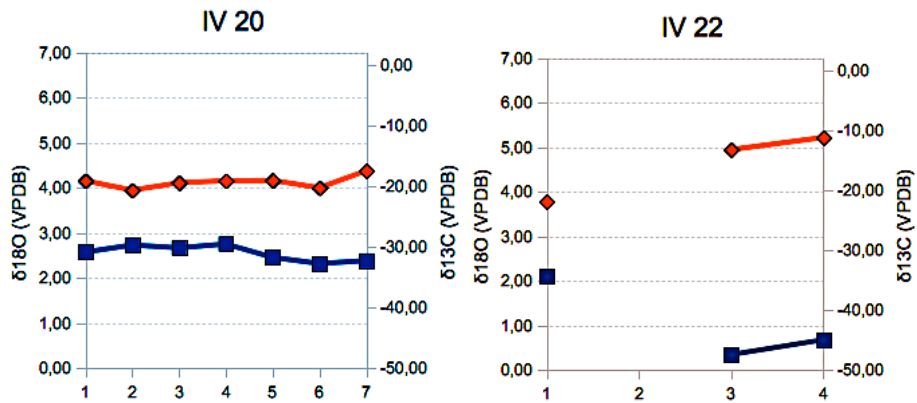


Figure 47: isotopes profiles for concretions samples of M86/5. In blue the $\delta^{13}\text{C}$, in red the $\delta^{18}\text{O}$. The values of both the isotopes are expressed in (VPDB).

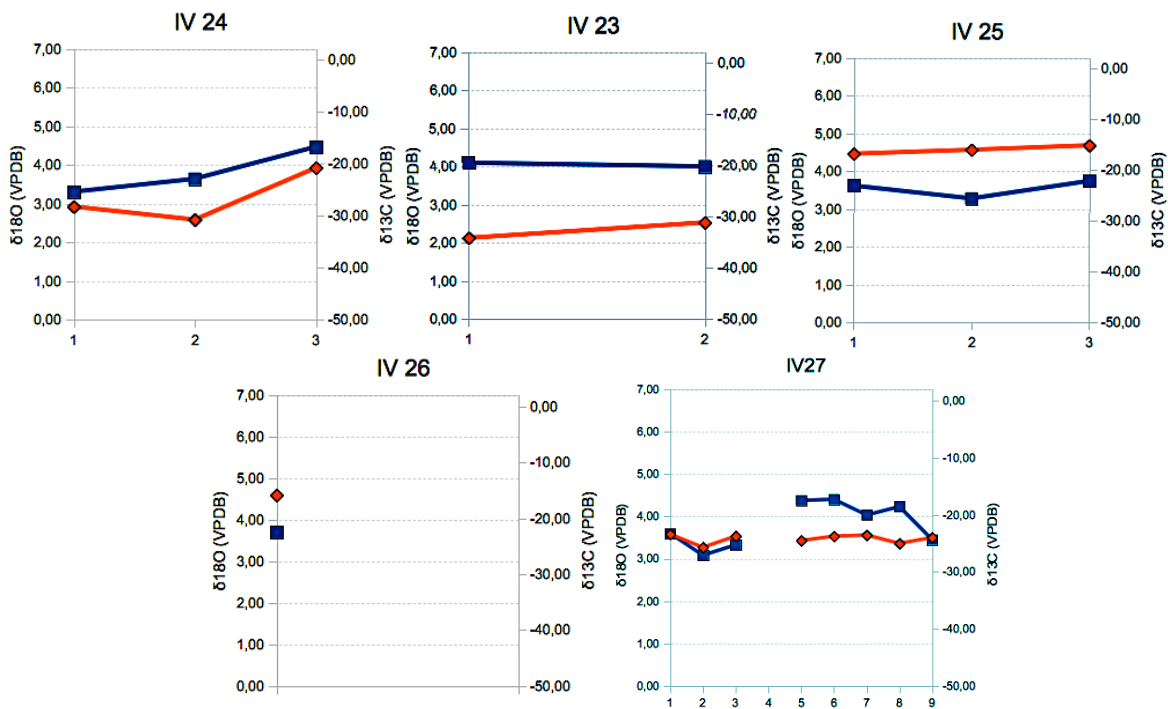


Figure 48: isotopes profiles for crusts samples of TTR-15 and 16. In blue the $\delta^{13}\text{C}$, in red the $\delta^{18}\text{O}$. The values of both the isotopes are expressed in (VPDB).

On the right side panel of figure 45, is showed the relationship between the dolomite fraction and the $\delta^{13}\text{C}$ composition. The dolomite content is very variable. Is possible to have a very clear distinction between two groups: the concretions, that have dolomite fraction contents near 0, and the crusts and chimneys in which the dolomite content is very variable. In the this case of this graph it is not possible to define any distinction or trend between the two variables considered.

The figures 46, 47 and 48 are graphs of the isotopic profiles for all the carbonate

samples. In some graphs samples there are gaps due to difficulties in the collection of the required powdered material or due to analytical errors during the ICP-MS measurements and had to be repeated and the results are still to be received. Anyway, analyzing all the profiles, it is possible to notice that they are very distinct between them. In some sample, like IV04, IV16, IV22 or IV19, they seems to cross each other and show inverse correlation between both isotopes. It means that as one increase and the other decreases. Other samples, like IV10 or and IV13, the two isotopes make the same bend; in other again they seems to do the opposite, like in IV16 or IV22. Other samples do not show any clear and distinctive variation along his profiles, are just confusing.

Chapter 7: Discussion

7.1 Types of authigenic carbonates

Based on the morphology, macroscopic and petrographic characterization and mineralogy, the studied samples can be classified in three different groups: (1) chimneys, (2) concretions, and (3) crusts. These have distinct and characteristic mineral compositions, as is possible to see in figure 37 in the *Carbonate Mineral Composition* ternary plot. The chimneys carbonate fraction is characterized by the predominance of dolomite. The concretions carbonate fraction is composed, almost exclusively, by calcite. The carbonate fraction of the crusts shows a more variable composition with the mineralogy including usually, both aragonite, calcite and dolomite. It is possible to identify as a distinctive characteristic of this type of carbonate the presence and higher contents of aragonite.

As illustrated in Figure 37, the *Principal Detrital Components Vs Total Carbonate fraction*, it is possible to observe that all the samples from the three types of carbonates are composed mainly by carbonate minerals, that as observed in the petrographic and isotopic composition, and the cement that lithifies a sediment detrital fraction is composed by quartz grains, clays, bioclasts and other minor detrital grains (feldspars, plagioclases, pyroxenes). The clay content is always minor than 10%. The *Mg content* on the calcite and dolomite minerals (Table 3 and Figure 37), is determined by the positions of main peaks of the carbonate phases on the XRD diffractograms after their correction based on the quartz peak as reference. This ternary plot indicates that the carbonate phases (calcite and dolomite) have stoichiometric or close to stoichiometric compositions. No Mg-calcite neither proto-dolomite are present.

The carbon and oxygen isotopic composition of the studied samples also discriminate very clearly the three different types of carbonates (figure 41). It is possible to notice that the chimneys, concretions and crusts define three domains with some overlapping in the chimneys and crusts domains. Concretions show more negative $\delta^{13}\text{C}$ values and fairly constant $\delta^{18}\text{O}$ values. The chimneys show high variability on the $\delta^{13}\text{C}$ values

7.2 Methane-derived origin of these carbonates

7.2.1 Fluids Nature: seawater and Methane

The inference of the isotopic composition of the carbon pool from the carbonate mineral one is complex, because the mineral composition may reflect mixing from the different carbon sources. Fractionation of the carbon will also depend on the extent to which the different carbon reservoirs are oxidized. However, it is possible to estimate the $\delta^{13}\text{C}$ composition of the fluids that permit the authigenic carbonates precipitation from, and is possible at least identify the different carbon sources.

The carbon isotopic composition of the studied samples: chimneys (with the exception of the sub-samples IV04.06 and IV16.02), crusts and concretions, indicate that they originated from a moderate to extremely ^{13}C -depleted reservoir, with some variable mixture with normal seawater ^{13}C reservoir (especially in samples IV08.02 and IV08.03). Therefore the C isotopic composition of these carbonates indicate a clear methane-derived origin of these authigenic carbonates.

For isotopic light carbon signature, two principal sources can be considered: (1) decomposition of organic matter, that result in typical pore waters $\delta^{13}\text{C}$ values of about -25‰ VPDB, and (2) methane and higher hydrocarbons oxidation products (Claypool and Kaplan, 1974; Rosenfeld and Silverman, 1959) that produces pore waters $\delta^{13}\text{C}$ values of less than -20‰ VPDB (-20‰ up to -110‰ VPDB). In the Gulf of Cadiz two potential sources of methane can be considered: thermogenic and biogenic origin (Hensen et al., 2007; Niemann et al., 2006; Nuzzo et al., 2007; Stadnitskaia et al., 2006). Typically, biogenic methane formed by CO_2 reduction or by fermentative decomposition of organic matter by micro-organisms at shallow depths is extremely fractionated in ^{13}C , typically with $\delta^{13}\text{C}$ values between -50‰ and -110‰ VPDB (Claypool and Kaplan, 1974; Schoell, 1988) and thermogenic methane is isotopic less fractionated ranging from -50‰ to -20‰ VPDB (Schoell, 1980, 1988).

Another potential important source of carbon to the total carbon pool from which these carbonates were precipitated is the dissolved carbon from normal seawater and HCO_3^- derived from dissolution of carbonate tests, both with $\delta^{13}\text{C}$ values $\sim 0\text{‰}$ (VPDB). Given the petrographic characteristics of the chimneys and the crusts indicate a weak diagenetic degree and therefore formation within shallow sediment column, and that in the case of the concretions were collected at 80 cm and 250 cm depth below the seafloor.

The studied samples have $\delta^{13}\text{C}$ values heavier than biogenic methane, therefore mixing with of the several carbon sources is probable. Thus, it is possible to propose that the authigenic carbonates most probably reflect a mixing of methane-rich fluids (thermogenic and biogenic methane) with non-methane carbon sources where seawater is the most important.

$\delta^{13}\text{C}$ values of the studied samples (figure 44) are typical from carbonates formed at methane vents (Bohrmann et al., 1998; Greinert et al., 2001; Hovland et al., 1987; Kulm and Suess, 1990; Kulm et al., 1986; Paull et al., 1992; Peckmann et al., 2001; Ritger et al., 1987) and correspond very well with methane-derived authigenic carbonates from other sites in the Gulf of Cadiz (Magalhães, 2007 and Magalhães et al., 2012), as illustrated in figure 49. In this comparison with methane-derived authigenic carbonate samples from other structures in the Gulf of Cadiz it is possible to notice that two sub-samples from chimneys (IV04.06 and IV16.02) are very out of the normal expected depleted ^{13}C values also reported in the literature as normal for MDAC. As discussed before, these sub-samples correspond to sedimentary infill's of burrows, being this the reason for these abnormal values. Also the sub-samples IV08.02 and IV08.03 present values of $\delta^{13}\text{C}$ very high -3.92‰ and -2.71‰ VPDB (Figure 49), close to the normal seawater composition (close to 0‰ VPDB). This is interpreted as being the result of the fact that sample IV08 present a very high level of bioturbation and bio-erosion. In fact, as illustrated in figure 28, this sample is highly burrowed, has high amount of remains of tube worms, benthic organisms attached to the burrow tunnels that are very close to the drilling points. It means that probably during the drilling procedure has been collected not only the carbonate rock material but also shell fragments or biological components that altered the results, especially the

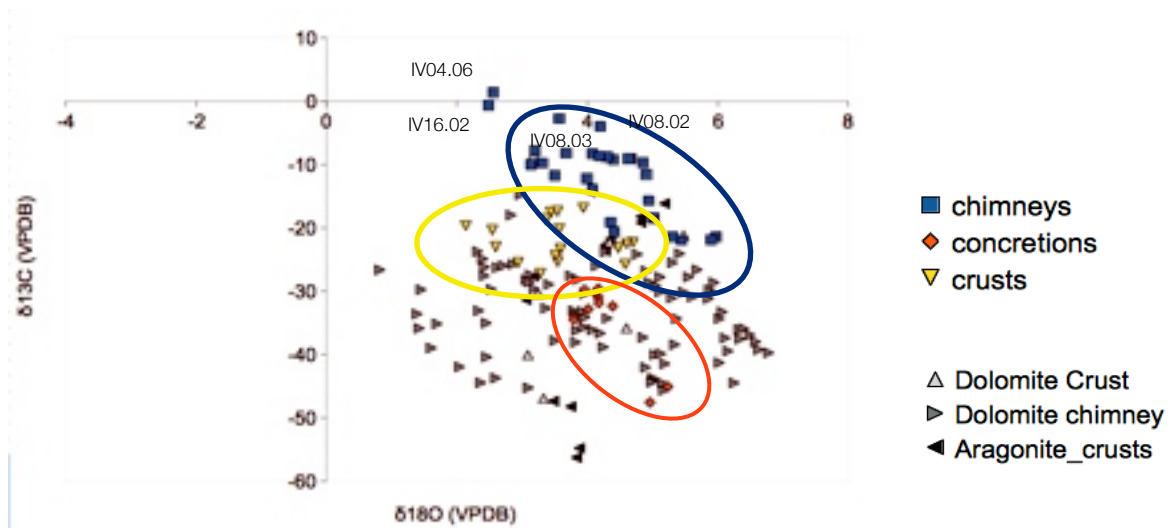


Figure 49: $\delta^{18}\text{O}$ and $\delta^{13}\text{C}$ values of the samples used in this thesis (colored ones) compared with the isotopic composition of samples collected in other sites of the Gulf of Cadiz (Magalhães, et al., 2012) plotted in black-gray color.

isotopes.

From figure 49 it is possible to recognize also that the isotopic composition of other MDAC samples collected in other sites of the Gulf of Cadiz (Magalhães, V. 2007) show that the crusts (Dolomite crusts in the figure) have highly variable isotopic compositions, similar to the observed in the crusts of this study. Also, the chimneys are very similar to the chimney samples in this study.

Relatively to the isotopic compositional variation within the individual samples, along radial and longitudinal profiles on the crusts and chimneys (figure 46, 47 and 48) no clear and distinctive trend can be defined. As already mentioned in the results section, there are some samples in which the two isotopes seem to increase or decrease together, some other cases in which the trend is opposite and others in which is not clear.

On the other hand, relatively to the relationship between the isotopic composition and the carbonate fraction (total carbonate, dolomite and calcite) it is possible to recognize a linear good correlation for the chimneys. In fact, looking at figures 42 and 44 is possible to define a general trend that is very clear for chimneys samples: as the carbonate content (of the cement) increases, the $\delta^{18}\text{O}$ becomes heavier and the $\delta^{13}\text{C}$ becomes more negative. This can be interpreted as reflecting

that as methane-derived authigenic carbonates are precipitated, increasing the cementation, these methane-derived isotopic signal (heavier $\delta^{18}\text{O}$ and depleted $\delta^{13}\text{C}$) will also increase, compared with the normal seawater signal ($\delta^{18}\text{O}$ and $\delta^{13}\text{C}$ values close to 0). This global trend between these two end-members is recognized on the chimney samples but is not observed along each individual sample. On the crusts and concretions this process of mixture is not recognized, possibly the number of analyzed samples is not sufficient to show this process.

7.2.2 Anaerobic oxidation of methane

The textural characteristics of the samples, corresponding to a formation within the sedimentary column, but with a low diagenetic degree, with the presence of pyrite, identified by XRD, and the recollection of the concretions at shallow sedimentary depths, indicates that these carbonates were formed within the sediments but below the zone of oxic diagenesis, in an anoxic environment. This implies anaerobic oxidation of methane (AOM) via sulphate reduction (SR) as typical in the methane-derived authigenic carbonates. Therefore, we can consider that these samples are formed as consequence of the upward migration of methane rich fluids, probably with minor amounts of reduced carbon-compounds, and the anaerobic oxidation of methane (AOM) in the Sulphate Reduction Zone (SRZ), according to the microbially mediated (Boetius et al., 2000) net chemical reaction (Reeburgh, 1980):



As the AOM increases the alkalinity of the pore fluids and isotopic light methane carbon is converted to bicarbonate, aragonite, Mg-calcite and dolomite, with light carbon isotopic ratio precipitates cementing the pore spaces of shallow sediments and their lithification, forming therefore these carbonate samples. Sulphide, that is another product of the coupling AOM + SR will be precipitated as pyrite, dissolved in the seawater and an important amount of it will be consumed by sulphide-based communities.

7.3 Relative formation ages

In relation to the formation ages of the different types of MDAC it is possible to distinguish the concretions from the chimneys and crusts. The concretions, as were sampled in situ through gravity coring, at 80 and 250 cm depth below the seafloor, the petrographic characteristics, with high porosity, absent of oxidized minerals (no iron oxides present) and the presence of pyrite, indicates a very recent or present-day formation. This is also supported by the pore water geochemical data, where the methane and sulfate profiles indicate these depths (80 and 250 cm depth below the seafloor) correspond to the present-day zone of sulfate-methane transition zone (Magalhães, pers. comm), therefore the zone where AOM-SR is more intense and the precipitation of MDAC is expected to occur more intensely. On the other hand, the petrographic and mineralogical characteristics of the crusts and chimneys, with high oxidized minerals (oxy-hydroxide minerals), absence of pyrite or other sulfate minerals indicate the contact of these samples with the oxidizing seawater after being formed within the sedimentary column. This is also supported by the intense colonization of the samples by benthic fauna and their intense burrowing. Therefore the crusts and chimneys correspond to older MDAC than the concretions. The crusts and chimney samples after being formed within the sedimentary column, would have to be exhumed from the sedimentary column, most probably due to the strong erosive effect of the sea bottom currents of the MOW that flows at the sites (MOW channel in front of the Gibraltar Strait, the Vernadsky ridge, the Pen Duick escarpment, the Mercator and Meknes mud volcanoes) where these samples were collected from.

The samples IV22.06 and IV22.07 have been recovered in a core on top of the Michael Ivanov Mud Volcano. This two sub-samples present the lower levels of $\delta^{13}\text{C}$, respectively -47.47‰ (VPDB) and -44.98‰ (VPDB). This can be related to the fact that near the sampling point, has been proved and investigate, during the M86/5 cruise, the presence of gas hydrates.

7.4 Formation model

The data collected permit to make some hypothesis on the formation processes of these different types of carbonate.

The chimneys and crusts, according to the formation model proposed by Magalhães (2007), are the result of expulsion of methane rich fluids along pathways of fluid circulation and escape, formed by (hydraulic) fracturing or along sedimentary discontinuities such as borrows. In fact if chimneys and crusts had formed above the seafloor, by upward growth of carbonates, in the same way of sulfide chimneys in hydrothermal vents, they should contain a very small or none detrital fraction, facts not supported by the petrographic observations of these thesis samples, where the detrital fraction composes a very significant fraction of the rock (usually about 50%). For the chimneys, considering their morphology, the degree of oxidation, the colonization and bioturbation by the benthic fauna, usually happen after the chimneys are cropped out. Therefore the chimneys with a more intense oxidation degree have been exposed to the seawater for longer periods of time and correspond to samples exhumed from shallower depths in the sediment column. In contrast, the ones without or with only weak oxidation signs and bioturbation have had a shorter period of exposure to the seawater and correspond to a formation deeper inside the sediment column. In general the dolomite crusts correspond to cemented sedimentary layers while the dolomite chimneys correspond to cemented fluid conduits.

Sediments with low permeability, like clay rich sediments will develop open vent channel chimneys and show lighter $\delta^{13}\text{C}$ and heavier $\delta^{18}\text{O}$. Sediments with high permeability will develop chimneys with closed vent channels and sometimes with concentric growth structures. The different concentric rings can reflect different episodes of venting with different intensities and different fluid compositions, or mixing fronts between the methane rich fluid and the seawater pore water.

In sites of higher flux of methane-rich fluids, migrating from deeper parts of the basin through the sediments, like occurs at the mud volcanoes, under anoxic but seawater ventilated environmental conditions (high sulfate concentrations), authigenic precipitation is dominated by aragonite and calcite. This is the formation

environment proposed for the crusts considered here.

Concretions are different: they show a main composition by calcite and very low level of dolomite (<1%), aragonite appear just in two sub-samples (IV20.06 and IV22.07). In this case, the range of the carbon isotopic composition varies between -29.54‰ and -47.47‰ VPDB. This characteristics fit very well with the MDAC concretions described by Greinet et al., 2001; Lein, 2004 and Magalhães et al., 2012. Relatively to the oxygen isotopic composition, the concretions described in this study, that were collected from the Michael Ivanov mud volcano show a significant enrichment in the heavier oxygen isotope. This enrichment can be explained with the presence of gas hydrates during the formation of these MDAC sample type. In fact, during the R/V Meteor cruise M86/5 gas hydrates were found and recollected from the Michael Ivanov mud volcano at depths of 80 cm bellow the seafloor. The concretions analyzed in this thesis can therefore be interpreted as having a formation related with the presence of gas hydrates.

It was also possible to notice that, relatively to the chimney samples analyzed in this work and comparing in with published results from other samples in the Gulf of Cadiz, the one from this work seem to cover a different range of $\delta^{13}\text{C}$ compositional values. In fact, the samples reported from Magalhães et al. (2012) show a range of $\delta^{13}\text{C}$ ranging between -30‰ and -60‰ VPDB, while our samples have values between -10‰ and -25‰ VPDB. Therefore it have been proposed four hypothesis that can explain this difference:

- The chimney samples reported in this study presents different sources areas than the previously reported in the Gulf of Cadiz (Magalhães et al., 2012). therefore these samples can reflect different gas compositions;
- The chimney samples analyzed in this thesis may represent a higher seawater influence with corresponding $\delta^{13}\text{C}$ values closer to 0 VPDB;
- The chimney samples reported in this study may exhibit late diagenetic alterations that have modified the $\delta^{13}\text{C}$ values
- Alternatively, the detrital minerals of the sediments, that are cemented by MDAC precipitated, may have different compositions that significantly change the $\delta^{13}\text{C}$ values of the bulk sample to slightly heavier compositions.

Chapter 8: Conclusions

In conclusion, in this work were described, for the first time, authigenic carbonate samples from six sites in the Gulf of Cadiz, for the first time in two of these sites. Results of this study prove that all the authigenic carbonates analyzed in this thesis are methane-derived (MDAC). The mineral composition and the isotopic values have permitted to divide the samples in three main types:

1. Chimneys, tightly carbonate-cemented, medium light grey to light brown color sandstone/mudstones. Those are sub-divided into two groups based on their morphology, one reddish-brownish, with high bioturbation, high cohesion and very well cemented; the other group of chimneys has yellow-grayish okra colors, without bioturbation signs and with lower cohesion. These two groups represent different intensities of exposition of the chimney samples to the seawater after their exhumation from the sediments in which they were formed. The formation of the chimneys is associated with the methane-rich fluids migration and escape into the top of the sedimentary column or into close to the sea bottom. In fact, the chimneys correspond to cemented fluids conducts. The mineralogy shows both calcite and dolomite minerals as main carbonate fraction, in some samples aragonite can be present in minor quantities (< 10%). The detrital fraction is, in general, high confirming the formation of these samples below the seafloor, within the sediments. Oxygen and carbon isotopes are typical and prove their formation by anaerobic methane oxidation and their methane-derived origin.
2. Crusts show both the three carbonate minerals: aragonite, calcite and dolomite, in variable percentages and have a formation process that is similar with the described for the chimneys. The detrital fraction on the crusts is in general lower than on the chimneys so, the crusts have been formed in an environment in the sedimentary column with higher pore spaces and therefore more superficial. The isotopic composition of the crusts is in agreement with the formation model described by Magalhães et al. (2012).
3. Concretions have a carbonate fraction dominated by calcite. The detrital content is higher than on the crusts or the chimneys. Concretions isotopic composition

agree with the isotopic composition of MDAC samples described in the literature. Comparing them with the other types of the studied authigenic carbonates show an enrichment in $\delta^{18}\text{O}$, due to the formation in the presence of gas hydrates (Greinet et al., 2001).

These samples show a clear relationship between carbonate fraction and the isotopic composition: an increase in the carbonate content is correlated with a decrease in $\delta^{13}\text{C}$ values and an increase in $\delta^{18}\text{O}$ values. In particular, considering the two main carbonate minerals, calcite and dolomite, it is possible to observe that an increase in the calcite content is followed by a decrease in the $\delta^{18}\text{O}$ values and the opposite variation of the $\delta^{13}\text{C}$ values. Increases of the dolomite content is followed by increases of the $\delta^{18}\text{O}$ values and decreases in the $\delta^{13}\text{C}$ values.

The majority of the studied samples have a detrital content higher than 30%, this is interpreted as indicating that the carbonate formation occurs within the sediments. The major components of the detrital fraction correspond to typical hemipelagic sediments. The crusts and concretions have pyrite, arsenopyrite and other iron sulfide minerals indicating a formation in anoxic environments, near the SRZ.

Improvements on the understanding of the methane-derived authigenic carbonates formation processes, especially in the case of the crusts, imply more analysis and more studies such as petrographic characterization with cathodoluminescence methods, Scanning-Electron Microscopic studies and Strontium isotopic studies, that were not available in this project timeframe. Also, the investigation of the relationship between gas hydrates and the formation of authigenic carbonates in the Gulf of Cadiz should be pursued, requiring the analyses of a larger number of concretion samples.

A future development of this work, including further analysis, is also important to understand if the observed differences between the chimneys described in this work and the chimneys in the Gulf of Cadiz described in the literature are resulting from one of the hypothesis that have been proposed in this thesis.

References

Web references

- <http://www.geol-pal.uni-frankfurt.de/Staff/Homepages/Petschick/PDFs/MacDiff%20Manual%20E.pdf>
- <http://pubs.usgs.gov/of/2001/of01-041/index.htm>
- <http://www.science.uottawa.ca/eih/ch9/9stront.html>
- <http://www.tulane.edu/~sanelson/geol212/carbonates.htm>
- <http://ocean.tamu.edu/Quarterdeck/QD5.3/sassen.html>
- http://www.martinhovland.com/mud_volcanoes.htm
- <http://www.isotechlabs.com/analytical/isotope/carbon.html>
- <http://www.logitech.uk.com/>
- <http://www.iso-analytical.co.uk/carbon.html>
- <http://www.isotope-analysis.com/>
- <http://www.geomar.de/en/research/expeditionen/detail-view/exp//314699/>
- http://www2.geo.ua.pt/mvseis/Mud_volcanoes.htm
- <http://pubs.usgs.gov/of/2001/of01-041/index.htm>

Papers

- Abbate, E., Balestrieri, M.L., Bigazzi, G., Ventura, B., Zattin, M., Zuffa, G.G.** 1999. An extensive apatite fission-track study throughout the Northern Apennines nappe belt. *Radiation Measurements*, 31: 673–676.
- Abbate, E., Bortolotti, V., Conti, M., Marcucci, M., Principi, G., Passerini, P., Treves, B.** 1986. Apennines and Alps ophiolites and the evolution of the Western Tethys. *Memorie della Societa` Geologica Italiana*, 31: 23–44.
- Abbate, E., Bortolotti, V., Principi, G.**, 1980. Apennine ophiolites: a peculiar oceanic crust. Rocci, G. (Ed.), *Tethyan Ophiolites: 1. Western Area vol. 1. Ofioliti, Spec. Issue*: pp. 59–96
- Aiello, I.W., Hagstrum, J.T., Principi, G.** 2004. Late Miocene remagnetization within the internal sector of the Northern Apennines, Italy. *Tectonophysics*, 383: 1–14.
- Akhmetzhanov, A. M., M. K. Ivanov, N. H. Kenyon, and A. Mazzini, eds.**, 2007, Deep-water cold seeps, sedimentary environments and ecosystems of the Black and Tyrrhenian Seas and the Gulf of Cadiz. Preliminary results of investigations during the TTR-15 cruise of RV Professor Logachev June-August, 2005: IOC Technical Series, v. 72: Paris, United Nations Educational, Scientific and Cultural Organization, 140 p.
- Akhmetzhanov, A. M., N. H. Kenyon, M. K. Ivanov, G. Westbrook, and A. Mazzini, eds.**, 2008, Deep-water depositional systems and cold seeps of the Western Mediterranean, Gulf of Cadiz and Norwegian continental margins. Preliminary results of investigations during the TTR-16 cruise of RV Professor Logachev May-July, 2006: Intergovernmental Oceanographic Commission technical series, v. 76: Paris, UNESCO, 91 p.
- Alaoui Mhammedi N., El Mounni, B., El Hmaid, A., Raissouni, A., El Arrim, A.** 2008. Mineralogical and geochemical study of mud volcanoes in north Moroccan atlantic margin. *African Journal of Environmental Science and Technology*. 2: 387-396.
- Aloisi, G., Pierre, C., Rouchy, J.M., Foucher, J.P., Woodside, J.** and the MEDINAUT Scientific Party. 2000. Methane-related authigenic carbonates of eastern Mediterranean Sea mud volcanoes and their possible relation to gas hydrate destabilisation. *Earth and Planetary Science Letters*, 5675: 1–18.
- Aloisi, G., Bouloubassi, I., Heijs, S.K., Pancost, R.D., Pierre, C., Sinninghe Damste, J.S., Gottschal, J.C., Forney, L.J., Rouchy, J.M.** 2002. CH₄-consuming microorganisms and the formation of Carbonate crusts at cold seeps. *Earth and Planetary Science Letters*, 203:

195-203.

- Amato, A., Cinque, A. and Santangelo, N.** 1995, Il controllo della struttura e della tettonica plio-quadernaria sull'evoluzione del reticolo idrografico dell'Appennino meridionale. *Studi Geologici Camerti*, vol. spec. 2: 23-30.
- Anderson, T. F., Arthur, M. A.** 1983. Stable isotopes of oxygen and carbon and their application to sedimentologic and paleoenvironmental problems. In: Arthur, M. A. ed. *Stable isotopes in sedimentary geology*. SEPM short course 10:1.1-1.151
- Artegiani, A., Bregant, D., Paschini, E., Pinardi, N., Raichich, F. and Russo, A.** 1977. The Adriatic Sea general circulation. Part I: Air-sea interactions and water mass structure. *Journal Physical Oceanography*, 27: 1492-1514.
- Bayon, G., Loncke, L., Dupré, S., Caprais, J.C., Ducassou, E., Duperron, S., Etoubleau, J., Foucher, J.P., Fouquet, Y., Gontharet, S. and others.** 2009. Multi-disciplinary investigation of fluid seepage on an unstable margin: The case of the Centre Nile deep sea fan. *Marine Geology*, 261: 92-104.
- Barnes, R.O. and Goldhaber, L.D.**, 1976 Methane Production and Consumption in Anoxic Marine Sediments, *Geology*, vol. 4, pp. 1977-1984.
- Ben-Avraham, Z., Smith, G., Reshef, M., Jungslager, E.**, 2002. Gas hydrate and mud volcanoes on the southwest African continental margin off South Africa. *Geology* 30, 927-930.
- Boccaletti, M., Bonini, M., Moratti, G., Sani, F.** 1999. Compressive Neogene-Quaternary tectonics of the hinterland area of the Northern Apennines. *Journal of Petroleum Geology*, 22: 37-60.
- Boccaletti, M., Coli, M., Decandia, F., Giannini, E., Lazzarotto, A.**, 1980. Evoluzione dell'Appennino Settentrionale secondo un nuovo modello strutturale. *Memorie della Società Geologica Italiana* 21: 359-374.
- Boetius, A., and Suess, E.** 2004. Hydrate Ridge: A natural laboratory for the study of microbial life fueled by methane from near-surface gas hydrates. *Chemical Geology*, 205: 291-310.
- Boetius, A., Ravenschlag, K., Schubert, C.J., Rickert, D., Widdel, F., Giesecke, A., Amann, R., Jorgensen, B.B., Witte, U. and Pfannkuche, O.** 2000. A marine microbial consortium apparently mediating anaerobic oxidation of methane. *Nature*, 407: 623-626.
- Bohrmann, G., J. Greinert, E. Suess, and M. Torres**, 1998, Authigenic carbonates from the Cascadia subduction zone and their relation to gas hydrate stability: *Geology*, v. 26, p. 647-650.
- Borenäs, K.M., Wåhlin, A.K., Ambar, I. and Serra, N.** 2002. The Mediterranean Outflow splitting a comparison between theoretical models and CANIGO data. *Deep-Sea Res., Part II*, 49 (19):4195-4205.
- Borges, J.F., Fitas, A.J.S., Bezzeghoud, M., and Teves-Costa, P.** 2001. Seismotectonics of Portugal and its adjacent Atlantic area. *Tectonophysics*, 331(4): 373-387.
- Bouloubassi, I., Aloisi, G., Pancost, R., Hopmans, E., Pierre, C. and Sinninghe Damste, J.R.** 2006. Archeal and bacterial lipids in authigenic carbonate crusts from eastern Mediterranean mud volcanoes. *Organic Geochemistry*, 37:484-500.
- Bryden, H.L., Candela, J., and Kinder, T.H.** 1994. Exchange through the Strait of Gibraltar. *Progress In Oceanography*, 33(3): 201-248.
- Campbell, K.A., Farmer, J.D., and Des Marais, D.** 2002. Ancient hydrocarbon seeps from the Mesozoic convergent margin of California: Carbonate geochemistry, fluids and palaeoenvironments. *Geofluids*, 2: 63-94.
- Capozzi, R., Picotti, V.** 2002. Fluid migration and origin of a mud volcano in the northern Apennines (Italy): the role of deeply rooted normal faults. *Terra Nova*, 14: 363-370.
- Capozzi, R., Picotti, V.** 2010. Spontaneous fluid emissions in the Northern Apennines: geochemistry, structures and implications for the petroleum system. *Geological Society, London, Special Publications* 348 (1), 115-135.
- Carmignani, L., Kligfield, R.** 1990. Crustal extension in the Northern Apennines: the transition from compression to extension in the Alpi Apuane core complex. *Tectonics*, 9: 1275-1303.
- Chand, S., Mienert, J., Andreassen, K., Knies, J., Plassen, L. and Fotland, B.** 2008. Gas hydrate stability zone modeling in areas of salt tectonics and pockmarks of the Barents Sea suggest an active hydrocarbon venting system. *Marine and Petroleum Geology*, 25: 625-636.
- Cherubin, L., Carton, X., Paillet, J., Morel, Y., and Serpette, A.**, 2000. Instability of the Mediterranean Water undercurrents southwest of Portugal: effects of baroclinicity and of topography. *Oceanologica Acta*, 23(5):551-573.
- Chiari, M., Cortese, G., Marcucci, M., Nozzoli, N.**, 1997. Radiolarian biostratigraphy in the sedimentary cover of ophiolites of south-western Tuscany, Central Italy. *Eclogae Geologicae*

- Hel- veticae, 90: 55–77.
- Conti, S., Fontana, D.** 1999a. Miocene chemohermes of the northern Apennines (Italy). *Geology*, 27: 927–930.
- Coleman, M. L.** 1993. Microbial processes: controls on the shape and composition of carbonate concretions. *Marine geology*, 113: 127-140.
- Coleman, D.F., Ballard, R.D.** 2001. A highly concentrated region of cold hydrocarbon seeps in the southeastern Mediterranean Sea. *Geo-Mar Lett* 21(3):162–167
- Conti, S., Fontana, D.** 2002. Sediment instability related to fluid venting in Miocene authigenic carbonate deposits of the northern Apennines (Italy). *International Journal of Earth Sciences*, 91: 1030–1040.
- Corfield, R. M.** 1995. An introduction to the techniques, limitations and landmarks of carbonate oxygen isotope palaeo- thermometry. In: Bosence, D. W. J.; Allison, P. A. ed. *Marine palaeoenvironmental analysis from fossils*. Geological Society special publication 83: 27-42.
- Cortese, G.** 1995. Radiolarian biostratigraphy of Tuscan cherts (Tuscan Succession) from Val di Lima (Tuscany, northern Apennines, Italy). In: Baumgartner, P.O. (et al.) (eds) *Middle Jurassic to Lower Cretaceous radiolaria of Tethys : occurrences, systematics, biochronology*. Lausanne: Institut de Geologie et Paleontologie. *Memoires de geologie Lausanne*, v.23: 813-816.
- Claypool, G. E., and I. R. Kaplan,** 1974, The origin and distribution of methane in marine sediments: *Marine Science*, v. 3, p. 99-139.
- D’Agostino, N., Jackson, J., Dramis, F. and Funicello, R.** 2001. Interactions between mantle upwelling, drainage evolution and active normal faulting: an example from the central Apennines (Italy). *Geophysical Journal International*, v. 147: 475-497.
- De Boever, E., Swennen, R., Dimitrov, L.** 2006. Lower Eocene carbonate cemented chimneys (Varna, NE Bulgaria): Formation mechanisms and the (a)biological mediation of chimney growth? *Sedimentary Geology*, 185: 159-173.
- Delacour, A. Früh-Green, G. L.; Bernasconi, S.M; Schaeffer, P.; Kelley, D. S** 2008. Carbon geochemistry of serpentinites in the Lost City hydrothermal system (30° N, MAR). *Geochimica et Cosmochimica Acta*, 72(15), 3681-3702.
- DeLong E.F.** 2000. Resolving a methane mystery. *Nature*, vol. 407: 578-579
- Dercourt, J., Zonenshain, L.P., Ricou, L.E., Kazmin, V.G., Le Pichon, X., Knipper, A.L., Grandjacquet, C., Sbertshikov, I.M., Geysant, J., Lepvrier, C.P., Pechersky, D.H., Boulin, I.J., Sibuet, J.C., Savostin, L.A, Sorokhtin, O., Westphal, M., Bazhenov, M.L., Lauer, J.P., Biju-Duval, B.** 1986. Geological evolution of the Tethys from the Atlantic to the Pamirs since the Lias. *Tectonophysics*, 123: 241–315.
- Díaz-del-Río, V., L. Somoza, J. Martínez-Frias, M. P. Mata, A. Delgado, F. J. Hernandez-Molina, R. Lunar, J. A. Martín-Rubí, A. Maestro, M. C. Fernández-Puga, R. León, E. Llave, T. Medialdea, and J. T. Vázquez,** 2003, Vast fields of hydrocarbon-derived carbonate chimneys related to the accretionary wedge/olistostrome of the Gulf of Cádiz: *Marine Geology*, v. 195, p. 177-200.
- Dimitrov, L.I.** 2002. Mud volcanoes the most important pathway for degassing deeply buried sediments. *Earth-Science Reviews*, 59: 49–76.
- Dimitrov, L.I.** 2003. Mud volcanoes a significant source of atmospheric emission from the mud volcanoes of Sicily (Italy). *Geophysical Research Letters* , 29 (8), 56(1/4).
- Dunham, R.J.** 1962. Classification of carbonate rocks according to depositional texture. In Ham, W.E. *Classification of carbonate rocks*. American Association of Petroleum Geologists *Memoir*, 1: pp. 108-121.
- Etiope, G., Baciu, C., Caracausi, A., Italiano, F., Cosma, C.** 2004. Gas flux to the atmosphere from mud volcanoes in eastern Romania. *Terra Nova*, 16: 179–184.
- Etiope, G., Klusman, R.W.** 2002. Geologic emissions of methane to the atmosphere. *Chemosphere*. VOL 49; 8, 2002: 777-789
- Faccenna, C., Becker, T.W., Lucente, F.P., Jolivet, L., Rossetti, F.** 2001. History of subduction and back-arc extension in the Central Mediterranean. *Geophysical Journal International*, 145: 809 – 820.
- Faccenna, C., Jolivet, L., Piromallo, C., Rossetti, F., Vignaroli, G.** 2008. Subduction polarity reversal at the junction between the Western Alps and the Northern Apennines, Italy. *Tectonophysics*, 450: 34–50.
- Fader, G.B.J.** 1991: Gas-related sedimentary features from the eastern Canadian continental shelf. *Continental Shelf Research* 11, 1123- 1153.
- Fairchild, I., Hendry, G., Quest, M., Tucker, M.** 1988. Chemical analysis of sedimentary rocks. In: Tucker, M. ed. *Techniques in sedimentology*. Oxford, Blackwell Scientific Publications:

274-354.

- Fantoni, R., Franciosi, R.**, 2008 - 8 geological sections crossing Po Plain and Adriatic foreland. *Rend. Soc. Geol. It.*, 3/1, Riassunti dell'84° Congresso Nazionale Sassari 15-17 settembre 2008 (Italy), 367-368.
- Fantoni, R., Bertello, F., Franciosi, R.**, 2008 - Reservoirs and source rocks in Mesozoic carbonate units of Italy. *Rend. Soc. Geol. It.*, 3/1, Riassunti dell'84° Congresso Nazionale Sassari 15-17 settembre 2008 (Italy), 365-366.
- Forwick, M., Baeten, N.J. and Vorren, T.O.** 2009. Pockmarks in Spitsbergen fjords. *Norwegian Journal of Geology*, vol. 89: 65-77.
- Foucher J.P., Westbrook G.K., Boetius A., Ceramicola S., Dupré S., Mascle J., Mienert J., Pfannkuche O., Pierre C. and Praeg D.** 2009. Structure and drivers of cold Seep Ecosystems, *Oceanography*. Vol 22, (1) : 92-109.
- Frepoli, A., and Amato, A.** 1997. Contemporaneous extension and compression in the northern Apennines from earthquake fault plane solutions. *Geophysical Journal International*, v. 129 : 368-388.
- Gay, A., Lopez, M., Berndt, C. and Séranne, M.** 2007. Geological controls on focused fluid flow associated with seafloor seeps in the Lower Congo Basin. *Marine Geology*, 244: 68-92.
- Gontharet, S., Pierre, C., Blanc-Valleron, M.M., Rouchy, J.M., Fouquet, Y., Bayon, G., Foucher, J. P., Woodside, Mascle, J.** and the NAUTINIL Scientific Party. 2007. Nature and origin of diagenetic carbonate crusts and concretions from mud volcanoes and pockmarks of the Nile deep-sea fan (eastern Mediterranean Sea). *Deep Sea Research, Part II, Topical Studies in Oceanography*, 54, (11-13): 1292-1311.
- González, J.F., Somoza, L., Lunar, R., Martínez-Frías, J., Martín Rubí, J.A., Torres, T., Ortiz, J.E., Díaz del Río, V., Pinheiro, L.M., Magalhães, V.H.** 2009. Hydrocarbon-derived ferromanganese nodules in carbonate-mud mounds from the Gulf of Cadiz: Mud-breccia sediments and clasts as nucleation sites. *Marine Geology*, 261: 64-81.
- Goldsmith, J.R. and Graf, D.L.** 1958. Relation between lattice constants and composition of the Ca-Mg Carbonates. *The American Mineralogist*, 43: 84-101.
- Graue, K.** 2000. Mud volcanoes in deepwater Nigeria. *Marine and Petroleum Geology*, 17: 959-974.
- Greinert, J., Bohrmann, G. and Suess, E.** 2001. Gas hydrate-associated carbonates and methane-venting at Hydrate Ridge: Classification, distribution, and origin of authigenic lithologies. In *Natural Gas Hydrates: Occurrence, Distribution, and Detection*, Geophys. Monogr. Ser., vol. 124, edited by C. K. Paull and W. P. Dillon, Washington, D. C.: 99-113.
- Greinert, J., Artemov, Y., Egorov, V., De Batist, M. and McGinnis, D.** 2006. 1300-m-high rising bubbles from mud volcanoes at 2080 m in the Black Sea: Hydroacoustic characteristics and temporal variability. *Earth and Planetary Science Letters*, 244: 1-15.
- Harrington, P.K.** 1985: Formation of Pockmarks by Pore-Water Escape. *Geo-Marine Letters* 5, 193-197.
- Hensen, C., Nuzzo M., Hornibrook E., Pinheiro L.M., Bock B., Magalhães V.H., and Brückmann W.** 2007 "Sources of Mud Volcano Fluids in the Gulf of Cadiz - Indications for Hydrothermally Altered Fluids." *Geochimica et Cosmochimica Acta* 71, no. 5 ,1232-48.
- Hernandez-Molina, F.J. et al.**, 2006. The contourite depositional system of the Gulf of Cadiz: A sedimentary model related to the bottom current activity of the Mediterranean outflow water and its interaction with the continental margin. *Deep-Sea Research Part II-Topical Studies in Oceanography*, 53(11-13): 1420-1463
- Hovland, M. & Judd, A.G.** 1988: Seabed Pockmarks and Seepages: Impact on Geology, Biology and the Marine Environment. Graham & Trotman Ltd., London, 293 pp.
- Hovland, M., Gardner, J.V. & Judd, A.G.** 2002: The significance of pockmarks to understanding fluid flow processes and geohazards. *Geofluids* 2, 127-136.
- Hudson, J.D.** 1977. Stable Isotopes and Limestone Lithification, *Journal of the Geological Society*, 133, (6): 637-660.
- Irwin, H., Curtis, C., and Coleman, M.**, 1977. Isotopic evidence for source of diagenetic carbonates formed during burial of organic-rich sediments. *Nature*, 269: 209-213.
- Ivanov MK, Kenyon N, Nielsen T, Wheeler A, Monteiro J, Gardner J, Comas M, Akhmanov G, Akhmetzhanov A**, Scientific Party TTR-9 Cruise, 2000. Goals and principle results of the TTR-9 cruise. UNESCO-IOC Worksh Rep 168:3-4
- Ivanov, M., Westbrook, G.K., Blinova, V., Kozlova, E., Mazzini, A., Nouzé, H. and Minshull, T.A.** 2007. First sampling of gas hydrate from the Voring Plateau. *Eos, Transactions of the American Geophysical Union*, 88(19): 209-212.
- Jolivet, L., Faccenna, C., Goffe, B., Mattei, M., Rossetti, F., Brunet, F., Storti, F., Funicello,**

- R., Cadet, J.P., D'Agostino, N., Parra, T.** 1998. Midcrustal shear zones in post orogenic extension: example from the Northern Tyrrhenian Sea. *Journal of Geophysical Research*, 103: 123–160.
- Jørgensen, N. O.,** 1989, Holocene methane-derived, dolomite-cemented sandstone pillars from the Kattegat, Denmark: *Marine Geology*, v. 88, p. 71-81.
- Judd, A., Long, D., Sanley, M.** 1994. Pockmark formation and activity, U.K. block 15/25, North Sea. *Bull Geol Soc Denmark* 41:34–49
- Judd, A.G. & Hovland, M.** 2007: *Seabed Fluid Flow: The Impact on Geology, Biology and the Marine Environment*. Cambridge University Press, Cambridge, 475 pp.
- Kvenvold, K.A., Rogers, B.W.** 2005. Gaia's breath—global methane exhalations. *Marine and Petroleum Geology* 22 : 579–590.
- Kelley, D.S., Karson, J.A., Blackman, D.K., et al.** 2001. An Off-Axis Hydrothermal Vent Field near the Mid-Atlantic Ridge at 30° N. *Nature*, 412 : pp. 145–148.
- Kelley, J.T., Dickson, S.M., Belknap, D.F., Barnhardt, W.A. and Henderson, M.** 1994. Giant seabed pockmarks: Evidence for gas escape from Belfast Bay, Maine. *Geology*, 22 : 59-62.
- Kennicut, M.C., Brooks, J.M., Bidigare, R.R., Fay, R.R., Wade, T.L. and McDonald, T.J.** 1985. Vent type taxa in a hydrocarbon seep region on the Louisiana Slope. *Nature* ,317:351–353.
- Kenyon, N. H., M. K. Ivanov, A. M. Akhmetzhanov, and G. G. Akhmanov, eds.,** 2006, Interdisciplinary geoscience studies of the Gulf of Cadiz and Western Mediterranean basins. Preliminary results of investigations during the TTR-14 cruise of RV Professor Logachev July-September, 2004: IOC Technical Series, v. 70: Paris, United Nations Educational, Scientific and Cultural Organization, 115 p.
- Kulm, L. D., and E. Suess,** 1990, Relationship between carbonate deposits and fluid venting: Oregon accretionary prism: *Journal of Geophysical Research-Solid Earth and Planets*, v. 95, p. 8899-8915.
- Kulm, L. D., E. Suess, J. C. Moore, B. Carson, B. T. Lewis, S. D. Ritger, D. C. Kadko, T. M. Thornburg, R. W. Embley, W. D. Righ, G. J. Massoth, M. G. Langseth, G. R. Cochrane, and R. L. Scamman,** 1986, Oregon subduction zone: venting, fauna, and carbonates: *Science*, v. 231, p. 561-566.
- Lein , A. Yu.**2004. Authigenic Carbonate Formation in the Ocean, *Lithology and Mineral Resources*, 39 (1): 1–30. Translated from *Litologiya i Poleznye Iskopaemye*, No. 1, 2004: 3–35.
- Lein, A.Yu., Bogdanov, Yu.A., Sagalevich, A.M., et al.**2002. White Columns of a Lost City. *Priroda*, 12 : pp. 40–46.
- Lein, A.Yu., Ivanov, M.V., Pimenov, N.V., and Gulin, M.B.**2002. Geochemical Characteristics of Carbonate Buildups Formed due to Microbial Methane Oxidation in Anaerobic Conditions. *Mikrobiologiya*, 71, (1): pp. 89–102.
- León, R. , Somoza, L. , Medialdea, T. , González, F. J. , Díaz-Del-Río, V. , Fernández-Puga, M. C. , Maestro, A. ; Mata, M. P.** 2007. Sea-floor features related to hydrocarbon seeps in deepwater carbonate-mud mounds of the Gulf of Cádiz: from mud flows to carbonate precipitates. *Geo-Marine Letters*, 27, (2-7): 237-247.
- Loncke, L., Mascle, J. and Fanil Scientific Parties.** 2004. Mud volcanoes, gas chimneys, pockmarks and mounds in the Nile deep-sea fan (Eastern Mediterranean): geophysical evidences. *Marine and Petroleum Geology*, 21: 669-689.
- Luff, R., Greinert, J., Wallmann, K., Klauke, I., Suess, E.** 2005. Simulation of long-term feedbacks from authigenic carbonate crust formation at cold vent sites. *Chemical Geology*, 216: 157-174.
- Luff, R., Wallmann, K. and Aloisi, G.** 2004. Numerical modelling of carbonate crust formation at cold vent sites: Significance for fluid and methane budgets and chemosynthetic biological communities. *Earth and Planetary Science Letters*, 221: 337–353.
- Lumsden, D.N.** 1979. Discrepancy between thin-section and X-ray estimates of dolomite in limestone. *Journal of Sedimentary Petrology*, 49: 429-435.
- MacDonald, I.R., Buthman, D.B., Sager, W.W., Peccini, M.B., Guinasso Jr., N.L.** 2000. Pulsed oil discharge from a mud volcano. *Geology*, 28: 907–910.
- MacDonald, I.R., Guinasso Jr., N.L., Sassen, R., Brooks, J.M., Lee, L., Scott, K.T.** 1994. Gas hydrate that breaches the sea floor on the continental slope of the Gulf of Mexico. *Geology*, 22: 699–702.
- Magalhaes, V.H.** Carbonates autigénicos e estruturas de escape de fluidos no Golfo de Cádiz. Tese apresentada do grau de Doutor em Geociências. Departamento de Geociências, Universidade de Aveiro. a.a. 2006-2007.
- Magalhães, V.H., Pinheiro, L.M., Ivanov, M.K., Kozlova, E., Blinova, V., Kolganova, J.,**

- Vasconcelos, C. , McKenzie, J.A., Bernasconi, S.M., Kopf, A.J., Díaz-del-Río, V., González, F.J., Somoza, L.** 2012. Formation processes of methane-derived authigenic carbonates from the Gulf of Cadiz. *Sedimentary Geology*, 243-244: 155-168.
- Maldonado, A., Nelson, C. H.** 1999. Interaction of tectonic and depositional processes that control the evolution of the Iberian Gulf of Cadiz margin. *Marine Geology*, 155: 217-242.
- Maldonado, A., Somoza, L., and Pallarés, L.** 1999. The Betic orogen and the Iberian–African boundary in the Gulf of Cádiz: geological evolution (central North Atlantic). *Marine Geology*, 155,(1–2): 9–43.
- Marshall, J. D.** 1992. Climatic and oceanographic isotopic signals from the carbonate rock record and their preservation. *Geological Magazine*, 129: 143–160.
- Mazurenko, L.L., Soloviev, V.A., Gardner, J.M., Ivanov, M.K.** 2003. Gas hydrates in the Ginsburg and Yuma mud volcano sediments (Moroccan margin): results of chemical and isotopic studies of pore water. *Marine Geology*, 195: 201–210.
- Mazzini, A., H. Svensen, M. Hovland, and S. Planke.** 2006. Comparison and implications from strikingly different authigenic carbonates in a Nyegga complex pockmark, G11, Norwegian Sea. *Marine Geology* 231:89–102.
- McKenzie, D.P.**1972. Active tectonics of the Mediterranean region. *Geophysical Journal of the Royal Astronomical Society*, 30: 109-185.
- Medialdea, T., Somoza, L., Pinheiro, L.M., Fernández-Puga, M.C., Vázquez, J.T., León, R., Ivanov, M.K., Magalhaes, V., Díaz del Río, V., and Vegas, R.** 2009. Tectonics and mud volcano development in the Gulf of Cádiz. *Marine Geology*, 261(1–4): 48–63.
- Medialdea, T., Vegas, R., Somoza, L., Vázquez, J.T., Maldonado, A., Díaz-del-Río, V., Maestro, A., Córdoba, D., and Fernández-Puga, M.C.** 2004. Structure and evolution of the “Olistostrome” complex of the Gibraltar Arc in the Gulf of Cádiz (eastern Central Atlantic): evidence from two long seismic cross-sections. *Marine Geology*, 209, (1–4):173–198.
- Michaelis, W., Seifert, R., Nauhaus, K., et al.**2002. Microbial Reefs in the Black Sea Fueled by Anaerobic Oxidation of Methane. *Science*, 297: 1013–1015.
- Milkov, A., Vogt, P.R., Cherkashev, G., Ginsburg, G, Chernova, N, and Andriashev, A.** 1999. Seafloor terrains of Håkon Mosby Mud Volcano as surveyed by deep-tow video and still photography. *Geo-Marine Letters*, 19: 38–47.
- Milkov, A., Vogt, P.R., Crane, K., A.Y. Lein, R. Sassen, and G.A. Cherkashev.** 2004. Geological, geochemical, and microbial processes at the hydrate bearing Håkon Mosby mud volcano: A review. *Chemical Geology*, 205: 347–366.
- Miller, D. J.,** 2006, Caracterização geoquímica e geológica de duas exsudações de Hidrocarbonetos na Bacia de Campos: Master thesis, Universidade Federal do Rio de Janeiro, COPPE, Rio de Janeiro, 181 p.
- Millot, C.** 2009. Another description of the Mediterranean Sea Outflow. *Progress In Oceanography*, 82, (2): 101–124.
- Mozley, P. S., Burns, S. J.** 1993. Oxygen and carbon isotopic composition of marine carbonate concretions: an overview. *Journal of sedimentary petrology*, 63: 73–83.
- Moore, J. C., and Vrolijk P.** 1992, Fluids in accretionary prisms, *Rev. Geophys.*, 30, 113-135.
- Muralidhar, K., A. Mazumdar, S. M. Karisiddaiah, D. V. Borole, and B. R. Rao,** 2006, Evidences of methane-derived authigenic carbonates from the sediments of the Krishna-Godavari Basin, eastern continental margin of India: *Current Science*, v. 91, p. 318-323.
- Naehr, T.H., Rodriguez N.M., Bohrmann, G., Paull, C.K., and Botz, R.** 2000. Methane-derived authigenic carbonates associated with gas hydrate decomposition and fluid venting above the Blake Ridge Diapir. In Paull, C.K., Matsumoto, R., Wallace, P.J., and Dillon, W.P. (Eds.), *Proc. ODP, Sci. Results*, 164 College Station, TX (Ocean Drilling Program): 285-300.
- Nadalig, K. Knittel, R. Amann, E.J. Sauter, M. Schlüter, M. Klages,** and others. 2006. Novel microbial communities of the Haakon Mosby mud volcano and their role as methane sink. *Nature*, 443: 854–858.
- Nelson C.H. , Maldonado, A.** 1999. The Cadiz margin study off Spain: an introduction. *Marine Geology*, 155: 3-8.
- Niemann, H., Duarte, J., Hensen, C., Omoregie, E., Magalhães, V.H., Elvert, M., Pinheiro, L., Kopf, A., and Boetius, A.** 2006. Microbial methane turnover at mud volcanoes of the Gulf of Cádiz. *Geochimica et Cosmochimica Acta*, 70: 5.336–5.355.
- Niemann H., T. Lösekann, D. de Beer, M. Elvert, T., Nissenbaum, A.,** 1984 Methane Derived Organic Matter and Carbonates, *Org. Geochem.*, vol. 5, no. 4, pp. 187–192.
- Nuzzo, M., F. Gill, C. Hensen, E. R. C. Hornibrook, R. D. Pancost, V. H. Magalhães, M. Haeckel, and L. M. Pinheiro,** 2007, The origins of light volatile hydrocarbon gases from mud volcano fluids, Gulf of Cadiz: ESF SEECAM Workshop. *Geological, Chemical and*

Biological Interactions at Cold Seeps and Carbonate Mounds.

- Oliver, G., Rodrigues, C.F., Cunha, M.R.** 2011. Chemosymbiotic bivalves from the mud volcanoes of the Gulf of Cadiz, NE Atlantic, with descriptions of new species of Solemyidae, Lucinidae and Vesicomidae. *ZooKeys*, 113: 1–38.
- Orpin, A. R.**, 1997, Dolomite chimneys as possible evidence of coastal fluid expulsion, uppermost Otago continental slope, southern New Zealand: *Marine Geology*, v. 138, p. 51-67.
- Patacca, E., Sartori, R., and Scandone, P.**, 1992, Tyrrhenian basin and Apenninic arcs: Kinematics relations since late Tortonian times. *Memorie della Società Geologica Italiana*, 45: 425-451.
- Paull, C., Ussler III, W., Maher, N., Greene, H.G., Rehder, G., Lorenson, T. and Lee, H.** 2002. Pockmarks off Big Sur, California. *Marine Geology*, 181: 323-335.
- Paull, C.K., Ussler III, W. & Borowski, W.S.** 1999. Freshwater ice rafting: an additional mechanism for the formation of some high-latitude pockmarks. *Geo-Marine Letters* 19: 164-168.
- Paull, C. K., J. P. Chanton, A. C. Neumann, J. A. Coston, C. S. Martens, and W. Showers**, 1992, Indicators of methane-derived carbonates and chemosynthetic organic carbon deposits: examples from the Florida Escarpment: *Palaios*, v. 7, p. 361-375.
- Peckmann, J., A. Reimer, U. Luth, C. Luth, B. T. Hansen, C. Heinicke, J. Hoefs, and J. Reitner**, 2001, Methane-derived carbonates and authigenic pyrite from the northwestern Black Sea: *Marine Geology*, v. 177, p. 129-150.
- Pickrill, R.A.** 1993. Shallow seismic stratigraphy and pockmarks of a hydrothermally influenced lake, Lake Rotoiti, New Zealand. *Sedimentology*, 40: 813-828.
- Pilcher, R. and Argent, J.** 2007. Mega-pockmarks and linear pockmark trains on the West African continental margin. *Marine Geology*, 244: 15-32.
- Pimenov, N.V., Rusanov, I.I., Poglazova, M.N.**, et al., 1997 Bacterial Overgrowths on Coral-Type Buildups at Gas Discharge Sites in the Black Sea, *Mikrobiologiya*, vol. 66, pp. 421–428.
- Pimenov, N.V., Rusanov, I.I., Poglazova, M.N.**, et al., 1998 Bacterial Mats on Coral-Shaped Carbonate Structures in Methane Seep Areas of the Black Sea, *Megaseeps, Zentrum für Meeres und Klimaforschung der Universität Hamburg, (Hamburg)*, vol. 14, pp. 37–50.
- Pimenov, N., Savvichev, A., Rusanov, I.**, et al., 1999 Microbial Processes of Carbon Cycle as the Base of Food Chain of Haa- kon Mosby Mud Volcano Benthic Community, *GEOMAR Lett.*, vol. 19, pp. 89–96.
- Pimenov, N.V., Savvichev, A.S., Rusanov, I.I.**, et al., 2000 Micro- bial Processes of Carbon and Sulfur Cycles on Cold Methane Seeps of the North Atlantic, *Mikrobiologiya*, vol. 69, no. 6, pp. 810–818.
- Pinheiro, L. M., Ivanov, M.K.** et al. 2003. Mud volcanism in the Gulf of Cadiz: results from the TTR-10 cruise. *Marine Geology* , 195(1-4): 131-151.
- Pinheiro, L.M., Wilson, R.C.L., Pena dos Reis, R., Whitmarsh, R.B., and Ribeiro, A.** 1996. The Western Iberia margin: a geophysical and geological overview. In Whitmarsh, R.B., Sawyer, D.S., Klaus, A., and Masson, D.G. (Eds.), *Proc. ODP, Sci. Results*, 149: College Station, TX (Ocean Drilling Program), 3–23.
- Plassen, L. & Vorren, T.O.** 2003: Fluid flow features in fjord-fill deposits, Ullsfjorden, North Norway. *Norwegian Journal of Geology* 83, 37-42.
- Principi, G., Treves, B.**, 1984. Il sistema corso-appenninico come prisma di accrezione. Riflessi sul problema generale del limite Alpi-Appennini. *Memorie della Società Geologica Italiana*, 28: 549-576.
- Reeburgh, W.S.**, 1976 Methane Consumption in Cariaco Trench Waters and Sediments, *Earth Planet. Sci. Lett.*, vol. 28, pp. 337–344.
- Reeburgh, W. S.**, 1980, Anaerobic methane oxidation: rate depth distributions in Skan Bay sediments: *Earth and Planetary Science Letters*, v. 47, p. 345-352.
- Reeburgh, W.S. and Alperin, M.J.**, 1988 Studies on Anaerobic Methane Oxidation, *Mitt. Geol.-Paleontol. Inst., Hamburg: Univ. Hamburg*, vol. 66, pp. 367–375.
- Reeburgh, W.S. and Heggie, D.T.**, 1977 Microbial Methane Consumption Reactions and Their Effect on Methane Distributions in Freshwater and Marine Environments, *Limnol. Oceanogr.*, vol. 22, pp. 1–9.
- Ricci Lucchi, F., Vai, G.B.**, 1994. A stratigraphic and tectonofacies framework of the “calcari a Lucina” in the Apennine Chain, Italy. *Geo-Marine Letters*, 14: 210–218.
- Ritger, S., B. Carson, and E. Suess**, 1987, Methane-derived authigenic carbonates formed by subduction-induced pore-water expulsion along the Oregon/Washington margin: *Geological Society of America Bulletin*, v. 98, p. 147-156.
- Rodriguez, C.L.** Comunidades macrobentónicas dos vulcões de lama do Golfo de Cádiz.

Dissertacao do grau de Doutor em Biologia. Departamento de Biologia, Universidade de Aveiro. a.a. 2008-2009.

- Rogers, J.N., Kelley, J.T., Belknap, D.F., Gontz, A. and Barnhardt, W.A.** 2006. Shallow-water pockmark formation in temperate estuaries: A consideration of origins in the western gulf of Maine with special focus on Belfast Bay. *Marine Geology*, 225: 45-62.
- Rosenfeld, W. D., and S. R. Silverman,** 1959, Carbon Isotope Fractionation in Bacterial Production of Methane: *Science*, v. 130, p. 1658-1659.
- Rosenbaum J. and Sheppard S. M. F.** 1986. An isotopic study of siderites, dolomites and ankerites at high temperatures. *Geochim. Cosmochim. Acta* 50, 1147–1150.
- Sassen, R., Brooks J.M., MacDonald I.R., Kennicutt M.C.** 1993. Association of oil seeps and chemosynthetic communities with oil discoveries, upper continental slope, Gulf of Mexico. In: *Proc 43rd Annu Conv AAPG, LA*, pp 349–356
- Sautkin, A., Talukder, A.R., Comas, M.C., Soto, J.I., Alekseev, A.,** 2003. Mud volcanoes in the Alboran Sea: evidence from micropaleontological and geophysical data. *Marine Geology* 195, 237–261.
- Serra, N., Ambar, I., and Boutov, D.,** 2010a. Surface expression of Mediterranean Water dipoles and their contribution to the shelf/slope–open ocean exchange. *Ocean Science*, 6, (1): 191–209.
- Serra, N., Käse, R.H., Köhl, A., Stammer, D., and Quadfasel, D.** 2010. On the low-frequency phase relation between the Denmark Strait and the Faroe-Bank Channel overflows. *Tellus, Ser. A*, 62,(4):530–550.
- Schoell, M.,** 1980, The hydrogen and carbon isotopic composition of methane from natural gases of various origins: *Geochimica et Cosmochimica Acta*, v. 44, p. 649-661.
- Schoell, M.,** 1988, Multiple Origins of Methane in the Earth: *Chemical Geology*, v. 71, p. 1-10.
- Scholz, F., C. Hensen, A. Reitz, R. L. Romer, V. Liebetrau, A. Meixner, S. M. Weise, and M. Haeckel.** 2009 "Isotopic Evidence (Sr-87/Sr-86, Delta Li-7) for Alteration of the Oceanic Crust at Deep-Rooted Mud Volcanoes in the Gulf of Cadiz, NE Atlantic Ocean." [In English]. *Geochimica et Cosmochimica Acta* 73, no. 18: 5444-59.
- Sibueta, M. and Olu, K.** 1998. Biogeography, Biodiversity and Fluid Dependence of Deep-Sea Cold Seep Communities at Active and Passive Margins, *Deep-Sea Research* 1, (45): 517–567.
- Somoza, L., Battista, B.M., Gardner, J.M., Lowrie, A.,** 2001. Gulf of Cadiz (western Spain): characterized by a complex petroleum system. Abstract. 21st Annual GCSSEPM Foundation Bob F. Perkins Research Conference. Petroleum systems of deep-water basins: global and Gulf of Mexico experience, December 2-5, 2001.
- Somoza, L., Gardner, J.M., Diaz-del-Rio, V., Vazquez, T., Pinheiro, L., Hernández-Molina, F. J.** and TASYO/ANASTASYA shipboard scientific parties, 2002. Numerous methane gas related seafloor structures identified in the Gulf of Cádiz. *EOS Transactions, American Geophysical Union* 83, 541-547.
- Somoza, L., Díaz-del-Río, V., León, R., Ivanov, M., Fernández-Puga, M. C., Gardner, J. M., Hernández-Molina, F. J., Pinheiro, L. M., Rodero, J., Lobato, A., Maestro, A., Vázquez, J.T., Medialdea, T., Fernández-Salas, L.M.,** 2003. Seabed morphology and hydrocarbon seepage in the Gulf of Cádiz mud volcano area: Acoustic imagery, multibeam and ultra-high resolution seismic data. *Marine Geology* 195, 153-176.
- Stadnitskaia, A., M. K. Ivanov, V. Blinova, R. Kreulen, and T. C. E. van Weering,** 2006, Molecular and carbon isotopic variability of hydrocarbon gases from mud volcanoes in the Gulf of Cadiz, NE Atlantic: *Marine and Petroleum Geology*, v. 23, p. 281-296.
- Stow, D., Hernandez-Molina, F.J., Hodell, D., and Alvarez Zarikian, C.A.** 2011. Mediterranean outflow: environmental significance of the Mediterranean Outflow Water and its global implications. *IODP Sci. Prosp.*, 339. doi:10.2204/iodp.sp.339.2011
- Strakhov, N.M.,** Calc–Dolomitic Facies of Modern and Ancient Basins, *Trudy IGN Akad. Nauk SSSR*, 1951, issue 124, Ser. geol., no. 45, pp. 211–218.
- Suess, E., Bohrmann, G., Von Huene, R., et al.** 1998. Fluid Venting in the Aleutian Subduction Zone. *Journal of Geophysical Research*, (103): 2597–2614.
- Suess, E., Carson, B., Ritger, S.D., et al.** 1985. Biological Communities at Vent Sites along the Subduction Zone off Oregon. *Bulletin of the Biological Society of Washington*,(6): pp. 475–484.
- Swart P.** 1983. Carbon and oxygen fractionation in Scleractinian corals: A review. *Earth-Science Reviews*, 19: 51–80.
- Takeuchi, R. Matsumoto, R., Ogihara, S. and Machiyama H.,** 2007, Methane-induced dolomite "chimneys" on the Kuroshima Knoll, Ryukyu Islands, Japan: *Journal of Geochemical Exploration*, v. 95, p. 16-28.

- Torres, M.E., J. McManus, D. Hammond, M.A. de Angelis, K. Heeschen, S. Colbert, M.D. Tryon, K.M. Brown, and E. Suess.** 2002. Fluid and chemical fluxes in and out of sediments hosting methane hydrate deposits on Hydrate Ridge, OR: I. Hydrological provinces. *Earth and Planetary Science Letters*. 201:525–540.
- Turova, T.P., Kolganova, T.P., Kuznetsov, K.B., and Pimenov, N.V.,** 2002. Phylogenetic Diversity of the Archean Component of Bacterial Overgrowths on Coral-Type Buildups in Methane Seepage Zones of the Black Sea, *Mikrobiologiya*, vol. 71, no. 2, pp. 230–236.
- UNESCO.**2006. Interdisciplinary geoscience studies of the Gulf of Cadiz and Western Mediterranean basins. IOC Technical Series, 70.
- UNESCO,** 2007 Deep-water cold seeps, sedimentary environments and ecosystems of the Black and Tyrrhenian Seas and Gulf of Cadiz. IOC Technical Series No. 72.
- UNESCO,** 2008 Deep-water depositional systems and cold seeps of the Western Mediterranean, Gulf of Cadiz and Norwegian continental margins. IOC Technical Series No. 76.
- Valentine, D.L. and Reeburgh, W.S.** 2000. New Perspectives on Anaerobic Methane Oxidation, *Environmental Microbiology*, 2: 477–484.
- Van Rensbergen, P., D. Depreiter, B. Pannemans, and J.-P. Henriët,** (2005a), Seafloor expression of sediment extrusion and intrusion at the El Arraiche mud volcano field, Gulf of Cadiz. *Journal of Geophysical Research* v. 110.
- Van Rensbergen, P., Depreiter, D., Pannemans, B., Moerkerke, G., Van Rooij, D., Marsset, B., Akhmanov, G., Blinova, V., Ivanov, M., Rachidi, M., Magalhaes, V., Pinheiro, L., Cunha, M., Henriët, J. P.** (2005b). The El Arraiche mud volcano field at the Moroccan Atlantic slope, Gulf of Cadiz. *Marine Geology*, 219: 1-17.
- Vanneste, H., Kastner, M., James, R.H., Connelly, D.P., Fisher, R.E., Kelly-Gerrey, B.A., Heeschen, K., Haeckel, M., Mills, R.A.** 2012. Authigenic carbonates from the Darwin Mud Volcano, Gulf of Cadiz: A record of palaeo-seepage of hydrocarbon bearing fluids. *Chemical Geology*, 300-301: 24,39.
- Voitov, G.I.,** 2001. Chemical and carbon isotope instabilities in the gryphon gases of mud volcanoes: an example of the southern Caspian and Taman' mud-volcano province. *Geochemistry International* 39, 373–383.
- Wilson, R.C.L., Sawyer, D.S., Whitmarsh, R.B., Zerong, J., and Carbonell, J.** 1996. Seismic stratigraphy and tectonic history of the Iberia Abyssal Plain. In Whitmarsh, R.B., Sawyer, D.S., Klaus, A., and Masson, D.G. (Eds.), *Proc. ODP, Sci. Results*, 149: College Station, TX (Ocean Drilling Program): 617–633.
- Yin, P., Berne, S., Vagner, P., Loubrieu, B., Liu, Z.,** 2003. Mud volcanoes at the shelf margin of the East China Sea. *Marine Geology* 194, 135–149.
- Youli Li,** 2002. Introduction to X-ray Diffraction, University of California, Santa Barbara.
- Zavatarelli, M., Raicich, F., Artegnani, A., Bregant, D., Russo, A.** 1998. Climatological biochemical characteristics of the Adriatic Sea, *Journal of Marine Systems*, 18, (1-3): 227-263.
- Zehnder, A.I.B. and Brock, T.D.**1979. Methane Formation and Methane Oxidation by Methanogenic Bacteria, *Journal of Bacteriology*,137: 420–432.
- Zehnder, A.J.B. and Brock, T.D.,**1980, Anaerobic Methane Oxidation: Occurrence and Ecology, *Appl. Environ. Microbiol.*, vol. 39, pp. 194–204.
- Zitellini, N., Gràcia, E., Matias, L., Terrinha, P., Abreu, M.A., DeAlteriis, G., Henriët, J.P., Daño-beitia, J.J., Masson, D.G., Mulder, T., Ramella, R., Somoza, L., and Diez, S.** 2009. The quest for the Africa–Eurasia plate boundary west of the Strait of Gibraltar. *Earth and Planetary Science Letters*, 280,(1–4): 13–50.

Books

- Alonso-Zarza, A.M. and Tanner, L.H.** 2010. Carbonates in Continental Settings: Geochemistry, Diagenesis and Application. Oxford: Elsevier. ISBN: 9780444535269
- Dove, M.P., De Yoreo, J.J., Weiner, S.** 2003. Biomineralization. Washington, D.C.: Mineralogical Society of America. (Reviews in mineralogy and geochemistry ; 54)
- Folk, R.L.** 1974. Petrology of sedimentary rocks. Austin: Emphill Publishing Company.
- Flügel, E.** 2004. Microfacies of Carbonate Rocks: Analysis, Interpretation and Application. Berlin ;

New York : Springer.

- Judd, A.G. and Hovland, M.** 2007. Seabed Fluid Flow: The Impact on Geology, Biology and the Marine Environment. Cambridge ; New York : Cambridge University Press. ISBN 9780521819503.
- Kiel, S.** 2010. The Vent and Seep Biota: Aspects from Microbes to Ecosystems. Dordrecht ; London : Springer. ISBN: 9048195713.
- Lisitsyn, A.P.** 1978. Protsessy okeanskoi sedimentatsii. Litologiya i geokhimiya (Oceanic Sedimentation Processes: Lithology and Geochemistry). Moscow: Nauka.
- Moore, D. M. and R. C. Reynolds, Jr.** 1997. X-Ray diffraction and the identification and analysis of clay minerals. 2nd Ed. Oxford University Press, New York.
- Morse, J.W. and Mackenzie, F.T.** 1990. Geochemisrty of sedimentary carbonates. Amsterdam: Elsevier Science & Technology . (Developments in sedimentary, 48)
- Schlager, W.** 1992. Sedimentology and sequence stratigraphy of reefs and carbonate platforms : a short course. Tulsa, Okla. : American Association of Petroleum Geologists.
- Schlager, W.** 2002. Sedimentology and sequence stratigrephy of carbonate rocks, Vrije Universiteit/Earth and Life Sciences De Boelelaan 1085, 1081 HV Amsterdam, Netherlands ISBN 90-806364-2-8
- Strakhov, N.M.** 1962. Osnovy teorii litogeneza (Principles of the Lithogenesis Theory), Moscow: Akad. Nauk SSSR.
- Tuker, M.E., Wright, V.P., Dickson, A.D.** 1990. Carbonate Sedimentology. Oxford: Blackwell Science. ISBN 0632014725
- Vai, G.B. and Martini, I.P.** 2001. Anatomy of an Orogen: The Apennines and Adjacents Mediterranean Basins. Dordrecht ; London : Kluwer Academic Publishers.

Annex I

R Statistic Script

I have used the follow procedure to make Box-plot Graphs using R statistics.

- I. Convert the excel file with the data in a .txt (ex: *iv04.txt*)
- II. Open R statistic and change the work spaces. To do that I went to “Misc” and select “*change work directory*”, then select the one that I need, in which I saved the .txt file.
- III. Import the file in R with `iv04<-read.table("iv04.txt")`
- IV. Now the file is imported to check it just wrote iv04 and enter the code; should appear the table like in figure 34.

```
> iv04<-read.table("iv04.txt")
> iv04
      V1      V2
1  Aragonite  3.49
2  Aragonite  0.00
3  Aragonite  0.00
4  Aragonite  0.00
5  Aragonite  0.00
6   Calcite 17.19
7   Calcite  0.00
8   Calcite  0.00
9   Calcite  6.82
10  Calcite  0.00
11 Dolomite 52.50
12 Dolomite  0.00
13 Dolomite 72.70
14 Dolomite 59.29
15 Dolomite  7.11
16 Detrital 26.82
17 Detrital  0.00
18 Detrital 27.30
19 Detrital 33.88
20 Detrital 92.89
```

Figure 50: screenshot of R-statistics showing an example of data input from .txt file.

- V. Now, if all the data are the correct ones, give the command to do a Boxplot graph with groups, this is important because it needed a division in the same samples between different minerals and fractions.

The script is: `boxplot(iv04$V2 ~ iv04$V1)`

where *V2* and *V1* are the variable that R have to consider respectively on the X and

Y axis. In this cases, the types of fractions on the horizontal axis and the values in % on the vertical.

VI. Then just give the enter command and the plot appear in a separate window.

VII. Go on "*file*"---> "*save as...*" and save it.

Annex II

GCD kit extension

The GCDkit is an extension of R specific for the GeoChemical Data. In this master thesis has been used to elaborate the ternary plot for the mineralogy.

To graph a ternary plot in GCDkit:

- I. Prepare a correct excel file, with the title of each column just in the first row and data start from the second. In this way the software read directly the different variables in the excel file.
- II. click on "*Data*" then "*load data files*" and select your file.
- III. then select the sheet where are your data and upload it in GCDkit.
- IV. Now the table is uploaded. You can check it going of "*data*"---> "*show table*"
- V. Now, to plot different groups of samples (in this case chimneys crusts and concretions) I have splitted data in group. Click on "*Data holding*" than "*Set group by...*" and in the end "*...labels*" , Now press Enter and it should appear the list of parameters contained in the sheet. The parameter that I have used was the "*Type*" column.
- VI. Now that the group are set click on "*Plots*" and then "*ternary plot*" and select from the list (it appear clicking the Enter button) the parameters that you want.
- VII. Select all the samples and let it run and the ternary plot appear in a separate window.

I have also changed the colors and the symbols for the groups to have simpler reading plot. To do this:

- I. Click on the menu "*Plot editing*" select "*Symbols/Colours by group*" and select "*Show Available symbols*" or "*Show available colours*"
- II. It will appear the list that shows the symbols and colours and a table to full-in with the groups in the first column (chimneys, concretions and crusts) and symbol and colour in the second and third.
- III. Enter the identification number for symbols and colours in the table.

- IV. Give the Enter command and close it.
- V. The plot is ready to be saved ("*File*"-->"*Save as...*")